國 立 交 通 大 學

奈 米 科 技 所

碩 士 論 文

轉酯化反應發展於微流道系統之研究

Development of real-time microfluidic reactor for the characterization of transesterification reaction

研 究 生：黃美榕

指導教授：柯富祥教授

中 華 民 國 九 十 七 年 六 月

轉酯化反應發展於微流道系統之研究

Development of real-time microfluidic reactor for the characterization of transesterification reaction

研究生：黃美榕 Student：Mei-Jung Huang

指導教授：柯富祥 Advisor：Dr. Fo-Hsiang Ko

國 立 交 通 大 學

奈 米 科 技 研 究

碩 士 論 文

A Thesis
Submitted to Institute of Nanotechnology
College of Engineering
National Chiao Tung University
in partial Fulfillment of the Requirements
for the Degree of
Master
in
Institute of Nanotechnology
June 2008
Hsinchu 300, Taiwan

中 華 民 國 九 十 七 年六 月

Acknowledgment

本研究之得以順利完成，首先感謝恩師 柯富祥教授這兩年來對學生不論是在學問研究方面及待人處世上的指導與教誨，以及對於研究內容及成果，均悉心校閱與指正，師恩浩瀚，學生銘感於心。另外，在研究期間承蒙俊淇學長這一路上的帶領，從一開始完全在狀況外的我，到現在能夠將論文完成，對本研究提供諸多寶貴意見，使得論文更佳紮實，於此謹致誠摯謝意。

在研究所這兩年生活中，特別感謝其昌學長、佳典學長、銘清學長、亦儂學長、志杰學長、群芳學姊、敬雅學姊、子銘學長的指導與照顧，教導我實驗室的生態與做人處事的道理，從學長姐們的身上學到許多書本中沒學過的事物，讓我受益良多。還有一路走來的同窗好友們中書、阿生、德玲、品麟的相互扶持與勉勵；以及戰友依蓁常常聽我在抱怨並適時的給我建議，常賦予生活上以及精神上的一劑強心針，在此致以無限的謝意。也感謝鄭捷學弟、柏軒學弟、嘉琦學妹、玟菲學妹以及京璋學弟在實驗研究上的協助與幫忙。

最後我要感謝一路支持我的家人—因為有爸爸媽媽的支持，大姐、婷、跟小蘭姐的關心及激勵，我才可以完成碩士學業，願將所有成就與你們分享。

轉酯化反應發展於微流道系統之研究

學生：黃美榕　　指導教授:柯富祥

國立交通大學

奈米科技研究所

碩士論文

摘　要

近年來，隨著奈米科技的日益進步，微小化系統也逐漸備受重視。微小化系統是一門延伸各領域的學問，需要化學、物理、生物、光學等各工程學科的結合製作與設計。能夠建立一個微小型系統並直接快速地偵測其中的生物或化學分子，也就是將以往傳統大型複雜的分析裝置，提供體積縮小化、平行分析化、降低生產成本及縮短反應時間等優勢，將對於分析及研究上提供重大的貢獻。

傳統上對與轉酯化反應多是利用鹼製程來進行催化油脂以生產脂肪酸酯類，亦是生質柴油。因具有反應時間短、成本低廉等優點亦是目前有發展工業化的製程，但是其中的廢液處理也造成嚴重的環境污染問題。若是利用脂肪分解酶來進行催化油脂以生產脂肪酸酯類，是具有無污染、環保的優勢。然而，較高的操作成本及冗長的反應時間是導致酵素製程不受青睞的最主要原因。對於脂肪分解酵素純化分離取得不易，再加上酵素無法進行重複回收再

利用，所以價格相較於鹼製程來的高昂。因此本研究注重於發展出一個可以減少成本、縮小試劑體積及縮短反應時間的轉酯化反應偵測系統。

本研究中將利用微小化系統的優勢以探討生物分子於微流道系統的表現。由於在實驗中，脂肪分解酶反應時間的長短取決於酵素的活性及酵素的安定性，因此將酵素經過固定化程序來進行提昇酵素活性及安定性為一個非常重要的步驟。我們利用化學蝕刻技術製作出形貌特徵為金字塔所形成的織構化表面，並結合自組裝技術來固定脂肪分解酶，由於織構化的表面可用以增加脂肪分解酶的鍵結及矽基材的穿透度，並進而發展出一套在微流道系統上偵測脂肪分解酶催化三酸甘油脂反應的方法。

研究中利用偵測與分析轉酯化反應的方法有：藉由 可見光與紫外光吸收光譜儀來測定，發現透射係數可以有判定的指標。實驗證實在不同反應時間中，穿透度有不同的變化，可用以觀察轉酯化反應的發生，然而此種光譜偵測的方法並不能確切地提供反應的轉化率；我們發現三酸甘油脂與脂肪酸酯類尾端氫原子化學位移的差異，並根據此差異來利用核磁共振儀偵測轉酯化反應，可以得到實際的反應轉化率；由於實驗中得知轉酯化反應對於光線有反應，因此我們利用這點結合太陽能板與微流道系統發展出一套光電偵測平台，並藉由特定波長的光訊號經由太陽能板以收集電子訊號。

實驗中，我們結合自組裝技術及化學蝕刻法以提高脂肪分解酵素經固定化程序的活性及安定性，並整合微流道系統來克服轉酯化反應中酵素製程的缺點。最後結合上述的偵測方法，以推測不同的方法對於轉酯化反應在微流道系統中的分析結果。

Development of real-time microfluidic reactor for the characterization of transesterification reaction

Student：Mei-Jung Huang Advisor：Dr. Fu-Hsiang Ko

Institute of NanoTechnology

National Chiao Tung University

ABSTRACT

Recently, the microfluidic technology has become very important and widely used in many research fields such as biochemical technology, semiconductor technology and electronics technology. The microfluidic technology, the studies on the motion of fluid and particles through the microchannels, is an emerging field that has given rise to a large number of scientific and technological developments over the last years.

In this study, we would like to develop a microfluidic reactor for production of the biodiesel of transesterification reaction. First, we immobilized lipase on the tetramethyl ammonium hydroxide (TMAH) textured surface with self-assembled monolayer (SAMs) of covalent bonding. The TMAH textured surface for anisotropic texturisation are usually growing pyramidal structures which are increasing the surface areas for lipase-immobilized and decreasing the reflectivity for advancing

light absorption. The immobilization of lipase on solid substrate is an essential step for many applications in the field of biocatalysis duo to the relevance for the performance to improve and optimize the lipase activity and stability. However, the transesterification by enzyme method is time-consuming compared to acid- or alkali-catalyzed. Development the microfluidic reactor system is an important way to improving the reaction rate and enhancing the conversion yield due to the high surface-volume ratio and advancing the mass and heat transfer. This experiment aims is to provide a new approach that could potentially analyze the real-time reaction of transesterification. Moreover, new generation of biosensors combining new bioreceptors with the ever-growing number of transducers is emerging.

The microfluidic reactor transducers of analysis systems are used in the optical spectroscopy (UV-Vis spectroscopy) for detecting the transmission of transesterification reaction. Following is detecting by nuclear magnetic resonance (NMR) for identifying the structure of biodiesel and then estimating the conversion of reaction. Since the response of transmission can be detected from transesterification reaction, the exploration of photo-electronic analysis, photodetector, can be used for monitoring the biocatalytic reaction in real-time. It is based on the phenomenon of different transmission and converted to electric signal. Since the detection of UV/Vis-NMR can confirm the conversion of transesterification and the detection of optical-electric (UV/Vis-photodetector) can be real-time monitoring the transesterification reaction. Combine with above analysis methods, the experiments provide a new approach for an easy and feasible way to analyze and detect the transesterification reaction.

Contents

List of Tables

Chapter 1

Chapter 2

Chapter 4

List of Figures

Chapter 1

Chapter 2

Chapter 3

Chapter 4

Chapter 1 Introduction

1.1 General Introduction

The interdisciplinary study of biology, chemistry, and electronics becomes more and more important than ever before. Combining the biotechnology and semiconductor technology, various types of biochips and biosensors have now been developed to detect and monitor the specific binding of biomolecular on the solid-state substrates. [1] The history of biosensors can trace back to 1962 with the development of enzyme electrodes by scientist Leland C. Clark. [2] Biosensors are known as immunosensors, optoelectrodes, chemical carries, resonant mirrors, glucometers, biochips, and biocomputers. The biosensors are described as a chemical sensing device in which a biologically derived recognition entity is coupled to a transducer, to allow the quantitative development of some complex biochemical parameter. And it is an analytical device incorporating a deliberate and intimate combination of a specific biological element and a physical element. A basic concept of biosensor in Fig. 1-1 and Fig. 1-2 shows it consists of a bioelement and a sensor element. The bioelement may be an enzyme, antibody, living cells, or tissue. The sensing element may be electric current, electric potential, and so on. [2]

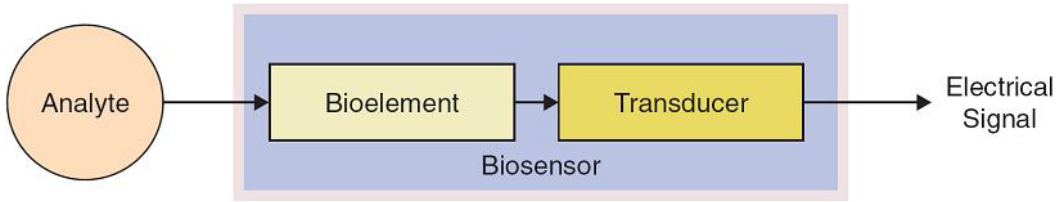

Figure 1-1 A schematic representation of biosensors. [2]

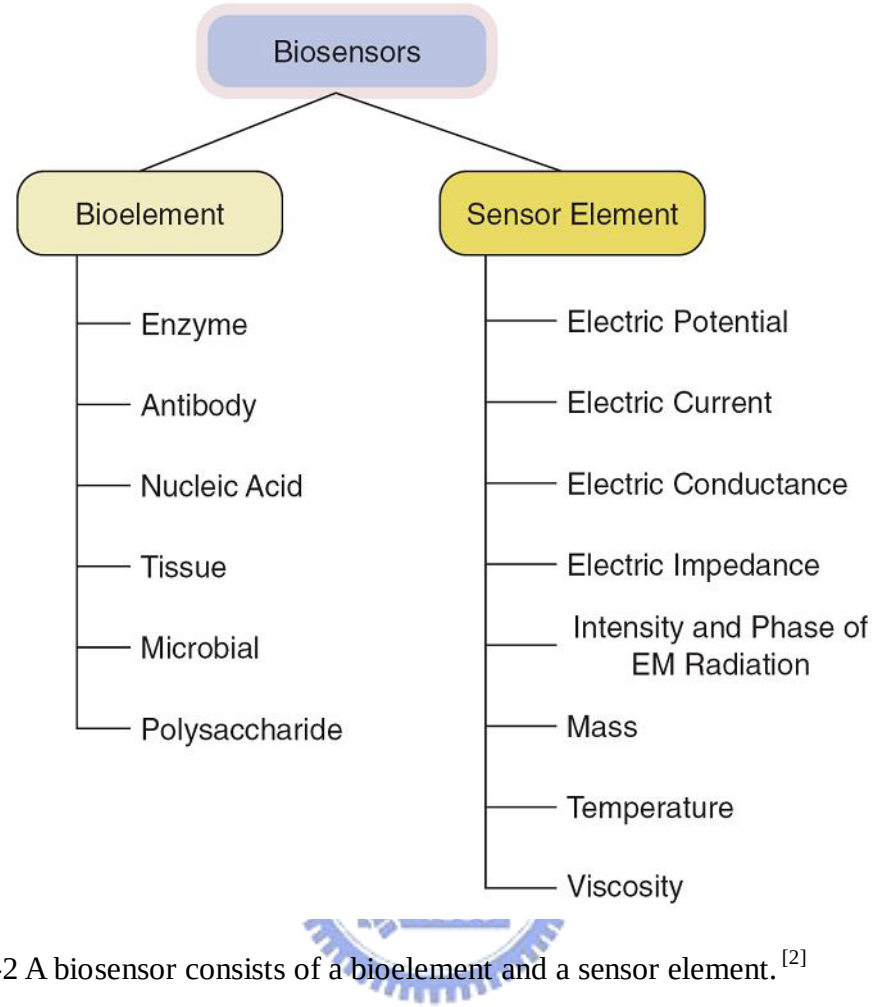

Figure 1-2 A biosensor consists of a bioelement and a sensor element. [2]

In this study, we try to develop a real-time microfluidic sensor and apply it for transesterification reaction detection applications. The sensor can be applied to green chemistry field. The biosensor is constructed by combining immobilized enzyme molecule as the bioelement, and the sensing element plays a role on optical element, electric current and chemical analysis. The transesterification reaction, in this process, is catalyzed by immobilized enzyme, lipase (triacylglycerol acylhydrolase, EC 3.1.1.3), for production of biodiesel fuel. Biodiesel has become more attractive because of its environmental benefits and the fact that it is made from renewable resources which indicates the vegetable oils or animal fats. The major advantage of biodiesel compared to other gasoline and petroleum diesel is that it is environmental

friendliness, and can be added in petroleum diesel with certain percentage to allay the energy issue.[3] As the rising energy demand and reducing petroleum reserves, fuels such as biodiesel and bioethanol are in the forefront of the alternative technologies. The price of bio-fuels will become more competitive to gasoline and petroleum diesel. Table 1-1 shows the economical feasibility of biodiesel.[4]

However, there are some challenges for biodiesel fuel production, with lipase catalysis, from the following reasons: (i) reaction efficiency is poor and (ii) the stable activity of enzyme is necessary. In the thesis, we try to fabricate a microfluidic system which possesses the higher surface-to-volume ratios and lower reagents consumption. to the microfluidic system is expected to enhance the throughput rate of chemical synthesis and the amount of chemical product[5] Since the free enzyme for transesterification loses its activity rapidly if it has no surface binding, we plan to retain the enzyme activity by means of immobilization onto the device surface.

Table 1-1 Economical feasibility of biodiesel.[4]

<table>
<tr><td></td><td colspan="2">Biodiesel</td><td>Petroleum</td></tr>
<tr><td rowspan="2">U.S.</td><td>B100</td><td>B20</td><td rowspan="2">$0.68/gallon
(taxes will add approximately $0.50 per gallon)</td></tr>
<tr><td>$1.5~2.0/gallon</td><td>$0.83~0.88/gallon</td></tr>
<tr><td rowspan="3">Europe</td><td>Vegetable oil</td><td>Waste grease</td><td rowspan="3">$0.20~0.25/l</td></tr>
<tr><td>$0.54~0.62/l</td><td>$0.34~0.42/l</td></tr>
<tr><td colspan="2">fiscal support from the government</td></tr>
</table>

B20 is nominally 20 percent biodiesel and 80 percent petroleum.
B100 is 100 % pure neat biodiesel.

1.2 Literatures Review

1.2-1 Biosensors

Biosensors are in general small devices based on direct spatial coupling between a biologically active compound and a signal transducer equipped with an electronic amplifier illustrated in figure 1-1. The response generated as a result of biochemical reaction is detected by a transducer to give a signal such as optical, electrical and thermal analysis in a given test sample. The biosensors can be of many types such as: resonant biosensors, optical detection biosensors, [6] thermal-detection biosensors, [7] ion-sensitive field-effect transistor (ISFET) biosensors, [8] [9] and electrochemical biosensors. [6][7]

The typically used bioelement enzyme is a large protein molecule that acts as a catalyst in chemical reactions but remains unchanged at the end of the reaction. The way of enzyme immobilization in the sensor has been investigated. It is an essential step for bioelement immobilization on the support materials. Mendes *et al.* [11] developed different immobilization procedures for horseradish peroxidase (HRP). The sensor of protein is efficiency immobilized on gold electrodes by different self-assembled monolayers (SAMs). The enzyme immobilization process uaes a cross linker to gold electrodes and modification with self-assembled monolayer which is constituted by structurally different thiols group that it is possible to develop distinct biosensors based on the $-NH_2$ terminal group of HRP. [10] The electrochemical impedance spectroscopy and surface plasma resonance are used to evaluate the analytical response of the biosensor with respective to H_2O_2. In figure 1-3 shows the performance, which are confirmed that a larger extent of enzymatic adsorption onto the Au–cysteamine electrode, and suggests the promising to sensor promising for H_2O_2 determination.

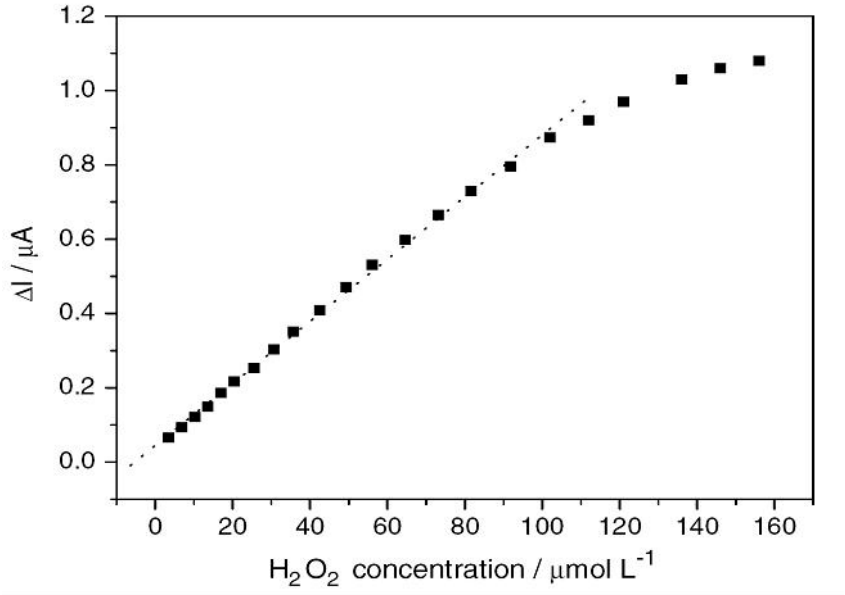

Figure 1-3 The analytical curve obtained for H_2O_2, using the developed biosensor with Au–cysteamine–glutaraldehyde–HRP. The linear response range, the detection limit and sensitivity presented by the proposed biosensor indicate that it can be used to determine hydrogen peroxide.[10]

A simple biosensor based on immobilized enzyme is developed for the monitoring of trace heavy metal ions. The biosensor system is designed based on the inhibition of urea activity, where the urea is immobilized on the membrane. When changing the pH, the bio-catalytic hydrolysis of urea changes the color from yellow to dark red, thus decreases in the reflectance response of the sensor measured at 615 nm by optical fiber sensor under the exposure to the heavy metal ions.[11]

The construction of the optical biosensor is shown in figure 1-4. The immobilized urease and pH indicator strip are placed into the specially fabricated flow-cell with approximate 10 μL. The flow-cell device, with inlet and outlet for solution flow, is directly faced to the circular end of a fiber optic bundle probe. The bottom of flow-cell is PTFE disk in order to provide a reflective surface.

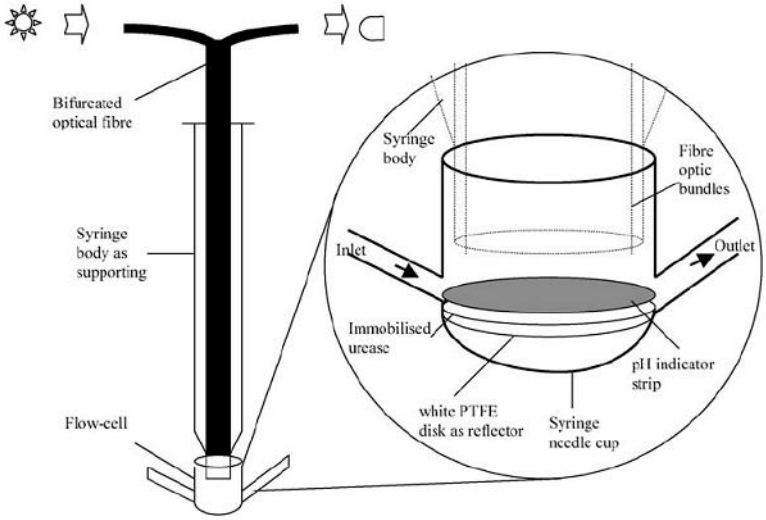

Figure 1-4 Flow-cell set-up and fiber optic biosensor configuration. [11]

The most commercially successful biosensors are glucose biosensors. The first historic experiment that served as the origin of glucose biosensors is carried out by Clark and Lyons. [2][12] They utilize the phenomenon of glucose oxidation with a glucose oxidase enzyme. The chemical reaction of glucose with oxygen is catalyzed in the presence of glucose oxidase shown in figure 1-5.

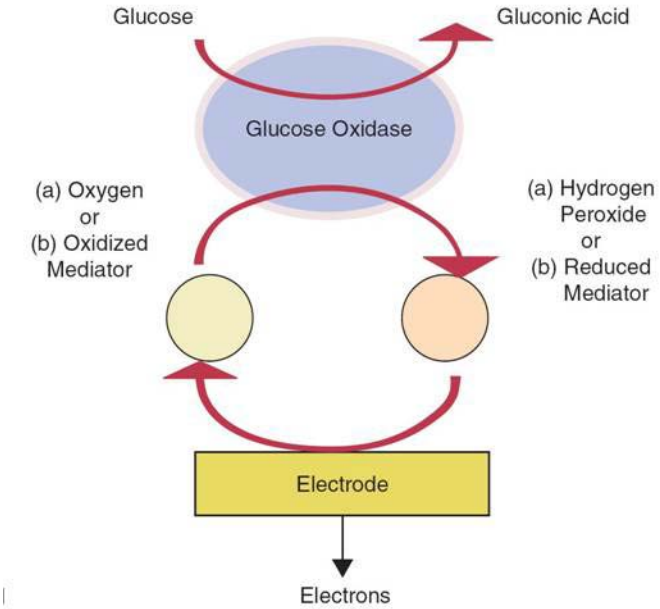

Figure 1-5 Working principle of glucose biosensors. [2]

As soon as the enzyme recognizes the glucose molecules, it acts as a catalyst to produce gluconic acid and hydrogen peroxide from glucose and oxygen. In the meanwhile, the reaction also produces electrons, and protons, thus reduces glucose oxidase enzyme. The effect of interference is corrected by using platinum (Pt) electrodes, which is covered with the enzyme, and measuring the differential current. The chemical reaction of increasing the glucose content, the more oxygen is consumed. On the other hand, the lowering of glucose content results in more hydrogen peroxide generation. Hence, either the consumption of oxygen or the production of hydrogen peroxide can be detected with the help of platinum electrodes, and this can serve as a measuring indicator for glucose concentration.

The biosensors are often used to cover sensor devices used in order to determine the analysis of substances and other parameters of biological. If the bioelement used as enzyme, the biological response of the biosensor is determined by the biocatalytic which converts the reactant to product. Immobilized enzymes possess a number of advantages which make them particularly applicable for use in such systems. It retains the activity and stability, which ensures that the same catalytic activity is present for a series of analyses.

In the field of biosensors, there are various technical difficulties and more research efforts needed to find better alternatives. The bioelements and chemicals used in the biosensors are inevitable to be prevented from leaking out of the biosensor; biomolecules are attached to the transducer as strongly as possible; the detection range should develop to be large, selective and more sensitive, and research should be focused on the development of low-cost biosensors. At present, the development of faster, reliable, accurate, portable, and low-cost biosensors has become an important issue for the further applications in this field.

1.2-2 Microfluidic System

The micorfluidic systems have several advantages for performing chemical reactions in comparison with the traditional technologies. The key advantages are the rapid heat exchange and rapid mass transfer, which cannot be achieved by the conventional batch system. As to the microfluidic systems used as analytical devices, the first approach is towards lab-on-a-chip devices. The lab-on-a-chip or micro-total-analysis system (μ-TAS) in conjunction with all of the components of the detection system has then to be integrated on a chip. These advances have also merged functions associated with sensing, actuation, and control to provide new platforms for chemical and biological research. The most important role of these systems is the function of analysis and detection system.

Noji *et al.* [13] developed a technique capable of PDMS microchamber in order to perform single protein analysis. Figure 1-6 shows the microchamber of molding soft polymer PDMS onto glass substrate with dimensions of up to 2 μm in diameter and 2 μm in height. The measurement is to study the rotation activity of F1-ATPase protein (F1 protein) motors, by a single protein isolated in a microchamber. The activity can be estimated by the mechanical properties of rotary motor, F1 proteins hydrolyze ATP (adenosin-triphosphate) into ADP + P (adenosin-diphosphate + Phosphorous), and release energy which is converted into rotational torque. F1 proteins would rotate with the consumption of ATP molecules. As soon as the F1 proteins attach to the glass surface, they begin to rotate. The direction of the rotation is the same as that observed for the γ subunit and ε subunit, a kind of subunits with a stoichiometry consisted by the F1-ATPase. Rotation is absolutely dependent on ATP hydrolysis and inhibiting ATPase activity.

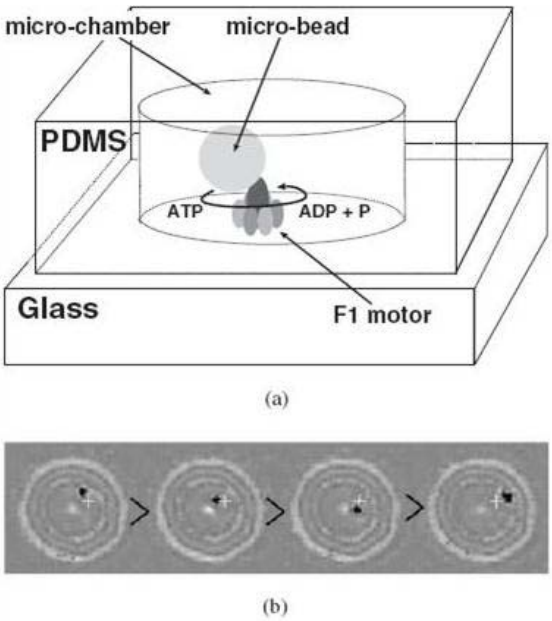

Figure 1-6 Schematic view of the rotation of a F1 protein motor in a PDMS microchamber. (a) A PDMS microchamber filled with buffer and one F1-protein-coated bead, and (b) View of a microchamber with a bead rotating in chamber. The PDMS mold exhibits good property of optical detection in the visible and near-UV wavelengths. [14]

The PDMS microreactors are usually defined as miniaturized reaction systems fabricated by using the methods of microtechnology and precision engineering. Miniaturized analytical assays are useful in many fields of biotechnology. The possibility of performing similar analyses in parallel is an attractive feature. The microreactor is the proposed for a wide range of devices having small dimensions, and a further division according to size into nano, micro and minireactors. Most of the currently constructed microreaction devices take advantage of microfluidics, which enables use of micro- and nano-liter volumes of reactive species and ensures high efficiency as well as repeatability of biomolecular processes. [15] For the use of microreactors in analytical chemistry and biochemical studies are that they can be coupled with numerous detection techniques such as fluorescence, absorbance,

electrochemical and chemiluminescence, and that pretreatment of the samples can be carried out on the chip. [16][17]

Most spectroscopic detections are used for fluorescent tag or some photo-label attachment on the substance. The absorbance technique is advantageous as it does not require fluorescent tag attachment on the substance. In the UV or visible range most of the molecules or atoms absorb light at several wavelengths and then give a specific signature. Measuring the absorbing species in a sample solution is accomplished by applying the Beer-Lambert law. [14] Zhu *et al.* developed an integrated microfluidic UV absorbance detection system with attomol-level sensitivity for BSA. [18] The fabrication for integration of bare photodetector chips into a polymer microfluidic substrate is shown in figure 1-7. Detection platforms fabricated using this approach exhibit exceptionally low concentration and mass detection limits down to 15 nM and 9.8 amol, respectively, for bovine serum albumin (BSA) as a model protein.

Based on the Lambert–Beer relation, the sensitivity of the detection system can be increased linearly by increasing the optical path length. The integrated detector is potentially used for monitoring protein separations without resolution loss due to sample dispersion when passing through the detection region.

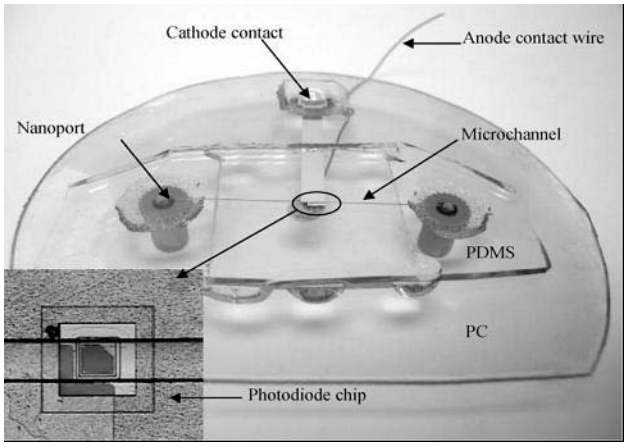

Figure 1-7 Photograph of a fabricated microfluidic substrate with integrated photodetector chip. [18]

Microfluidic systems, such as the enzymatic microreactors, have been developed in order to facilitate in biochemical analysis, and have applications in biocatalysis. The immobilization enzyme is often used with the achievements in chemical and biochemical microreaction. A centrifugal microchip that uses a compact disk (CD) player-like apparatus has also been described. [19][20] This method was applied to antibody specificity, with the analysis process carried out by controlling the rotation speed shown in figure 1-8(a). This microfluidic system does not require the usual pump mechanism. Centrifugal and capillary forces were used to control the flow sequence of different solutions involved in the process. The microfluidic device was fabricated on a plastic CD. Each step of the analysis process was carried out automatically by controlling the rotation speed of the CD. This method is useful for the development of analytical microbioreaction systems for multiple analyses of single samples.

Hisamoto *et al.* [21] reported that a nylon membrane could be formed at the interface of two solutions formed in a microchannel shown in figure 1-8(b). Peroxidase is immobilized on this membrane, which is used as a chemicofunctional membrane. The synthesis of a chemically functional polymer membrane is reported by an interfacial polycondensation reaction and multilayer flow inside a microchannel. Single and parallel dual-membrane structures are successfully prepared by using organic/aqueous two-layer flow and organic/aqueous/organic three-layer flow inside the microchannel followed by an interfacial polycondensation reaction.

Methods for the immobilization of enzymes on a microfluidic surface have also been developed because they can have the advantage of the larger surface area of microreaction systems. In these systems, a biotin–avidin system was most frequently used to immobilize enzymes. The biotinylated polylysine was physically immobilized on a glass surface to capture streptavidin-conjugated alkakine phosphatase [22] shown

in figure 1-8 (c). The device consists of a glass slide onto which enzyme has been immobilized in a well-defined region with a sharp interface that runs perpendicular to the direction of flow. By flowing substrate solution over the enzyme surface and measuring product concentration as a function of distance from the enzyme front, it can be determined the intrinsic kinetics of the reaction under steady-state conditions.

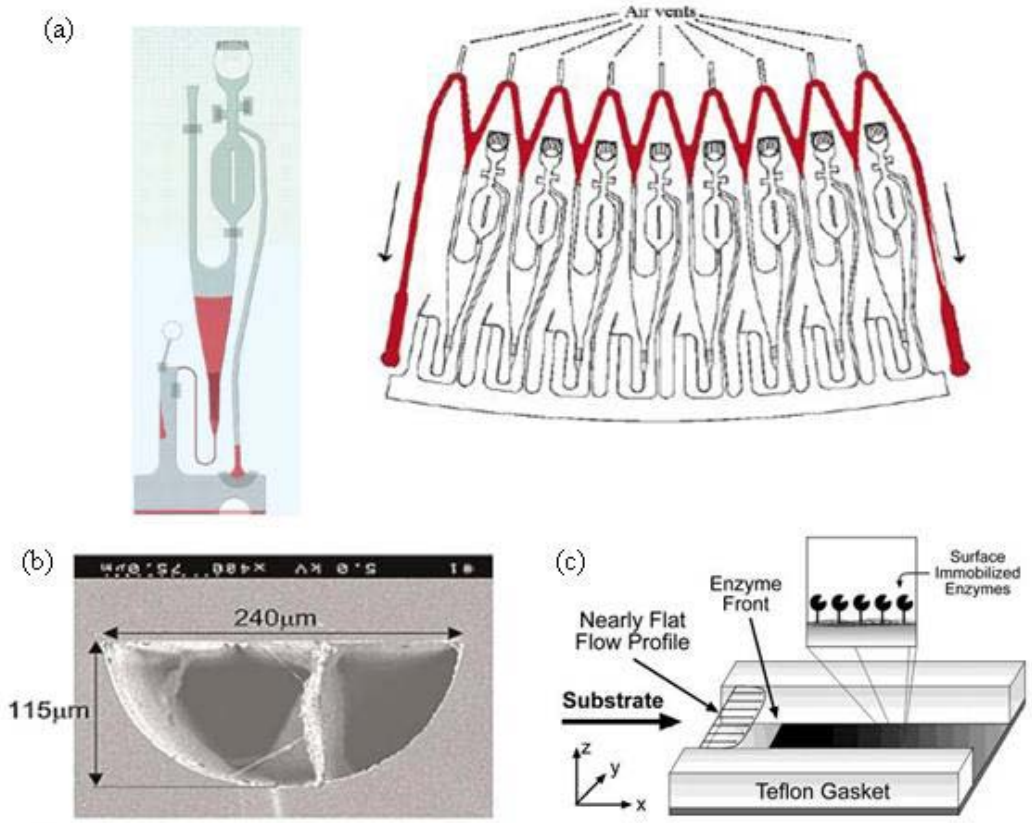

Figure 1-8 Images of immobilization technique for enzyme microreactor. (a) Schematic view of analysis structure CD and CD structure schematically drawn with a unit of eight parallel structures for analysis. (b) The membrane of a cross-linking enzyme-aggregate formed at microchannel surface. (c) The microreactor consists simply of a surface onto which enzyme has been immobilized. A Teflon gasket defines the walls of the channel. Flow over the surface is essentially uniform across the width of the channel. [19][20][21][22]

Numerous analytical micro enzyme-reactors have been developed that take advantage of the reduction in reaction time and the minimal amount of reagents used in microchannel systems. However, the range of immobilized enzymes available with satisfactory characteristics is still limited. The characterization of enzyme activity is a function of new biocatalysts and their substrates and the substrate concentration in the microreactors.

1.2-3 Biodiesel Analysis

Biodiesel is a renewable and a non-petroleum-based fuel made by a reaction of alcohol with vegetable oils, animal fats, or greases through a refinery process called transesterification reaction. The analytical methods of biodiesel discussed in this module can be divided into three categories: chromatographic methods, [23] [24] [25] spectroscopic methods, [26] [27] and physical-property based methods. [28]

Chromatographic methods are used to separate a mixture of compounds based on theirbphysical properties. The major chromatographic methods are gas chromatography (GC) and liquid chromatography (LC), often termed high-performance liquid chromatography (HPLC). In GC, the mixture is separated mainly by the boiling point and the structure of the individual compounds. To carry out a GC analysis, low concentrations of samples are usually dissolved in an organic solvent and then injected into the gas chromatograph. In this case, a sample needs to be derivatized with a silylating reagent in order to obtain a useful gas chromatogram. Derivatization improves their performance considerably, and can provide better resolution between compounds with similar properties. When the detector detects a material eluting from the column at a certain retention time, this will be shown by a peak in the chromatogram. Bunyakiat *et al.* [23] calculated the biodiesel conversion

from GC analyses and standardization by the following equation:

$$\% \text{ biodiesel conversion} = W_{ME} / W_{FA} \times 100 \text{---------- 1}$$

Where W_{ME} is the weight of methyl ester in liquid product that is obtained from gas chromatography; and W_{FA} is the weight of fatty acid in each vegetable oil.

Chiou and Wu [24] used LC to analyze the reaction production of biodiesel. LC generally separates a mixture based on the solubility of its components in a solvent while passing the mixture through a column which is similar to GC. It is usually conducted at room temperature.

Recently, spectroscopic methods that have been used for biodiesel include nuclear magnetic resonance (NMR) and near-infrared (NIR) spectroscopy. In both cases, certain characteristic peaks for oil and biodiesel in the spectra indicate how far the conversion of oil to biodiesel has progressed. NIR is easy to use and can give spectra in less than a minute. One of the advantages of these methods is that no derivatization is needed. Knothe [27] used ^{1}H NMR spectroscopy for determining the blend level of biodiesel in conventional diesel duel. Spectroscopic methods, on the other hand, give results in which all components of a mixture contribute simultaneously to the resulting spectrum. They can be used for quantification if appropriate components in the mixture exhibit unique peaks well separated from those of other components.

Spectroscopic or chromatographic methods have been used most often for assessing biodiesel fuel quality and monitoring transesterification. In contrast to chromatographic methods, spectroscopic methods analyze the intact sample. However, it usually results in additional instrument costs. The chromatographic methods only detect if a compound is eluting, not its identity or structure. The identity or structure needs to be established through the use of standards as far as possible. Thus, using a

spectroscopic method of detection in combination with a chromatographic method yields more detailed information. The most common analysis methods are GC-MS and LC-MS.

Physical characterization methods are based on the difference in viscosity between the vegetable oil and the corresponding biodiesel. For example, the viscosity of soybean oil is 32.6 mm^2/s at 38°C and that of biodiesel is 4.41 mm^2/s at 40°C. The viscosity difference forms the basis of an analytical method for detecting by the viscometry applied to determining the conversion of vegetable oil to methyl ester. This can apply to monitor the progress of the transesterification reaction. It is noted that physical characterization methods do not provide much detailed analytical information than spectroscopic or chromatographic methods.

1.3 Motivation

The world energy demand issue continues to increase. The most feasible way to meet this growing demand is by utilizing alternative fuels. The biodiesel can be produced from transesterification reaction by means of chemical catalysis, acid- and alkali-catalyzed, and enzyme-catalyzed. The first two catalytic methods are received the greatest attention and used widely. As for the enzyme-catalyzed reaction, this reaction is considered natural and green. However, the reaction requires much longer reaction time and higher cost than other two methods. [23] For solving these problems, a new concept of micro systems needs to be developed. The special detection performed inside the microfluidic systems has the advantages in the fields of enhancing reaction efficiency. Furthermore, the microfluidic reactor requires much smaller sample volumes for the analysis system. This design conducts many measurements and consumes small volumes of samples, which is very importance for

raising the price of feedstock materials recently.

In this study, we would like to propose a new approach for the analysis and detection of transesterification reaction by means of fabricating a biosensor with enzyme-immobilized in microfluidic reactor system. The analysis of UV-Vis spectroscopy is an easy and feasible way of detecting the transesterification reaction, which idea has not been proposed for the detection of biodiesel before. Compared to other spectroscopic detections used fluorescent tag or some photo-label attachment on the substance, the UV-Vis method possesses the advantage of without any label such as fluorescent tag attachment. Under this approach, our ultimate goal is to develop a cheap and portable microfluidic reactor for faster production of the biodiesel. Our research demonstrates the potential application for the analysis and detection of transesterification reaction.

1.4 Thesis Organization

In this study, we report the enzyme-based biosensor of transesterification reaction for the production process of biodiesel. Our experimental flow is shown in figure 1-9.

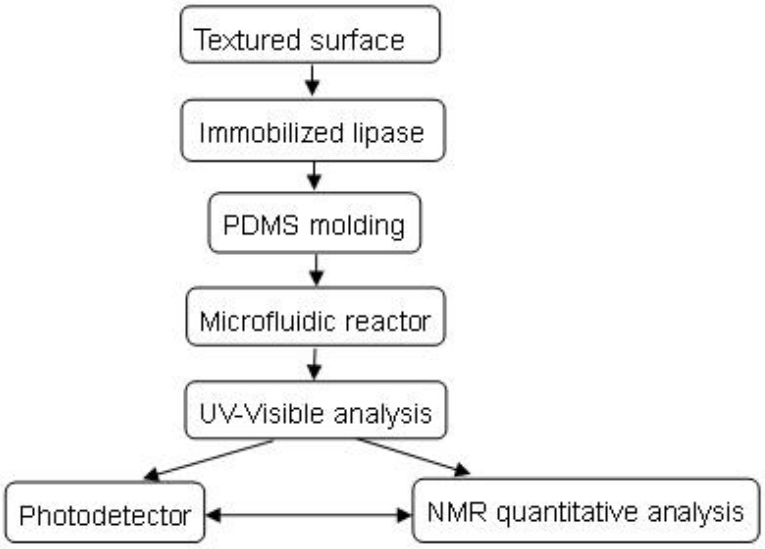

Figure 1-9 The overall flow of this study.

The thesis is divided into five chapters. In chapter 1 is the general overview of the background and motivation of this study. Literature surveys the fabrication of biosensors, microfluidic systems, and reviews of biodiesel analysis. The principles and operations of this experiment are introduced in chapter 2. The detailed fabrication processes and immobilized steps are presented in chapter 3. In chapter 4, we discuss the activity of immobilized enzyme, microfluidic reactor performance and the analytical results of transesterification reaction. Finally, we summarize the contribution of our research in chapter 5.

Chapter 2 Principles and Operations

2.1 Transesterification Reaction

Alkyl esters of short chain fatty acid are called biodiesel. ‘‘Bio’’ represents its renewable and biological source in contrast to traditional petroleum-based diesel fuel; ‘‘diesel’’ refers to its use in diesel engines. We can obtain these esters (biosiesel) from triglycerides (oil) by transesterification with alcohol. Fig 2-1 shows the transesterification reaction of triglyceride. [4] The transesterification can be carried out by chemical, enzymatic or non-catalytic method. [23] The chemical method can produce biodiesel and glycerol in the presence of a strong acid or base catalyst, in which normally be H_2SO_4 and NaOH or KOH respectively. The alkali-catalyzed transesterification is much faster and less corrosive than the acid-catalyzed reaction and has been used for industrial scale. However, this reaction generates by-product i.e., waste water and requires high quality of feedstock during the producing of biodiesel. If oil has high free fatty acid and water content, acid-catalyzed transesterification reaction is more suitable. [4][29] The enzymatic one is lipase-catalyzed which considered its energy-intensive process, but the high cost of enzyme and lower conversion of transesterification will be an important issue. Another approach is the non-catalytic, under supercritical methanol condition, just few minutes to product biodiesel and it is the fastest way of these methods. Because this type of non-catalytic method is under supercritical methanol condition, it takes most expensive production cost. [23] Table2-1 compares various biodiesel production processes.

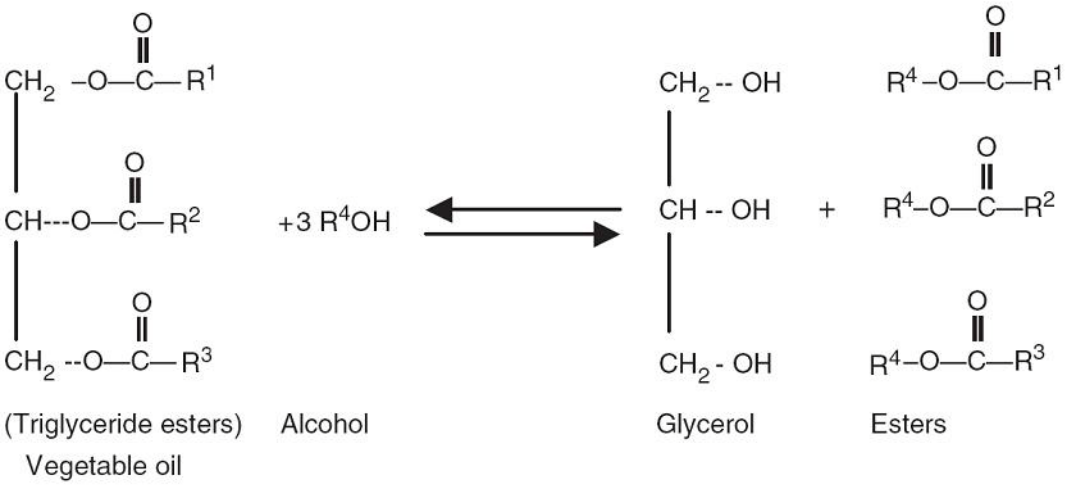

Figure 2-1 Transesterification reaction of triglyceride. And R^1, R^2, R^3, R^4 represent various alkyl group. [4]

Table 2-1. Various Biodiesel Production Processes. [4][23][29-30]

	Chemical		**Enzyme**	**Non-catalytic (Supercritical)**
	Acid	**Alkali**		
Condition	30~65 ^{0}C	60~80 ^{0}C	Near R.T.	>239.4 ^{0}C >8.09MPa
Reaction rate	Middle (1hr~)	Fast (30min~1hr)	Slow (1hr~)	Fast (sec~min)
Waste water	Yes	Yes	No	No
Yield	Normal to high	Yes	Low to high	High
Note points	1. Low cost. 2. Suitable for high FFA and water content. 3. Difficult to purification. 4. Complicated process.	1. Low cost. 2. Need high quality TG. 3. Difficult to purification. 4. Anhydrous alcohol process.	1. High cost. 2. Enzyme inactivity. 3.Environment-friendly process. 4. Lower conversion yield compare to chemical method.	1. High cost. 2. Large amount of supercritical methanol. 3. Easy to purification. 4. Only need to remove methanol in the end of process.

FFA: free fatty acid

TG: triglyceride

Transesterification of triglycerides (vegetable oils and animal fats) to generate esters and glycerol to obtain a new engine fuel (biodiesel) is a well-prove process. Renewable biomass has also been considered as potential feedstock for vegetable oils to produce biodiesel. The main advantages of biodiesel as diesel fuel are liquid nature portability, ready availability, renewability, higher combustion efficiency, lower sulfur and aromatic content and higher biodegradability. [3] Table 2-2 shows the biodiesel emissions compared to conventional diesel.

Table 2-2 Biodiesel emissions compared to conventional diesel. [4]

Emission type	B100 (%)	B20 (%)
Regulated		
Hydrocarbon	−93	−30
Carbon monoxide	−50	−20
Particulate matter	−30	−22
NO_x	+13	+2
Non-regulated		
Sulfates	−100	−20
PAH (polycyclic aromatic hydrocarbons)	−80	−13
Ozone potential of speciated HC	−50	−10

As the energy is shortage and contamination problem around the world recently, the regeneration, biocompatibility, biodegradability, and environmental acceptability of biomass become noteworthiness theme. Although this is an environment-friendly process, the high price of biodiesel will be an important issue. The high price of biodiesel is in large part due to the high price of the feedstock and another part is depends on the price of the crude petroleum. [4] Nowadays more and more countries including Netherlands, Germany, Belgium, Austria, USA and Japan not only develop their renewable biomass process, but also promulgate the policy or tax relief to encourage people using the renewable biomass.

2.2 Lipase

In this experiment, we would like to generate esters through biocatalytic reaction with enzymes, lipase (triacylglycerol acylhydrolase, EC 3.1.1.3), which can normally be placed into three types by different positional specificities shown in figure 2-2. [31] [32]

A. *Non-specific lipase:* This kind of lipases can completely catalyze the triglycerides to free fatty acid and glycerol. Examples of this type of lipases are *Candida rugosa*, *Corynebacterium acnes* and *Stephylococcus aureus*. And they show no marked specificity as regards the position on triglycerides molecule.

B. *1, 3-specific lipase*: The second type of lipases catalyses the release the fatty acids from the outer 1- and 3-positions glycerides specifically. 1, 2(2, 3)-diglycerides and 2-monoglycerides are chemical unstable and undergo acyl migration to give 1, 3-diglycerides and 1(3)-monoglycerides, respectively. Examples of the lipases are generated from *Aspergillus niger* and *Rhizopus arrhizus* species.

C. *Fatty acid specific lipase:* The lipases catalyses the specific release of a particular type of fatty acid from glycerides. Most extracellular microbial lipases show little fatty acid specificity.

(i) Nonspecific lipase:

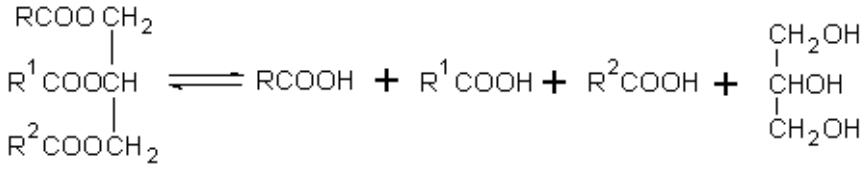

(ii) 1, 3-specific lipase:

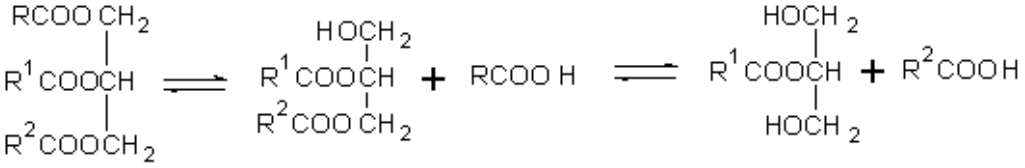

(iii) Fatty acid specific lipase:

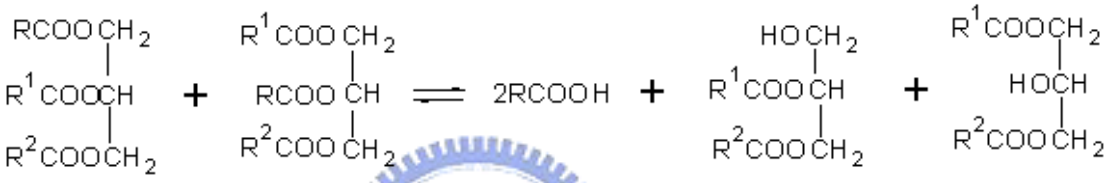

Figure 2-2 Products formed by lipase-catalyzed hydrolysis of triglycerides. [31] [32]

Above-mentioned, we choice the *Candida rugosa lipase* as the biocatalysis enzyme because the non-specific lipase and the commercial availability in large quantities at a relatively low cost. Lipases can catalyze the hydrolysis and synthesis of esters at lipid/water interfaces, a phenomenon known as interfacial activation, which involves the displacement of a surface structure named the lid. [23] Lipases show a 'lid' controlling access to the active site which is yellow part in figure 2-3. The lipase three-dimensional structures were the first revealed by X-ray crystallography in 1990. [33] And the interfacial activation might be due to the presence of an amphiphilic peptidic loop covering the active site of the enzyme in solution, just like a lid or flap.

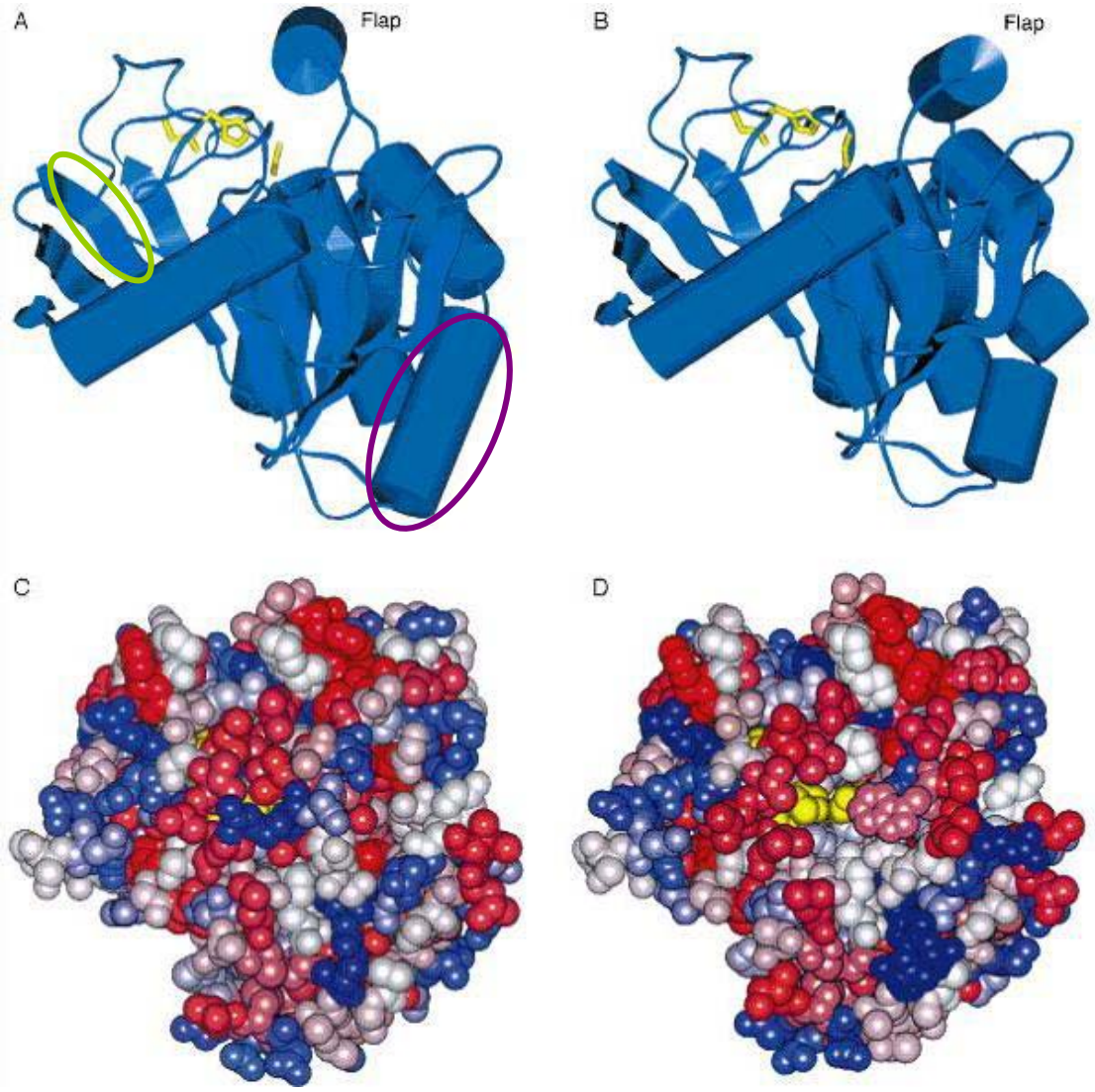

Figure 2-3 Structure of lipase in closed conformation (A, C) and open conformation form (B, D). The purple one stands for and β strands and the green one is α helices. Upon opening of the lid, the catalytic triad (yellow) becomes accessible (D), and the region binding to the interphase becomes significantly more apolar. [33]

The lipases, whose structure has been constructed by members of the α/β-hydrolase fold family with a common architecture, compose of a specific sequence of α-helices and β-strands.[33] A lid is amphlpathic structure, and lipase used as catalysts in aqueous as well as water media. Interface-activated lipases occur in alternative conformation states with different activity: in the close conformation, the

hydrophilic side faces the solvent, whereas the hydrophobic one is directed towards the protein core. The lid covers the enzyme active site, making it inaccessible to the substrate molecules. On the other hand, in open conformation the hydrophobic side faces the solvent, and the enzyme active site becomes exposed to the substrate-binding region.[31][33] Therefore, not only the amphipathic nature of the lid but also its specific amino acid sequence might be of importance for activity and specificity of lipases.

2.3 Texturisation of the Pyramidal Structure

There are lots of researches for random pyramidal texturing structures, due to decrease reflectivity of silicon solar cells and increase the short circuit current of the devices. [34] Anisotropic etching of silicon plays an important role for fabricating various three-dimensional structures such as thin membranes and silicon microbridges for solar cell systems and IC processing. [34][35] The most commonly and simple way is using chemical etching solutions, NaOH or KOH. However, these chemical solutions containing K+ or Na+ ions are toxic, pollutant and the passivation layers (SiO_2 or SiN) deposited on the surface of the cell are contaminated after texturisation. An alternative to texturisation is tetramethyl ammonium hydroxide (TMAH). It was found that TMAH is not pollutant, not toxic and its use leads also to good etching characteristics of a pyramidal structure. [34-36] Moreover, the etching rate and surface morphology can be controlled by the etching parameters, such as concentration of the solution, temperature and the addition of surfactant.

In this study, we investigate the etching process of silicon wafers with TMAH solutions of varying concentration under different temperature and surfactant conditions. This experiment with texturing the silicon substrates can generate the

pyramidal structures which provide that aims of increasing the surface areas and decreasing reflectivity. The appearance of increasing surface areas has better perform of the immobilization lipase on the surface compared to the substrate without pyramidal structures. When decreasing the reflectivity, it can convert light signal to electric signal more completely, which has the same characteristics with solar cell. [37]

2.4 Immobilization Technology

The technology of immobilization is using chemical or physical method to immobilized enzyme onto the support or substrate. Enzymes are often immobilized onto solid supports to increase their thermal and operational stability, and recoverability. [31] Immobilization of enzymes has generally been used to obtain reusable enzyme derivatives. This enables recycling of the biocatalyst and hence lowers the cost. The most important part of biosensor is the immobilization of a desired enzyme. Furthermore, the usefulness of immobilized enzyme depends on factors such as the immobilization method, the chemical and physical conditions (pH, temperature and contaminants), thickness and stability of the membrane used to couple the enzyme. [7]

Various methods available for enzyme immobilization of biosensor can be showed in figure 2-4: membrane entrapment, physical adsorption, matrix entrapment, and covalent bonding, the four general classes: [2]

A. Membrane entrapment is based on entrapment of a solution containing the biologically active material on the surface of the sensor using a semipermeable membrane. In the scheme, a semipermeable membrane separates the analyses and the bioelement, and the sensor is attached to the bioelement. Membrane must have pores that small enough to retain the biologically active material,

and be matched to the biosensor so that it does not affect the response of transducer.

B. Physical adsorption is based on a combination of van der Waals forces, hydrophobic forces, hydrogen bonds, and ionic forces to attach the biomaterial to the surface of the sensor. This simplest method of immobilization is exposed to the biological material on the surface directly. Because of the weakly bond in molecule the sensor performance might be affected in changing of temperature, pH value.

C. Porous entrapment is based on forming a porous encapsulation matrix around the biological material that helps in binding it to the sensor. And it is typically accomplished by formation of a gel containing biologically active material. This kind of method would not produce toxic by-products, and will increase the reactive areas by fixed biological components

D. Covalent bonding is treated as a reactive group to which the biological materials can bind. This method is using chemical adsorption much stronger, thus biosensor lifetime would be longer. And the biological active material is directly on the surface of the sensor, thus it can reduce response time. The surface treatment to immobilize biomolecules, ex: Self-assembly monolayer (SAM): functional groups for coupling with proteins, such as NH_2, COOH, SH, silane.[24]

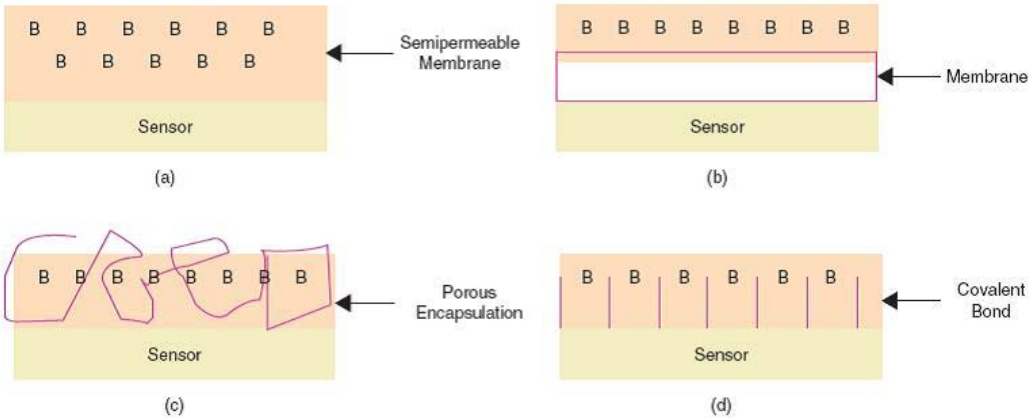

Figure 2-4 The bio and sensor element in biomaterial-sensor coupling can be divided into four general classes (a) membrane entrapment, (b) physical adsorption, (c) matrix entrapment, and (d) covalent bonding. [2]

As mentioned above, there are several methods for immobilization of enzymes. Some of these ways might have disadvantages and change the performance of enzyme .For example, the physical adsorption method is prone to leaching and shows instability whereas the covalent linking results in reduced activity of the biomolecule.[7] However, according to the researches ninety percent of the soluble enzyme was immobilized, and the immobilized enzyme was substantially more stable than the free enzyme.[38] The free enzyme lost its activity rapidly, and we could retains enzyme activity by immobilization technology method. In this experiment, we immobilized the enzyme onto the substrates by chemical methods, which covalent bonds are formed with the lipase. Protocols for covalent enzyme immobilization often begin with a surface modification or activation step.

2.5 Microfluidic System

The microfluidic technology, which studies the motion of fluid and particles through the microchannels, is an emerging field that has given rise to a large number of scientific and technological developments over the last years. Microfluidics technology currently in development could have a revolutionary impact on the next generation of assays, particularly as lab-on-a-chip applications. [39] The history of microfluidics technology starts in the early 1950s, when an effort to dispense small amounts of liquids in the nano and subnanoliter ranges, which basically is today's ink-jet technology. Common methods of fabricating microfluidic devices and systems are including valves, mixers, and pumps, capable of controlling fluid flow by utilizing the physics of the microscale (μL) or nanoscale (nL). [40] Fluid flow at the microscale exhibits unique phenomena that can be leveraged to fabricate devices and components capable of performing functions useful for chemical reactions and biological operations.

In miniaturization size of experiment enable precise control of the decreasing fluid volumes and reduce consumption of reagents and improve of controlling over the mass and heat transfer.[5] Because of the large surface-to-volume ratio of small fluid flow, microscale reactions might occur much faster and be revolutionized in the fields of high-throughput synthesis and chemical production.

The materials of microfluidic devices have been fabricated in silicon, [41] glass [42] or quartz [43] because of the similar technology available in the microelectronics industry. However, for applications in the biochemistry field and polymeric materials are a desirable choice because of their lower cost, good possibility, and biocompatibility. [40] Table 2-3 lists the comparison of the materials of polymers and other substrates. [40-44] In this study, we would like to use the elastomer

polymer material, polydimethylsiloxane (PDMS), an inexpensive one but powerful material and it offers several advantages compared with silicon or glass.

Table 2-3 Compare the different materials of microfabrication. [40-44]

Matrerial	Polymer	Silicon	Glass	Quartz
Feature aspect ratio	>10:1	>10:1	2:1	>10:1
Minimum feature size	<1 μm	<1 μm	<1 μm	<1 μm
Bioassay compatibility	Fair to very good	fair	fair	fair
Optical detection	Good to excellent	Poor to fair	Good	excellent
Cost	Inexpensive	Inexpensive to expensive	Inexpensive	expensive

2.6 Quantitative Analysis

2.6-1 Ultraviolet-Visible Spectrophotometer

In optical detection, the ultraviolet-visible molecular absorption spectroscopy is based on the measurement of transmittance and absorbance. There is a linear relationship between concentration absorber (c) and absorbance (A) in figure 2-5, 2-6 and table 2-4. [45]

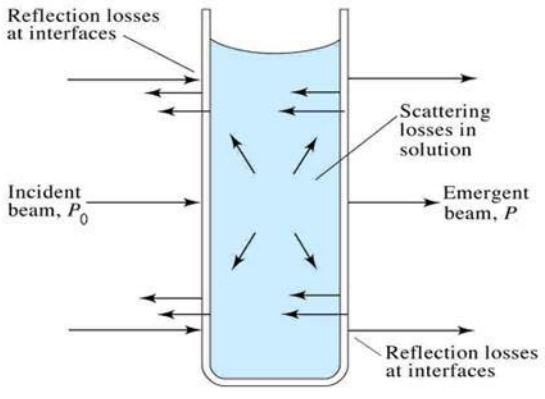

Figure 2-5 Reflection and scattering losses with a solution contained in a typical glass cell. In this example, the light passes through the air-glass, glass-solution, solution-glass, and glass-air interfaces. [45]

$$A = -\log T = \log (P_0 / P) = \varepsilon bc$$

Figure 2-6 The equation of Beer-Lambert low, [c] is linearly related to absorbance. [45]

The radiation of initial radiant power P_0 is attenuated to transmitted power P by a solution containing c moles per liter of absorbing solution with a path length of b centimeters

Table 2-4 Important terms and symbols for absorption measurements. [45]

Term and symbol	Definition	Alternative name and symbol
Incident radiant power, P_0	Radiant power in watts incident on sample	Incident intensity, I_0
Transmitted radiant power, P	Radiant power transmitted by sample	Transmitted intensity, I
Absorbance, A	$\text{Log}(P_0/P)$	Optical density, D ; extinction, E
Path length of sample, b	Length over which attenuation occurs	l, d
Concentration of absorber, c	concentration in specified units	
Molar absorptivity, ε	A/bc	Molar extinction coefficient

In this study, we use ultraviolet-visible spectrophotometer to analyze the protein quantitative method of lipase-immobilized. We also found that the reaction before and after transesterification would change its characteristics of the transmittance at the wavelength of 400 nm. According to this phenomenon, we can detect the transesterification reaction of optical responses with time.

2.6-2 Nuclear Magnetic Resonance Spectroscopy

Determining the structures of compounds is an important part for chemistry synthesis. Nuclear magnetic resonance (NMR) spectroscopy helps to identify the carbon-hydrogen framework of the compound. This instrumental technology not only identifies the functionality at a specific carbon but also determines what the neighboring carbons look like. Therefore, NMR can be used to determine the entire structure of a molecule.

The most important applications for the organic chemist are proton NMR (^{1}H-NMR) and carbon-^{13}NMR spectroscopy. NMR spectroscopy developments have coincided with leaps in technology, such as readily available dedicated computers for Fourier transformation, efficient spectrometer control, and stable high-field superconducting magnets. [46] In principle, NMR is applicable to any nucleus possessing spin. The electrons are changed, spinning particles with two allowed spin states of nuclei: +1/2 and -1/2. Spinning charged nuclei generates a magnetic field of a small bar magnet. In the absence of an applied magnetic field, the nuclei spin are randomly oriented. However, if the sample in an applied magnetic field, the nuclei twist and align in the larger magnet. [47]

In this experiment, we have discussed the compound of triglyceride (oil) and esters (biodiesel) with different groups of protons. Therefore, this difference in the spin dynamics inspired us to analyze the structure of these two compounds by ^{1}H-NMR spectroscopy.[27] Furthermore, we can estimate the yields in percentage for production of biodiesel by calculating the relative peak position and areas of the NMR spectra.

2.6-3 Photodetector

Photodetectors are devices used for detection of light and converted electric signal from optical radiation with the source of visible, infrared, or ultraviolet wavelength. The important issues of these detectors are its signal to noise ratio, spatial resolution, ability to operate through a range of high to low input light levels, and spectral response. They are often used in sensing objects or encoding data by a change in transmitted or reflected light. There are many types of photodetectors which may be appropriate in a particular case: [48]

A. Photodiode is a semiconductor device with p-n or p-i-n junction, where detects of light and generates a photocurrent. A particularly sensitive device is avalanche photodiodes, which can potentially provide higher gain bandwidth performance.

B. The metal-semiconductor-metal (MSM) photodetector is containing two Schottky barrier contacts of doped semiconductor material. The MSM device can be used as a photodetector by shining light on the top surface of the structure. When light impinges the electrodes of the semiconductor, it generates electric carriers, and is collected by the electric field and thus can form a photocurrent.

C. Phototransistor is similar to photodiode but relatively more complicated to fabricate and generally require sizeable chip area. However, it is attractive for detection applications since it can achieve high gain through transistor action.

In this experiment, we integrated the photodiode device, such as a solar cell, and microfluidic systems for real-time sensing the transesterification reaction by lipase-immobilized on the solar cell surface.

Chapter 3 Experimental

3.1 The Texturing Process by TMAH.

TMAH is not pollutant, non toxic and its use leads to a pyramidal structure. We can control the parameters by temperature, the concentration of the solution, and the addition of surfactant to grow the optimization pyramidal structure for our study. In many research, the Si surface with texturing morphology by TMAH is usually used to produce for solar cell and other optoelectronic devices. [36][37] In this work, we have analyzed the surface morphology and reflectivity after texturisation with TMAH in various experimental conditions.

In order to decrease reflectivity and increase the surface area of silicon substrate, anisotropic etching of silicon is a major way to form the three-dimensional pyramidal structures. All etching experiments are carried out by the single-crystalline [100] p-type silicon. In this experiment, the texturing process is used with TMAH solution due to the good etching characteristics and low contamination that has been mentioned before. The etching rate depends on the composition, temperature and silicon surface properties. Therefore, the optimized setup of etching conditions with respect to solution concentration and environment effect is needed to consider. We investigated the etching process of silicon wafers with different concentration of TMAH solutions and varying temperature. Before the etching process, the wafers are immersed in buffered oxide etch (BOE) to remove any oxide present. We discuss here an analysis method of the surface morphology based on the scanning electron microscope (SEM) and atomic force microscope (AFM). To determine the temperature influence, experiments are carried out at temperatures ranging from 60 °C to 80 °C in the water batch and agitation at 100 rpm. The SEM and AFM morphology in 2.38 % TMAH solution at 60 °C, 70 °C and 80 °C are shown in figure 3-1, 3-2 and

3-3, respectively.

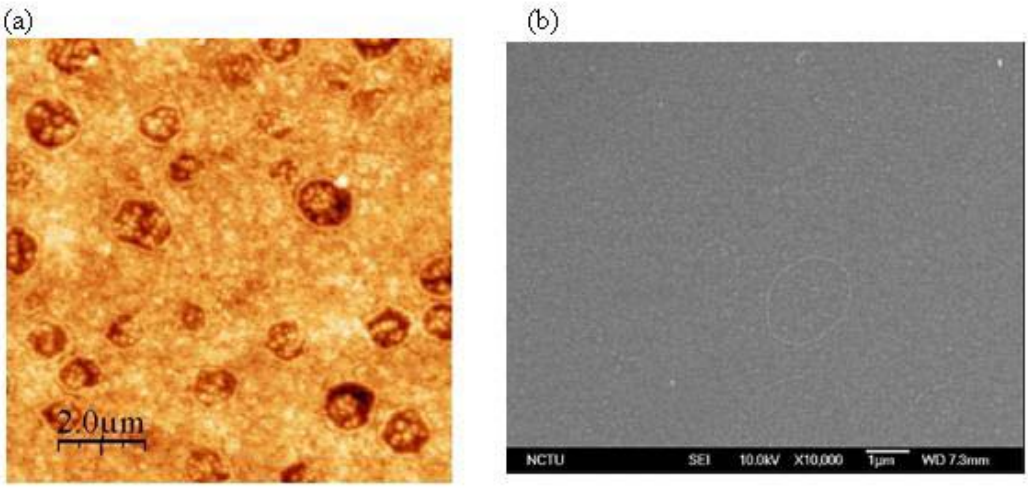

Figure 3-1 Anisotropic etching of silicon with 2.38 % TMAH solution. (a) shows AFM morphology in area is 10 μm × 10 μm, and (b) shows the SEM morphology at 60 ℃ 60 min.

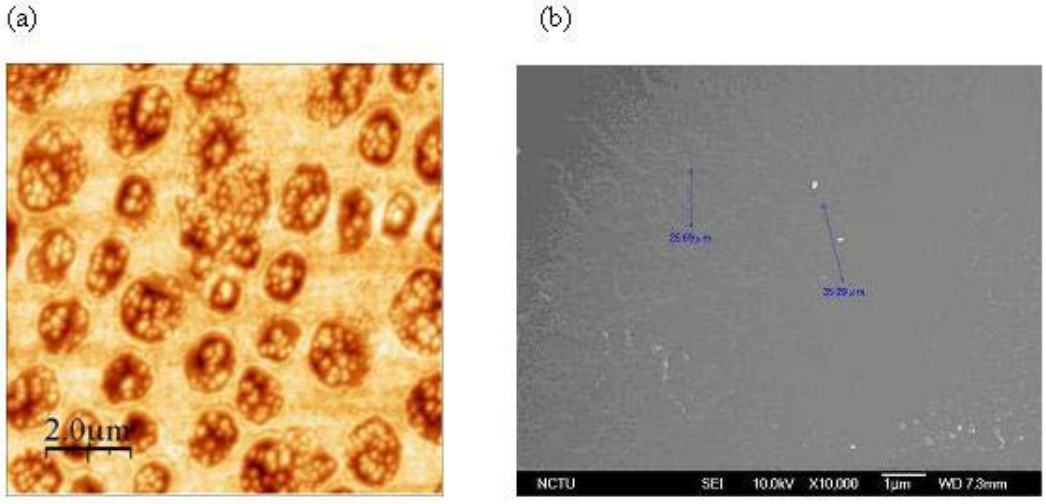

Figure 3-2 Anisotropic etching of silicon with 2.38% TMAH solution. (a) shows AFM morphology in area is 10 μm × 10 μm, and (b) shows the SEM morphology at 70 ℃ 60 min.

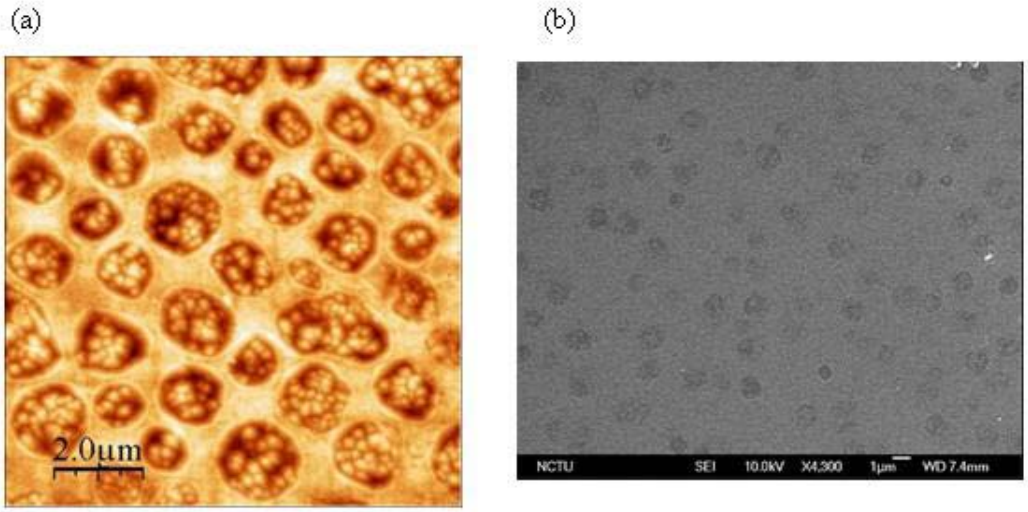

Figure 3-3 Anisotropic etching of silicon with 2.38 % TMAH solution. (a) shows AFM morphology in area is 10 μm × 10 μm, and (b) shows the SEM morphology at 80°C 60 min.

According to figure 3-1 to 3-3, we can see that there are many bubbles sticking on the surface, furthermore these bubbles affect the growing of pyramidal structure. When increasing the temperature, that has the tendency towards the more hydrogen bubbles onto the substrate. It has been known that the general texturing reaction could be described in figure 3-4. [49]

$$Si + 2H_2O + 2HO^- \rightarrow SiO_2(OH)_2^{2-} + 2H_2$$

Figure 3-4 The reaction of general texturing silicon surface. [49]

We can know from the reaction that the reaction will generate the hydrogen gas to form many bubbles, and this may cause the bubbles to stick on the silicon surface in the process of texturing. We find the enhancement using isopropyl alcohol (IPA) as a surfactant diminishing the adherence of hydrogen bubbles on the etched surface to

avoid the formation of big hydrogen bubbles, and IPA lift the bubbles away by the evaporation with increasing temperature during etching process. [36]

Here we prepare TMAH solution and IPA for avoiding the formation of big hydrogen bubbles on the surface of silicon. Figure 3-5 to 3-7 show the morphology of AFM and SEM of 1.67 % TMAH solution and 30 % IPA at 60 ℃, 70 ℃, and 80 ℃, respectively.

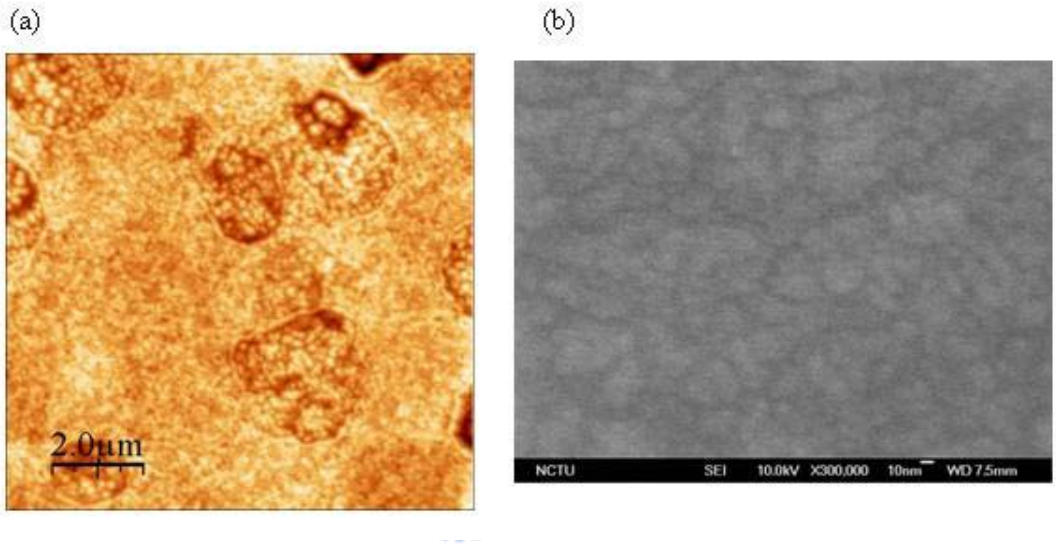

Figure 3-5 Anisotropic etching of silicon with 1.67 % TMAH solution and 30 % IPA. (a) shows AFM morphology in area is 10 μm × 10 μm, and (b) shows the SEM morphology at 60 ℃ 60 min.

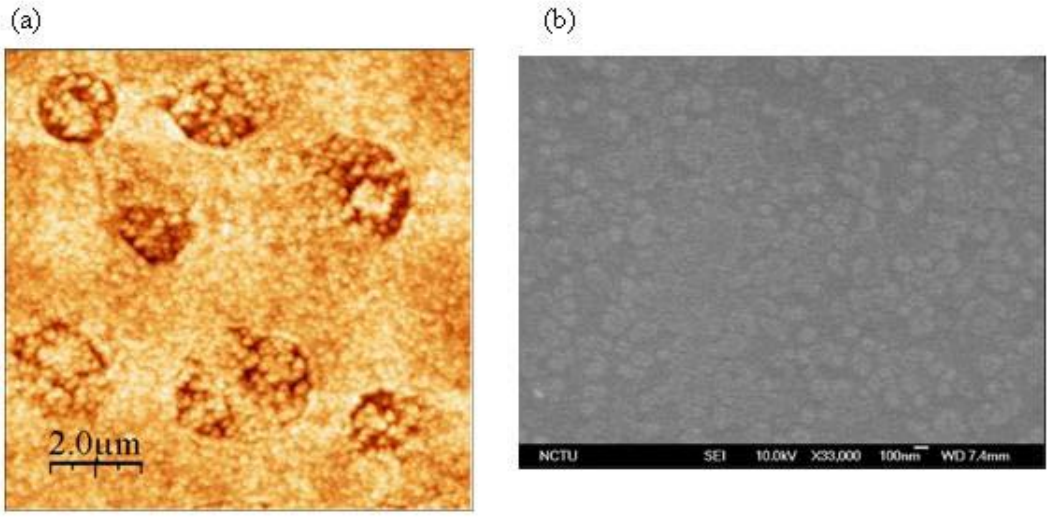

Figure 3-6 Anisotropic etching of silicon with 1.67 % TMAH solution and 30 % IPA. (a) shows AFM morphology in area is 10 μm × 10 μm, and (b) shows the SEM morphology at 70 ℃ 60 min.

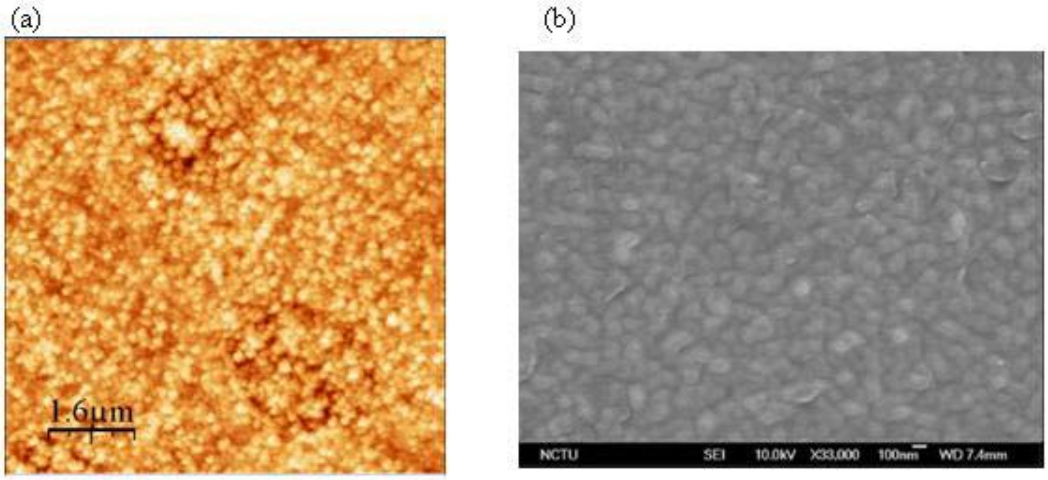

Figure 3-7 Anisotropic etching of silicon with 1.67 % TMAH solution and 30 % IPA. (a) shows AFM morphology in area is 10 μm × 10 μm, and (b) shows the SEM morphology at 80 ℃ 60 min.

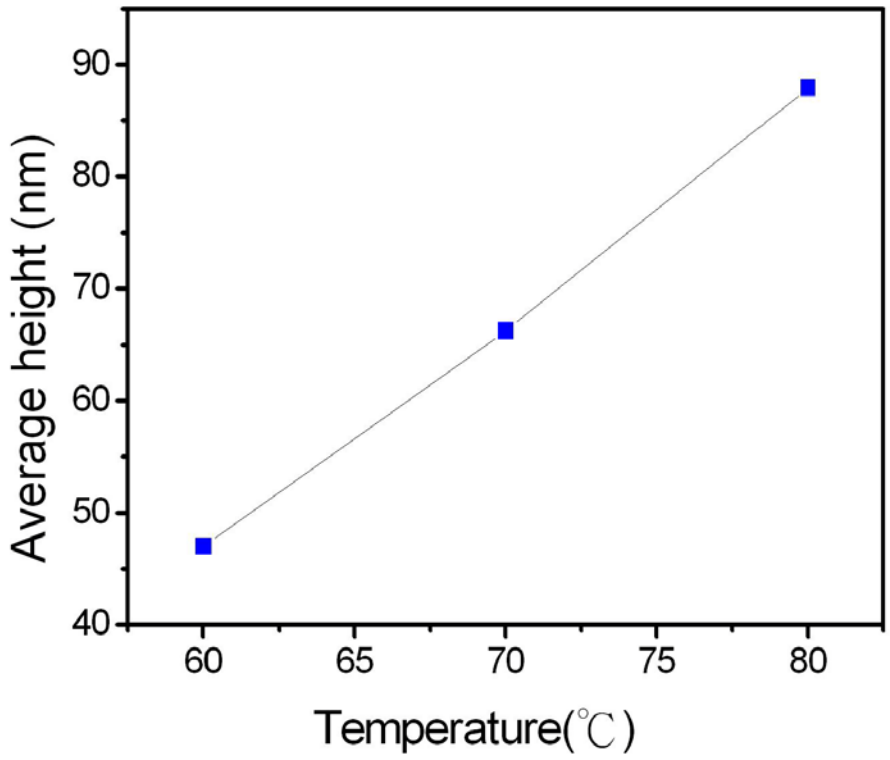

Figure 3-8 The relationship shows the average height of etching silicon as a function of temperature.

From the figure 3-5 to 3-7, we can determine the temperature influence, in figure 3-8, on increasing temperature, the etch rate of the (100) and (110) crystallographic planes increased faster than the each rate of the (111) crystallographic plane. When temperature increases, this difference of etch rate results in higher pyramids. [36]

According to figure 3-5 to 3-7, the adding of IPA can diminish the adherence of hydrogen bubbles to the etched surface. However, there are still few bubbles sticking on the surface, and not completely forming the pyramidal structure during etching process. Here we prepare the varying concentrations of TMAH with the addition of IPA at 80 °C which has higher etching rate in figure 3-8. In order to make the hydrogen bubbles not sticking to the silicon surface, and form the pyramidal structure, we put the silicon wafer in vertical direction rather than in horizontal direction.

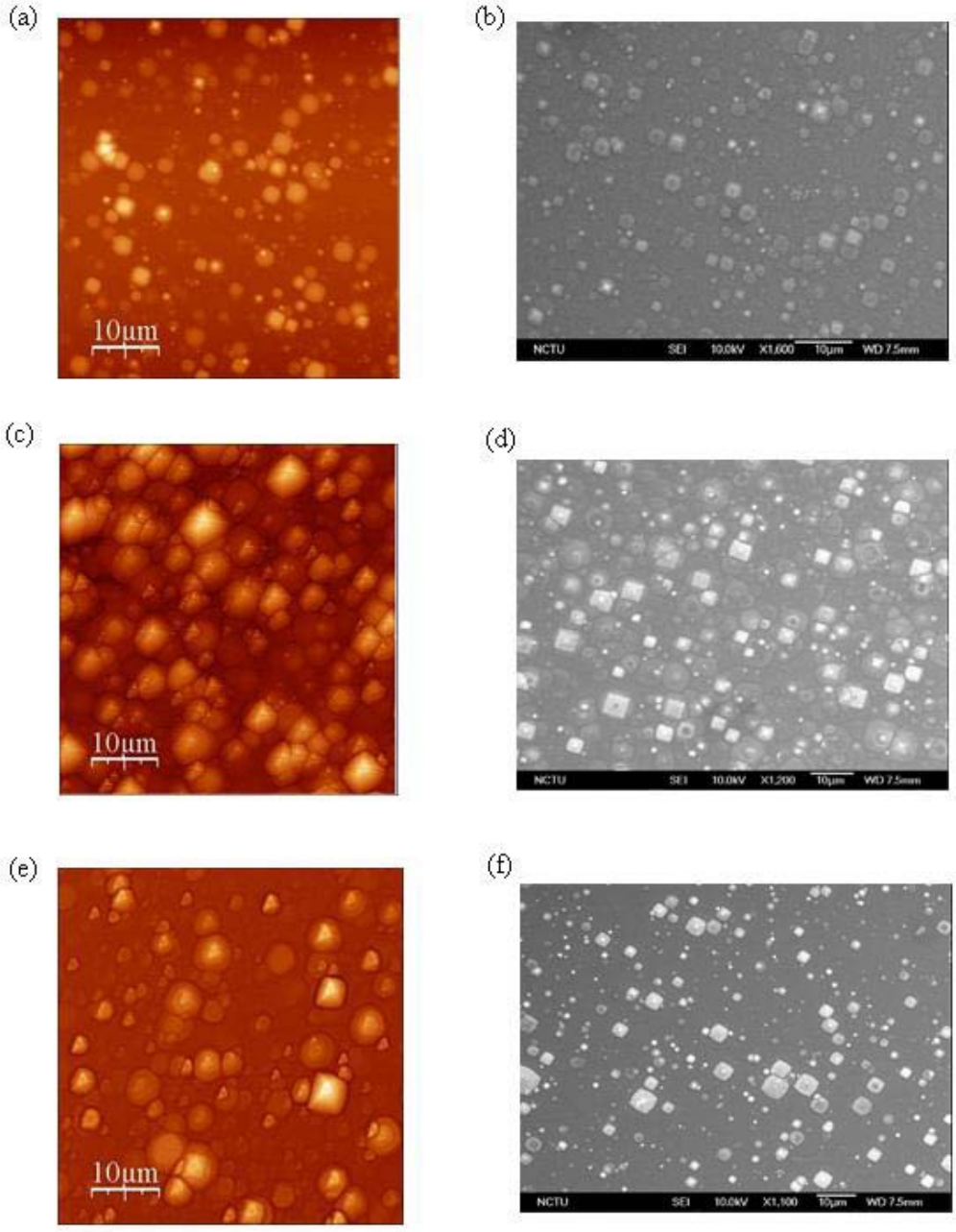

Figure 3-9 The morphology of AFM and SEM with different concentration of TMAH and IPA at 80 °C. 60 min. (a) and (b) are using 1.67 % TMAH solution and 30 % IPA solution. (c) and (d) are using 1.19 % TMAH solution and 50 % IPA solution. (e) and (f) are using 0.714 % TMAH solution and 70 % IPA solution.

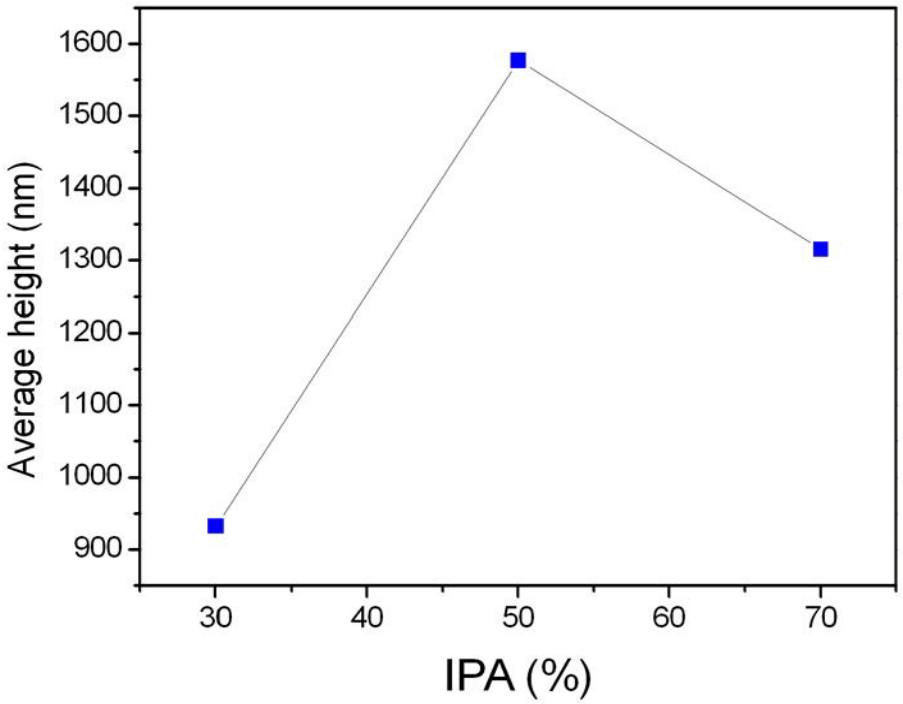

Figure 3-10 The etching height in different concentration of TMAH and IPA at 80 °C.

In figure 3-9 and 3-10 indicate that the solution content higher IPA can diminish the adherence of hydrogen bubbles completely on the etched surface and improve the growing of three-dimensional pyramidal structures. However, the solution with 0.714 % TMAH and 70 % IPA has lower average etching height and lower distribution of pyramidal structures. That reason may result from it lacks the ability to etch the silicon due to fewer TMAH concentrations. Figure 3-9 and 3-10 shows the uniform of growing pyramidal structures morphology and higher average etching height under the solution with 1.19 % TMAH and 50 % IPA.

In this experiment, we have optimized texturing solution contains 1.19 % of TMAH and 50 % of IPA under the temperature of 80 °C. The optimization process of growing the three-dimensional pyramidal structures is for decreasing reflectivity and increasing the surface area of silicon substrate. [36] The analysis method of N&K analyzer is discussed in chapter 4.

3.2 Enzyme Immobilization

The phenomenon associated with the immobilization of proteins on a solid surface is important in many fields of biotechnology and biosensors. The simplest way to link a biological molecule onto a surface is by physical adsorption, but this strategy is not adequate for analytical purposes because, in general, it produces a weak surface modification that can not resist to stirring and washing during the immobilization process. In order to prevent this kind of incompatibility and to link the molecule of interest to the substrate, basically in chemical modification of the enzyme with a linking structure is able to preferentially react with the substrate.

In this experiment, the process of lipases-immobilized on the solid substrates is attached by SAM with covalent bonding. The investigation of the lipases immobilization efficiency on SAM is an essential step to understand the neighboring chemical effect and the terminal groups contribution to the immobilization process, due to the fact that it provides an opportunity to explore the chemical environment with molecular.

First, we SAM of 3-mercaptopropionic acid (3-MPA) act as an anchor layer onto gold substrate through covalent bonding, because the thiol group(-SH) of 3-MPA is a strong bonding with gold surface conjugated S-Au leakage.[50] The terminal carboxylic acid groups of 3-MPA self-assembled are activated to the *N*-hydroxysuccinimide (NHS) ester, followed by reaction of this 3-MPA-NHS ester monolayer with the amino groups of lipases to create multiple amide bond linkages to the surface. This is accomplished by mixing the NHS with a carboxyl containing molecule and a carbodiimide coupling agent such as EDC, 1-ethyl-3-[3-(dimethylamino)propyl] carbodiimide. A "zero-length" cross-linking reagent, has been routinely used to form stable, covalent protein/protein complexes

through the formation of amide bonds between complementary amino and carboxyl groups. [10][51] As EDC reacts with the carboxyl group and forms an amine-reactive intermediate, an *O*-acylisourea. The intermediate is unstable in aqueous solutions and is therefore not useful in two-step conjugation procedures without stabilization of the intermediate using *N*-hydroxysuccinimide. [52]

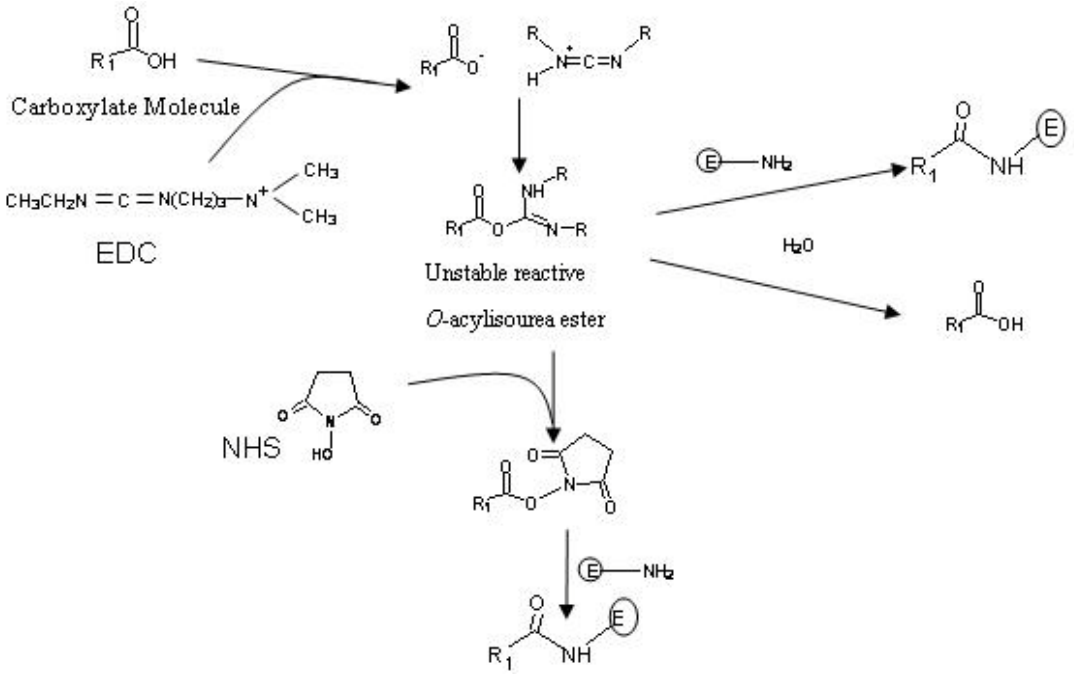

Figure 3-11 EDC reacts with a carboxyl group, forming an amine-reactive O-acylisourea intermediate. This intermediate may react with an amine group, yielding a conjugate of the molecule joined by an amide bond. [24] However, the intermediate is also susceptible to hydrolysis, making it unstable and short-lived in aqueous solution. The addition of NHS stabilizes the amine-reactive intermediate by converting it to an amine-reactive NHS ester, thus increasing the efficiency of EDC-mediated coupling reactions. [52]

As showed in the figure, the amine-reactive NHS ester intermediate has sufficient stability to permit two-step crosslinking procedures, which allows the carboxyl groups on the protein to remain unaltered. Following is the immobilization

procedure and the process showed in figure 3-12.

Step 1: First, the silicon wafer is cleaned by H_2SO_4: H_2O_2=3:1, twice, each time for 40-45 min. And 5 nm Cr and 10 nm Au are deposition onto the silicon substrate by thermal coater.

Step 2: A clean gold surface is immersed in 0.02M 3-MPA aqueous solution for 2hrs at room temperature, then rising with DI water to remove excess physically adsorbed compounds.

Step 3: EDC/NHS (2 mM EDC, 5 mM NHS) are added to the Au-modified surface for 20 min.

Step 4: Lipase is obtained from *Candida rugosa* type VII and diluted to a concentration of 0.75 % with doubly deionized water for 1 hr of immobilization.

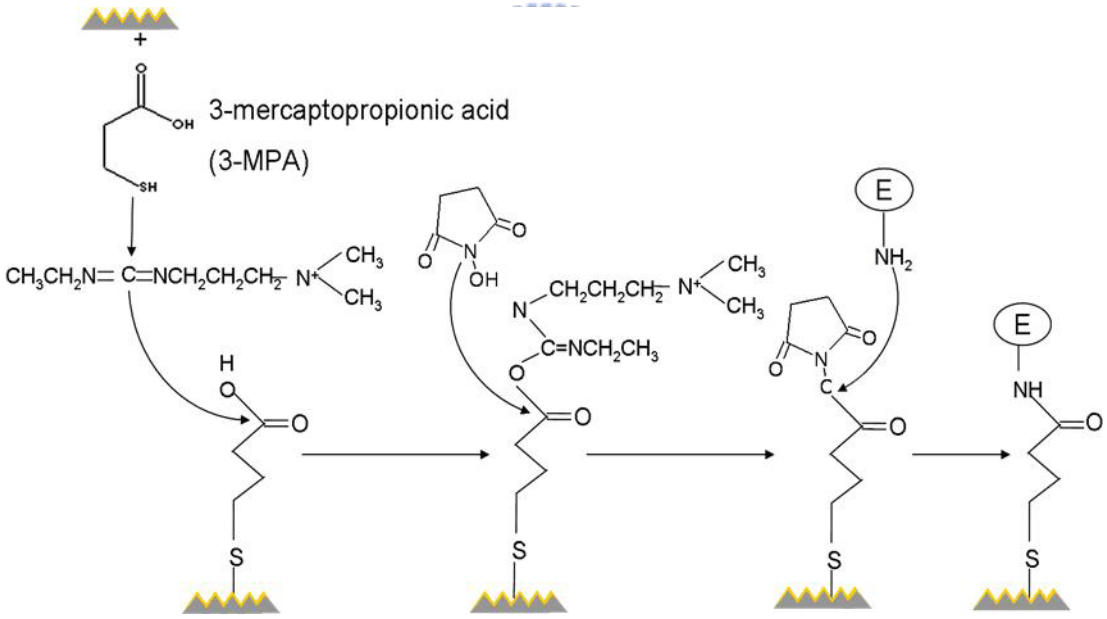

Figure 3-12 Reaction scheme for forming amide bonds with a self-assembled monolayer of 3-MPA onto the TMAH texturing surface with a gold thin film. In the first step, the MPA carboxylic acid groups are reacted with the carbodiimide, EDC, and then reacted with NHS to form the NHS ester. Subsequent reaction of this active intermediate with an aqueous solution of amino groups (NH_2) results in the attachment of lipases to the surface by SAM.

3.3 The Characterization of the Lipase-Immobilized

3.3-1 Bradford Quantitative Analysis

The Bradford assay is a protein determination method, a simple and accurate procedure for determining concentration of solubilized protein. The assay method based on Bradford is available from Bio-Rad, a dye-binding which can react to protein solution, and color change in response to various concentrations of protein. Therefore, we can measure the change of color with an UV-Vis spectrophotometer or microplate reader. The blue dye can bind to primarily basic and aromatic amino acid residues. When the dye binds to protein, it is converted to a stable unprotonated blue form that is detected at 595 nm in the assay using an UV-Vis spectrophotometer. [53] Spector [54] found that the extinction coefficient of a dye-albumin complex solution was constant over a 10-fold concentration range. Therefore, the Beer's law may be applied for accurate quantization of protein by selecting an appropriate ratio of dye volume to sample concentration.

Every protein-chemical reagent combination has not been assayed completely, and there is possible some interferences of the reagents by interactions the dye with certain proteins. However, there are chemical reagents not directly affecting the development of dye color, such as bovine serum albumin (BSA) and gamma globulin, show little or no interference. The standard procedure is using different concentration of dilution protein standards, and combining the dye-protein to show the typical standard curve of the Bio-Rad protein assay with BSA. Then, we can compare the unknown protein sample to the standard curve and provide a relative measurement of protein concentration.

Following are the standard procedure for standard curve of the Bio-Rad protein assay with BSA.

Step 1: Prepare the 0.1 ml of six BSA protein standard dilutions. The protein standard concentration is 6.25 μg/ml, 12.5 μg/ml, 25 μg/ml, 50 μg/ml, 100 μg/ml and 200 μg/ml respectively.

Step 2: Add 4ml diluted Bio-Rad dye reagent (Bio-Rad: RO water =1:4) and vortex 10 seconds.

Step 3: Incubate the standard at room temperature for 5 minutes.

Step 4: Measure the absorbance at 595 nm with UV-Vis spectrophotometer.

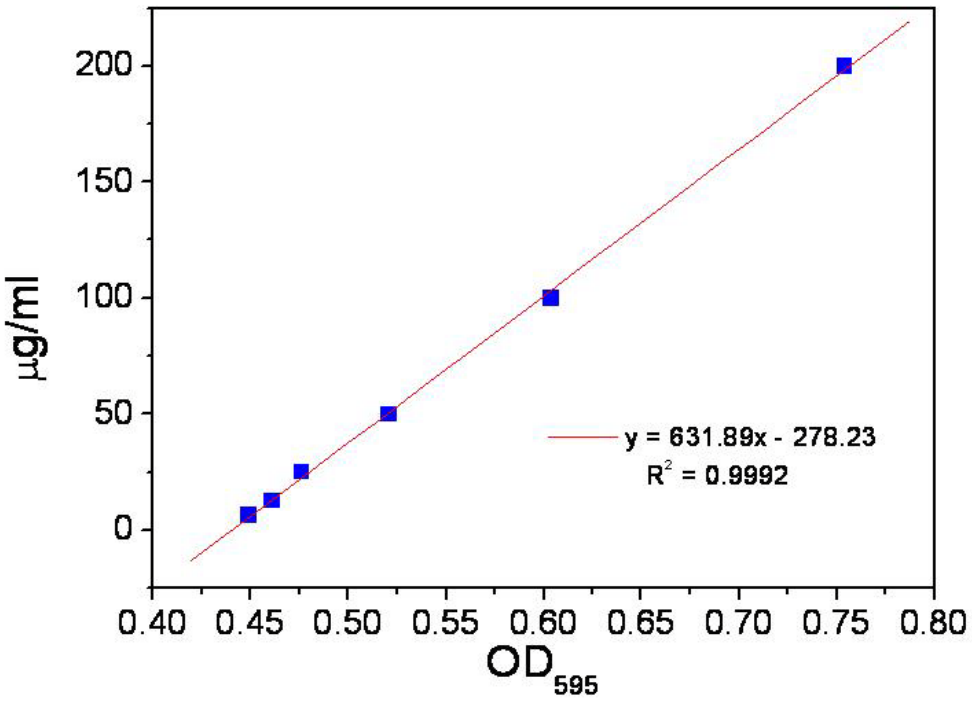

Figure 3-13 The typical standard curve of the Bio-Rad protein assay with BSA.

3.3-2 Measurement of Lipase Activity

The enzymatic activity of lipase can be measured by nitrophenyl derivatives. Many enzymatic activities, involving glycosidase and phosphates, are carried out with h or *p*-) nitrophenyl derivatives as substrates. The (*o*- or

p-)nitrophenol relaesed by hydrolysis of these substrates contains a variable amount of the (*o*- or *p*-) nitrophenoxide anion which absorbs at a conveniently accessible wavelength (400–420 nm).[24][55][56] The proportion of the nitrophenoxide anion present in the amount of nitrophenol depends on two parameters: pH and temperature, and the enzymatic activity is be measured by monitoring the absorbance of the hydrolysis product of nitrophenyl derivatives with the UV–Vis spectrophotometer.

In this experiment, the lipase activity is measured by a colorimetric assay in which the cleavage of p-nitrophenyl palmitate (p-NPP), and a yellow water-soluble product, p-nitrophenolate (p-NP), is formed by the hydrolysis of pNPP. And the reaction shows in figure 3-14.

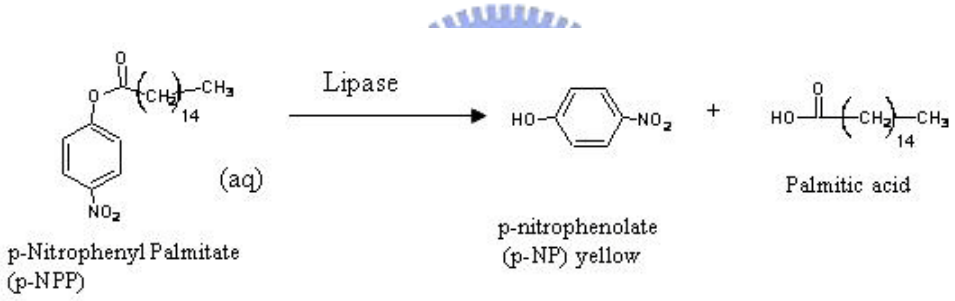

Figure 3-14 The hydrolysis reaction of pNPP on the catalyst activity of lipase.

The activities quantification method allows determination the influence of chemicals on enzymatic activities. The lipase is incubated for a while, and then the substrate (p-NPP) is added to this medium to quantify the activity of lipase. One unit of lipase activity was defined as 1.0 μmole of p-NP released/min. If the enzyme still possesses activity, the concentration of p-NP gradually raises and the absorbance wavelength also gradually increases. The influence of catalytic activities is be noticed a change in the reaction mixture after addition of sodium carbonate or sodium hydroxide to stop the reaction. In order to understand the chemical behavior, and

identify the products responsible for the p-NPP reactions which is initiated by these catalytic activities of lipases. [24][57-58]

Determination of lipase activity under severe conditions, extremes of pH and temperature, are needed to be considered. Besides that, the concentration conditions of lipase also need to carry out. This part will be discussed in chapter 4.

Following are the procedure for p-NPP hydrolysis reaction of catalysis by lipase.

Step 1: Prepare the 0.5 % p-NPP in IPA solution under 37 ℃ until the completely dissolve.

Step 2: Prepare the 0.1 ml free lipase and 1ml buffer for control group, in contrast the 0.1 ml immobilized lipase and 1ml buffer for experiment group.

Step 3: Add the p-NPP solution to the control group and experiment group for 5 minutes of the hydrolysis reaction in an optimistic temperature.

Step 4: Each 0.1 ml solution of step 3 is sampled and added to 2 ml 0.5 N Na_2CO_3 in 30 °C water-bath to stop the reaction.

Step 5: The assays are carried out for a fixed time and then absorbance reading at 410 nm is recorded at room temperature by UV-Vis spectrophotometer.

3.4 Specific Activity and Relative Specific Activity

Specific activity is used in measuring of enzyme activity in each milligram of protein. This is defined as the amount of substrate the enzyme catalyzed per mg protein in the enzyme preparation, per unit of time. Therefore, the lipase activity is expressed as U/(min×mg).[59] In this experiment, one unit (U) of enzyme activity was defined as the amount of enzyme which catalyzedthe production of 1 umol p-NP per minute under the experimental conditions. [24][57-58]

In biochemistry, the absorbance measurement of a sample by spectrophotometry can be used in measurements of enzyme activities, determinations of protein

concentration, enzymatic kinetic constants, measurements, protein characterization during isolation and purification, and any number of other important biochemical methods. The absorbance of a sample is directly proportional to concentration and cell thickness. It is based on the Beer-Lambert equation. A molar extinction coefficient for p-nitrophenol under this assay is 15,000 $M^{-1}cm^{-1}$.[24] Percentage of relative specific activity (RSA) is calculated as the ratio of specific activity of free or immobilized enzyme to the specific activity at the optimum conditions shown in following equation which is describing the relationship between the ratio of specific activity of free and immobilized enzyme.

$$\text{Relative specific activity (\%)} = \frac{\text{Specific activity of immobilized enzyme}}{\text{Specific activity of free enzyme}} \times 100$$

3.5 Triglyceride Synthesis by Lipase-Catalyzed

In this study, the enzymatic process for biodiesel production using a *Candida rugosa lipase* of immobilized on the substrate which is been textured. The triglyceride synthesis of transesterification in this experiment is for production of biosiesel. Biodiesel has been widely studied using many different types of vegetable oils such as soybean, rapeseed, sunflower and peanut oils.[30] These alternative energy resources of vegetable oils are one of the renewable fuels and environment-friendly. The vegetable oil we used is peanut oil because of the lowest price and obvious transmission change after transeaterification reaction.

The biocatalysts of lipase we used for these studies are *Candida rugosa lipase* because of its superiority in catalyzing transesterification reaction and its commercial availability in large quantities at a relatively low cost. A catalyst is usually used to improve the reaction rate and yield. To complete a transesterification reaction, a 3:1

molar ratio of alcohol to triglycerides is needed shown in figure 2-1. Although the reaction is reversible, excess alcohol may be required to shift the equilibrium to the product side. [25] However, the lipases could be denatured by high molar equivalents of methanol to oil.[60] In this experiment, the transesterification reaction for the production of biodiesel fuel is performed from peanut oil and short-chain alcohol, methanol, using immobilized *Candida rugosa lipase* obtained with 3:1 molar ratio of methanol to peanut oil.

We investigate the transesterification reaction on the microfluidic platform and detect the new approach of analysis method. This part will be discussed in chapter 4.

3.6 Construction of a Microfulidic Reactor

3.6-1 PDMS Molding

In this section we will describe the process for polydimethylsiloxane (PDMS) molding. PDMS is the choice of material for optical transparency, elasticity, durability, flexibility and bio-compatibility for microfluidic reactor with biological sample. Besides that, PDMS can be reproduced with high fidelity on the micro scale by replica molding and the optically transparent down to 280nm so it can be used for detection schemes such as UV-Vis detector and fluorescence. [61] Because PDMS is elastomeric, it will conform to smooth and andrelease from delicate features of a mold without damaging itself.

Following are the process for PDMS molding.

Step1. The PDMS is polymerized by mixing 10:1 (w/w) ratio Sylgard 184 with curing agent and stirred thoroughly.

Step2. Put in the vacuum pump to degas PDMS mixture and then pour the PDMS mixture to mother mold (shown in Figure 3-15).

Step3. Cure PDMS in hotplate until PDMS is solidified, and the temperature is 110 ℃.

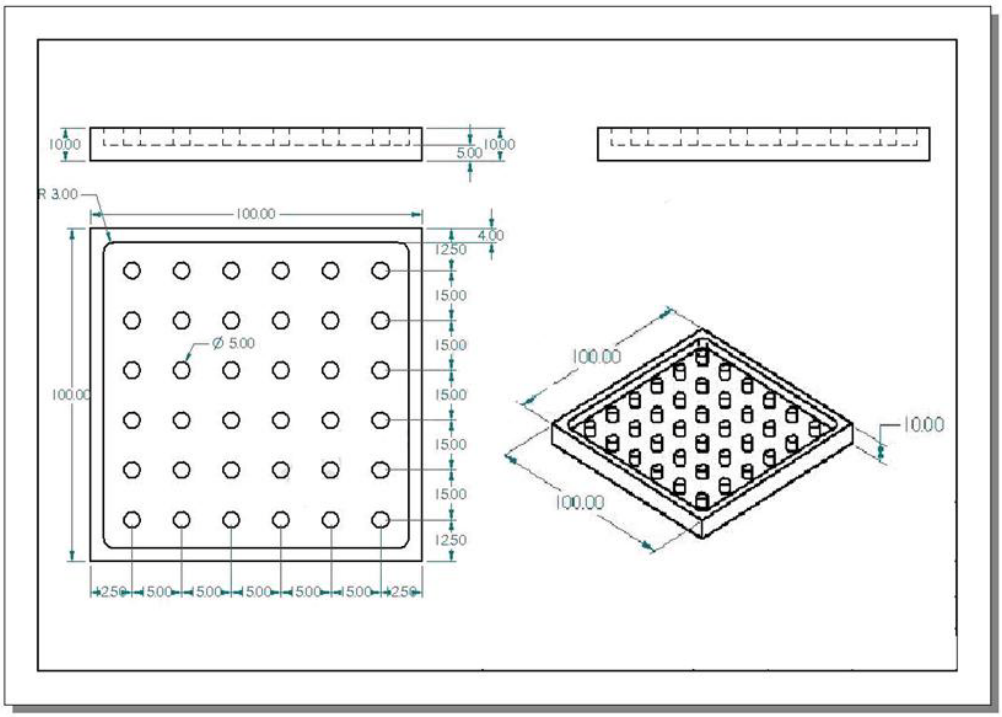

Figure 3-15 Illustration of PDMS mother mold.

The mold is made of aluminum, and the size is 10 cm by 10 cm square containing 36 cylinders. Each cylinder is 5 mm of the diameter and of 5 mm of the height. We can make lots of reaction chamber at the same time by replica molding. The reaction chamber is open-head in one side; therefore the volume of the chamber can be calculated. The volume of reactor chamber is 0.0981 cm^3.

After preparing the PDMS stamp, we imprint the needle shape to transfer a channel in the both sides of chamber under 220 ℃ temperature and 353.28 kg/m^2 pressure for 6 hours shown in figure 3-16.

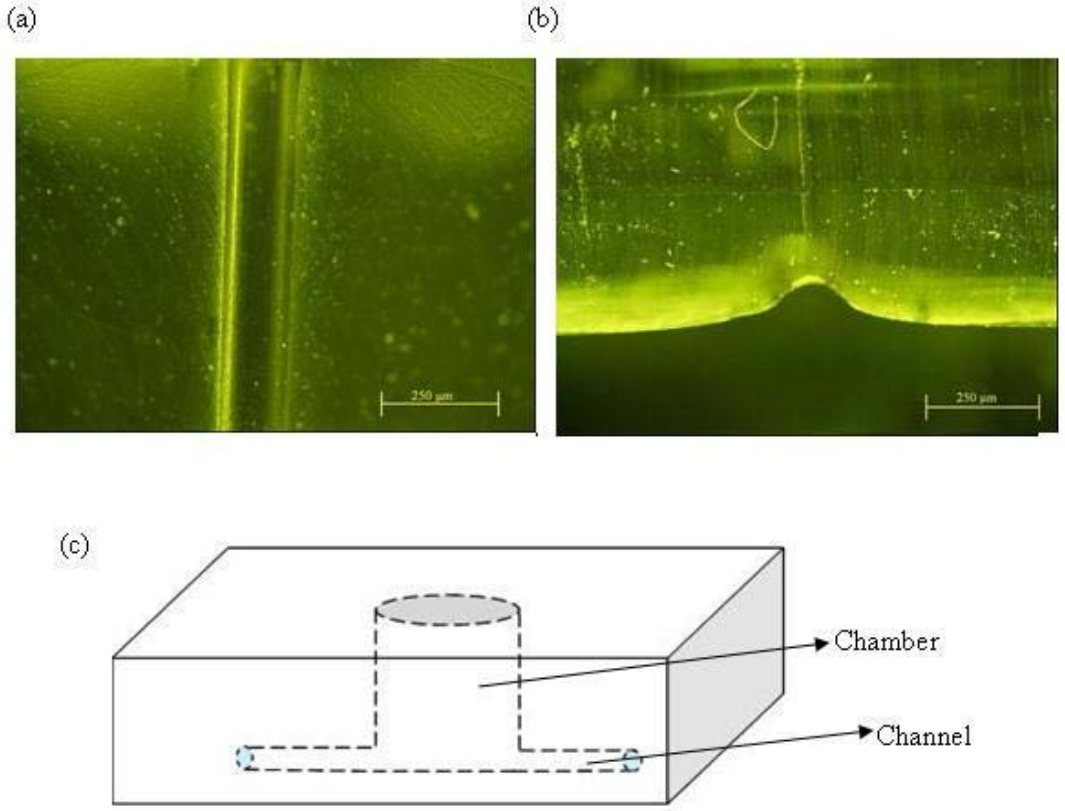

Figure 3-16 Example of the microreactor made of PDMS. (a) the top view of the channel by optic microscope, (b) the side view of the channel by optic microscope, and (c) the scheme of the PDMS chamber and microchannel.

3.6-2 Adhesion of PDMS Elastomer to Substrate

One of the most important issues is in the selection of appropriate materials for a device. PDMS belongs to group of siloxanes shown in figure 3-17. [62]

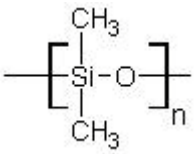

Figure 3-17 The chemical structure of PDMS.

Untreated PDMS presents hydrophobic surface, which makes the microchannels difficult to wet with aqueous solutions and easily generate bubbles. For some time it has been known that exposing PDMS to various energy sources can alter its surface properties. Energy sources such as oxygen plasmas have been the most popular way in PDMS chip making. The surface Si-CH_3 groups along the PDMS backbone are transformed into Si-OH groups by the reactive oxygen species in the plasma. Then condensation of silanols (Si-OH) with appropriate groups, such as OH, COOH on another surface leads to the formation of the Si-O-Si structure when the two layers contact together. [62] This is usual way of surface chemistry for PDMS and silicon substrate. For PDMS and glass, this condensation reaction yields Si-O-Si bonds after loss of water. However, in this experiment the reactant of transesterification reaction we used is oil and alcohol. Exposing PDMS to O_2 plasma can not bond well for adhesive PDMS with silicon and glass, even cause the overflowing.

As mentioned first, PDMS belongs to group of siloxanes and it has the similar group of materials which is called silicoketones or silicones. Furthermore, the adhesion behavior of PDMS elastomers in contact with substrates functionalized with a number of chemical groups that are capable of reactions with silicone elastomers. [63] We try to bond PDMS and substrate by silicone sealant for adhesion and this way would not overflow when pumping chemical reactant into PDMS reactor. However, the transparent silicone sealent becomes fold and less transparent when completely drying. This may result non-uniform binding between PDMS and substrate and affect the transparency of PDMS and the optical analysis.

An improved method with an adhesive layer can leave selectively coating a patterned substrate and a very thin layer of uniform adhesion. [64]

Step 1: Prepare the liquid PDMS by mixing 10:1 (w/w) ratio with curing agent.

Step 2: Place a thin film of liquid PDMS on the solidified PDMS stamp. Then,

put the stamp onto the substrate (silicon or glass).

Step 3: Placed them into an oven at 60 °C for 20-30 min to cure the PDMS prepolymer.

Because the liquid PDMS is elastic, it can flat well after PDMS and substrate are brought into contact. Therefore, the liquid PDMS can form uniform layer of adhesive and bond very strongly to avoid the overflowing shown in figure 3-18. This way is simple and fast for the bonding of the substrates to form enclosed microfluidic networks. Also this method retains the layer of their original material and can maintain their desired functions essentially unaffected by the adhesive.

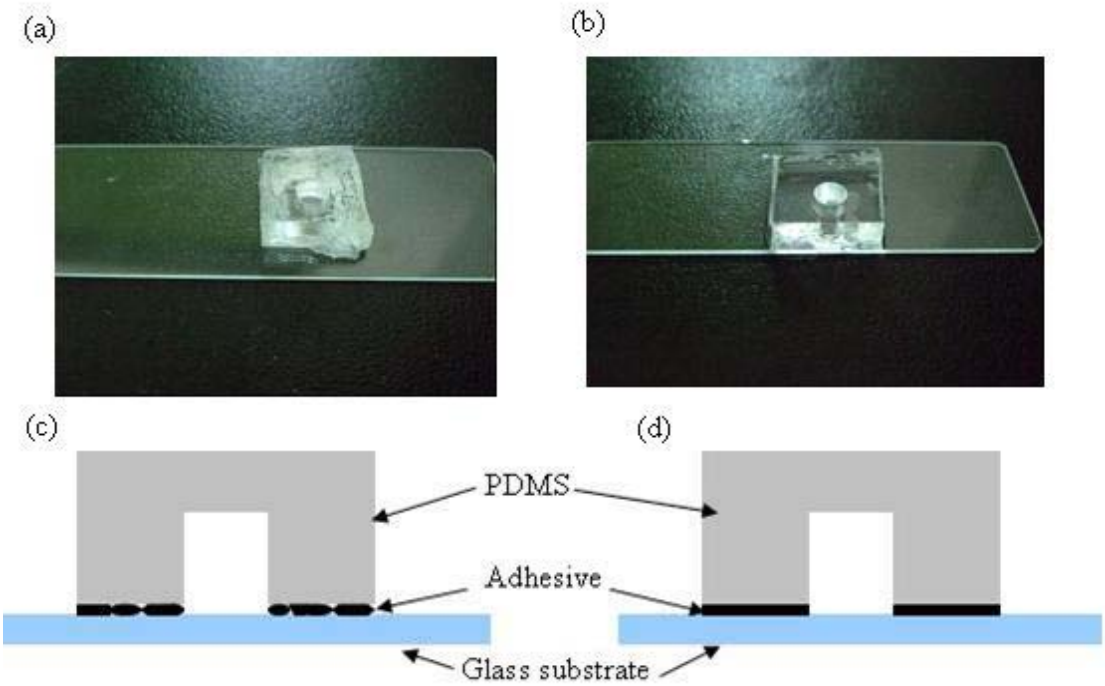

Figure 3-18 Schematic view of the adhesion between PDMS molding and glass substrate. (a) and (c) show it bonds the PDMS and glass by silicone sealant adhesive. (b) and (d) show an improved method that bonds the PDMS and glass by liquid PDMS adhesive. Here we use the glass as the substrate in order to observe the interface between PDMS and substrate clearly.

3.6-3 Fabrication and Integration of the Microfluidic Reactor

Some steps of fabrication procedure are discussed before. In this section, we would like to introduce the details of the whole fabrication process and then integration the microfluidic system.

Step 1: Prepare the PDMS molding. (This is discussed in 3.6-1)

Step 2: Screw through the PDMS stamp to make tunnels in both sides and vertically down the channel.

Step 3: Adhesion of PDMS stamp to the substrate.

Step 4: Put hollow needles through the vertically tunnels and then with Teflon tube. The needle is 0.6mm with outside diameter (O.D.) and Teflon tube is 0.56mm with I.D. and 1.16mm with O.D.

The fabrication process displays in the figure 3-19. This microfluidic platform provides a setup of fluidic operations, which are designed for easy combination within a well defined and low cost fabrication technology. The platform use minute volumes of samples and can allow saving of reagents and speeding up the analysis time. Due to tendency to use easily fabricate as well as low cost approaches, microfluidic reactor made of PDMS are more and more popular in various analytical devices. Additionally, the surface-to-sample-volume ratio becomes larger. Therefore, it increases the influence of material properties on the measurement.

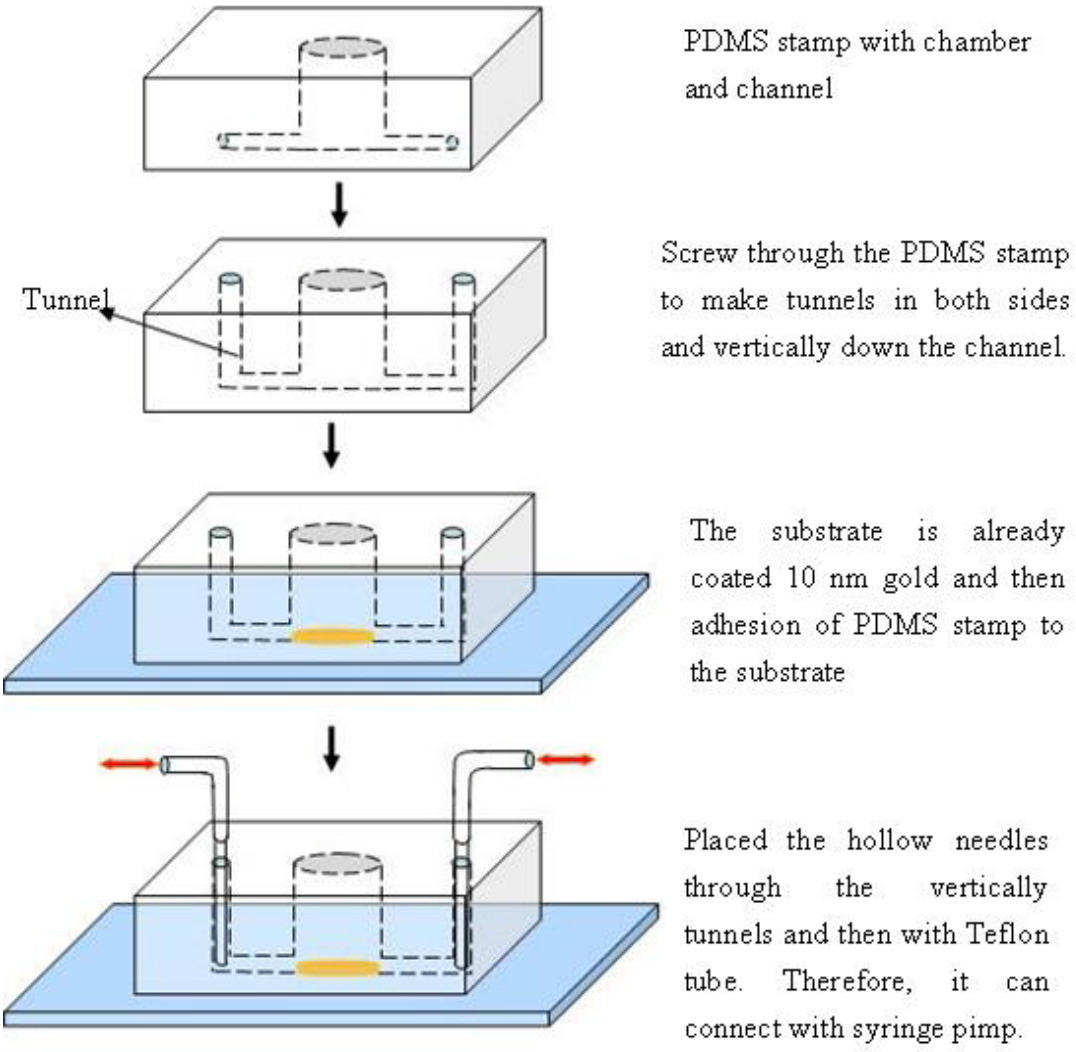

Figure 3-19 Schematic diagrams of fabrication and integrations in microfluidic reactor. The microfluidic system contains the microchannels and the reaction chambers.

The scheme of microfluidic system and syringe pump (Model 270 Series, KD Scientific Inc., Holliston, USA) is showed in figure 3-20. The volume of rector chamber is 0.0981 cm^3, and we set the parameters of syringe pump is 0.06 ml with cut-off volume and flow rate is 0.67 ml/min for fast and repeat pumping in order to mixing the reactant of oil and alcohol.

Figure 3-20 Schematic of the testing apparatus used for microfluidic system with syringe pump. (a) is microfluidic reactor with textured surface by TMAH, and (b) is textured surface of solar cell.

We investigate the lipase-immobilized on anisotropic texturing surface by of TMAH/IPA solution and detect the transesterification reaction in the microfluidic reactor platform for analysis. In the study, we find that there are some absorbance responses of UV-Vis spectroscopy by detecting the biocatalysis reaction. According to this phenomenon, the optical detection can be connected with the spectroscopic methods of NMR in order to more specific identify the structure of triglyceride and esters. The microfluidic reactor platform for the detection of UV/Vis-NMR system is shown in figure 3-20 (a). Under the same phenomenon of UV-Vis spectroscopy, the

optical response can be connected with the photoelectric devices or solar cell. Since random pyramidal texturing of silicon substrates allows increasing the short circuit current of the device, and it is usually achieved, in commercial solar cells. [34][36][37] The microfluidic reactor platform for the detection of UV/Vis-photodetector system is shown in figure 3-20 (b).

Chapter 4 Results and Discussion

4.1 Optimal Conditions of Anisotropic Texturisation

4.1-1 Surface Morphology of the Pyramidal Structure and Its Reflectivity Analysis

As mentioned in chapter 3-1, we have been determined the conditions of etching silicon wafer with 1.19 % of TMAH and 50 % of IPA solution under the temperature of 80 °C. The anisotropic texturisation are usually leading to pyramidal structures and the higher pyramids the more surface areas for lipase-immobilized. Therefore, we discuss the optimal texturing time for growing the optical pyramidal structures, reflectivity analysis by N&K analyzer and surface energy by contact angle. Figure 4-1 indicates the texturing time of 1.19 % of TMAH and 50 % of IPA solution at 80 °C and the silicon wafers are all carried out with vertically direction.

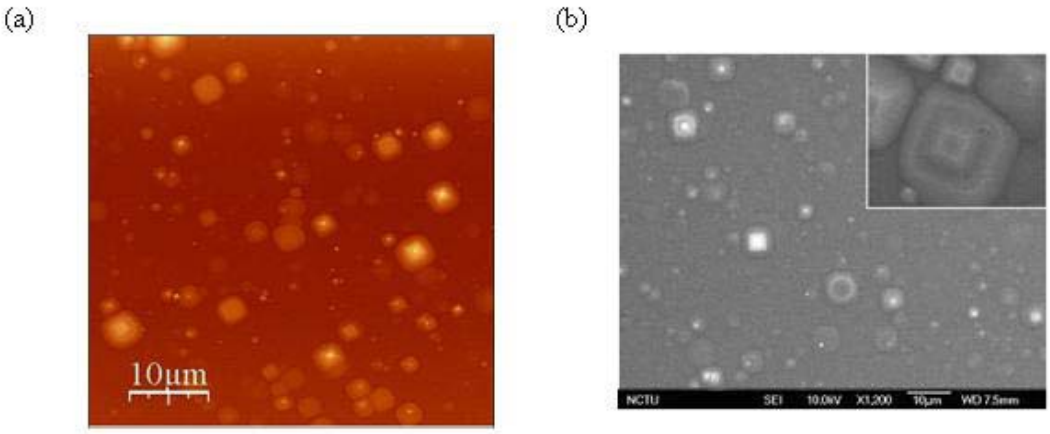

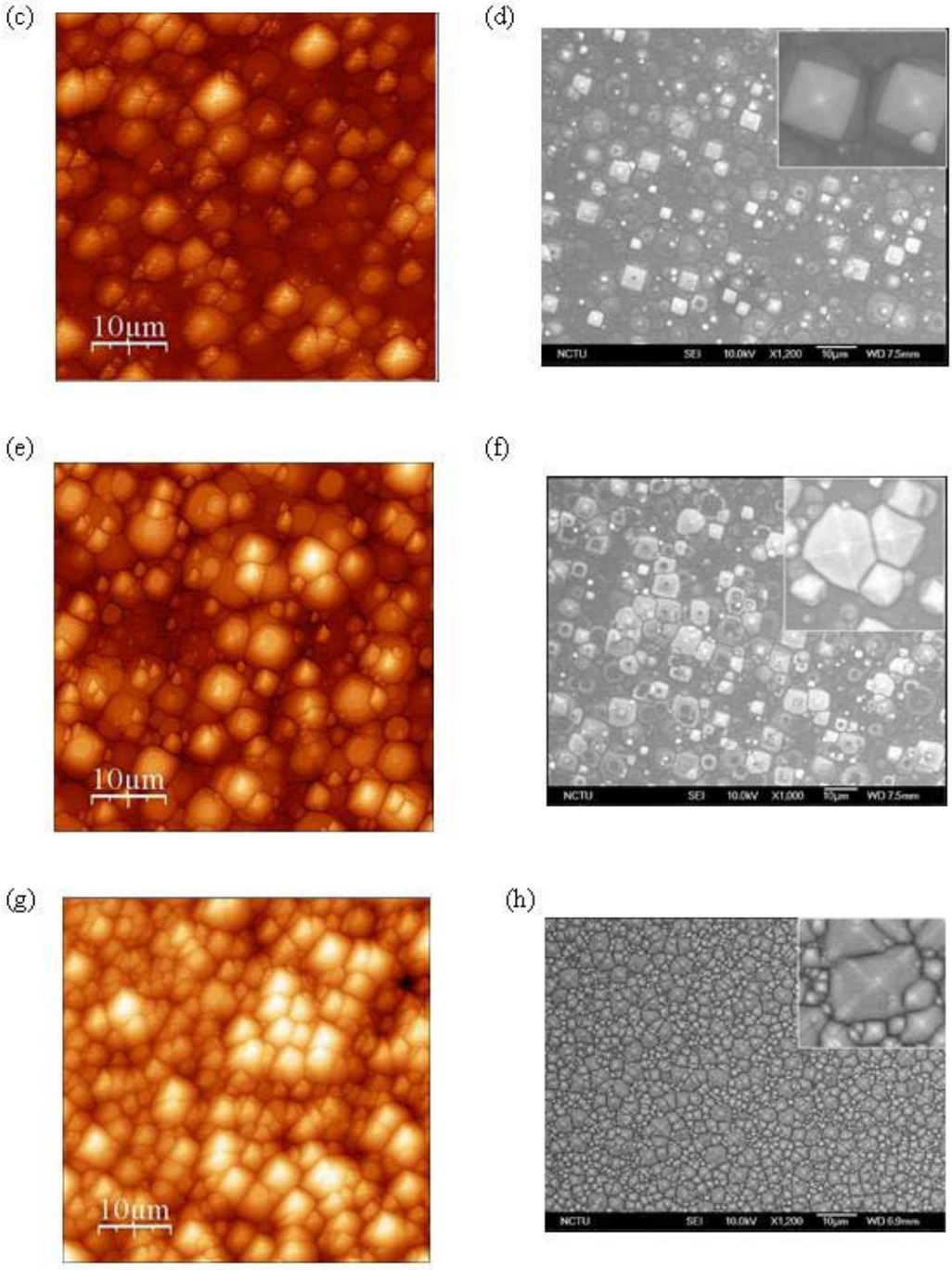

Figure 4-1 The AFM and SEM texturing morphology of 1.19 % of TMAH and 50 % of IPA solution at 80 °C with varying time. (a) and (b) are textured under 30 mim; (c) and (d) are under 60 min; (e) and (f) are under 90 min; (g) and (h) are 120 min.

According to the figure 4-1, the longer etching time has the higher density of pyramidal structures on the silicon wafer and the etch rate of the (100) and (110) crystallographic planes increased faster than the each rate of the (111) crystallographic plane. The morphology of pyramidal structures can be observed from the SEM. The different etching time grows the different average height of pyramidal structures shown in figure 4-2. With longer etching time leads to faster etching rates and grows the higher pyramidal structures.

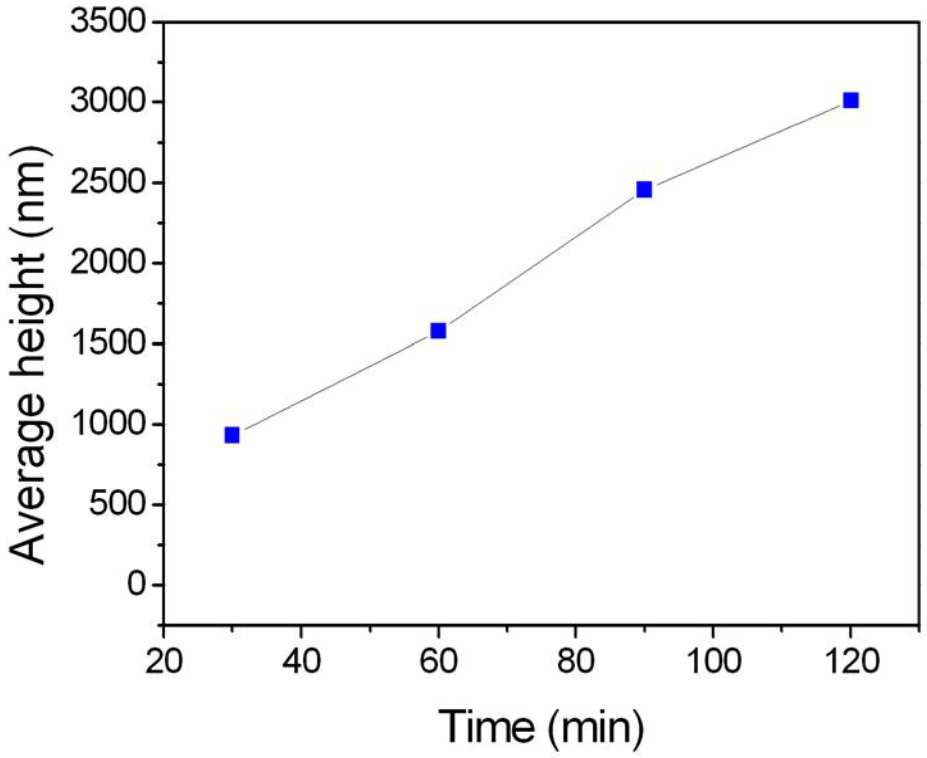

Figure 4-2 Average height of pyramidal structures with different time. The highest density and optimal pyramids is at 120 min, and the average height is 3.01 μm.

The mechanism of TMAH etching follows alkaline silicon etching and can be summarized into three separate steps: [49] [65] [66]

$$(CH_3)_4NOH \longrightarrow (CH_3)_4N^+ + OH^- \quad 2$$

$$Si + 2OH^- \longrightarrow Si(OH)_2^{2+} + 4e^- \quad 3$$

$$4H_2O + 4e^- \longrightarrow 4OH^- + 2H_2 \quad 4$$

$$Si(OH)_2^{2+} + 4\,OH^- \longrightarrow SiO_2(OH)_2^{2-} + 2H_2O \quad 5$$

The mechanism reactions taking place on the silicon surface. In a first step of equation 2, TMAH is reduced to form hydroxyl ions. In the second step (Eq. 3), the silicon atoms at surface react with these hydroxyl ions to form oxidized silicates $Si(OH)_2^{2+}$ and four electrons are injected from each silicon atom into the conduction band. Simultaneously, water is reduced to provide more hydroxyl ions which are bonded to the silicate formed in second step. The reaction of equation 4 and 5 produces soluble silicic acid, with hydrogen gas as a byproduct. As shown by the previous equations, it means the water will be present and the silicon will be etched. When the concentration of water increases, more hydrogen and therefore more bubbles are present. However, the bubbles will stick on the silicon surface and affect the etching rate discussed in chapter 3-1. They will block the diffusion of reactants and products from the surface of contact between the bubble and the silicon. The hydrogen is generated on the silicon surface and can form bubbles which can reduce a natural upward flow of reaction between the solution and silicon surface and causing some difficulties in etching rate. We add the IPA as surfactant to diminish the adherence of hydrogen bubbles on the etched surface. Therefore, roughness increases with etching time and progressively the etch rate in (100) and (110) directions because pyramids expose slowly etching crystal (111) planes.

With above methods, the texturization efficiency depends on the concentration, temperature and etching time of dissolved solution. It presents an alternative method

to create uniform and reproducible pyramidal texture on silicon wafer with help of surfactant isopropyl alcohol (IPA) and agitation. The roughness increases when TMAH concentration decreases since the amount of water and IPA present in the solution increases in same time and therefore produces less hydrogen. Initially the number of pyramids at the surface is small, but as etching continues, new pyramids are formed and begin to superimpose over previous hillocks where the number and the size of the pyramids are observed by SEM and the average height are observed by AFM.

With growing pyramidal structures, the difference of etching rate results in higher pyramids and leads to a lower reflectivity shown in figure 4-3. By textural effects, the surface scattering features and lower reflectance across all wavelengths in pyramidal structures. In figure 4-3 (b), the scheme expresses the light shines through the pyramidal structures. The higher pyramids leads to a lower reflectivity hence the light absorption is increased. This absorption can be further improved by an optimized texturisation. [36] In this experiment, the best condition of anisotropic texturisation is etching under 1.19 % TMAH and 50 % of IPA solution at 80 ^{0}C for 120 min. Since the lipase is immobilized on the substrate with a thin gold film, we can coat with 5 nm Cr and 10 nm Au on the optimal texturing silicon substrate. The reflectivity is relatively lower than non-treated sample shown in figure 4-4. The reflection of the front surface needs to be minimized and the incident light will shine into the hole aperture to increase the light collection and the high-efficiency of silicon solar cells. This improvement is currently achieved by a textured surface covered by coated a gold film onto the anisotropic texturisation substrate. [67] It shows a large decrease of the reflectance over the entire spectrum. This difference is explained by light trapping improvement for following detection.

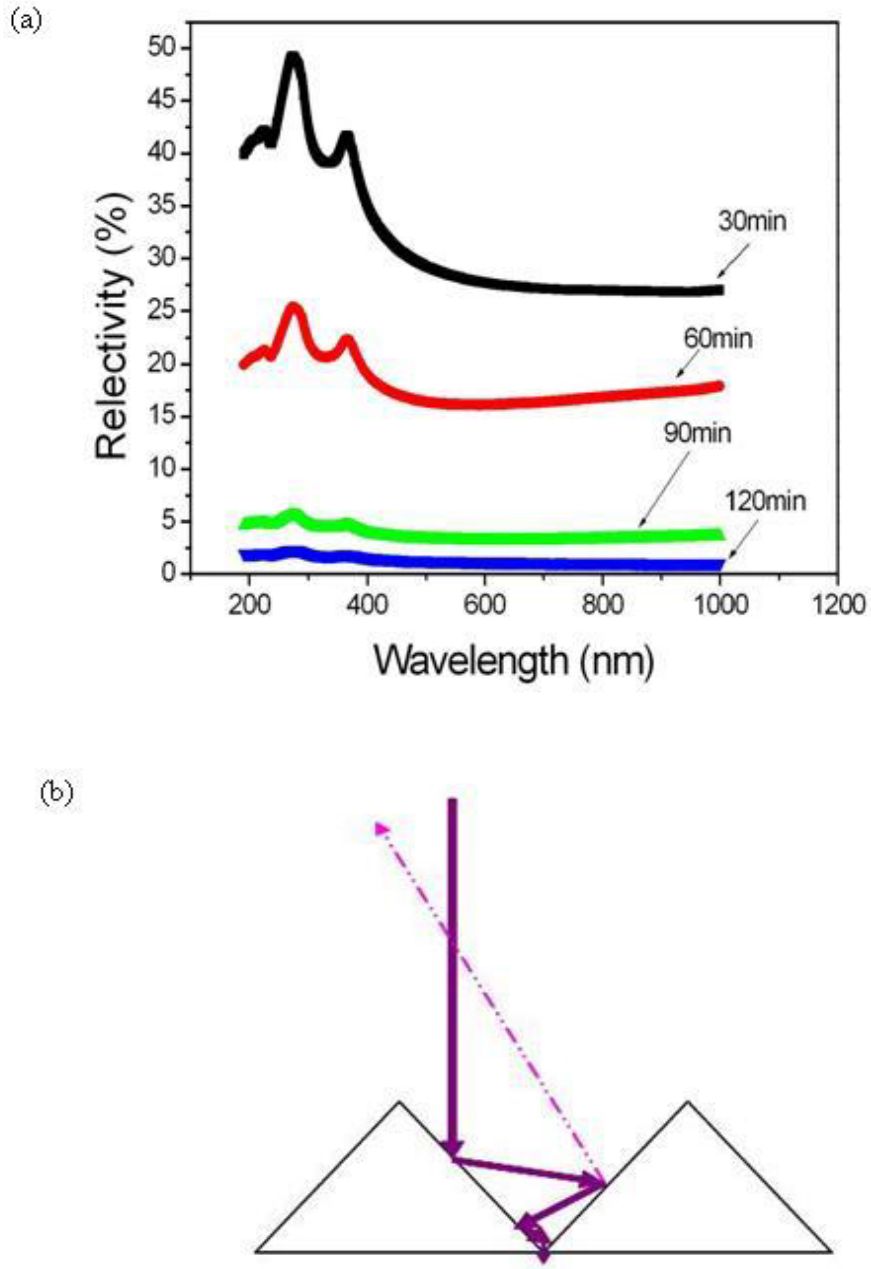

Figure 4-3 Comparison of different conditions of etching surface. (a) The reflectivity of silicon surface with pyramidal structures during different texturing time. (b) The scheme of a light beam at normal incidence on a textured surface. The light is shined through a hole aperture and the incident light could be recorded by photodetector devices such as solar cell. However, there is not all incident light will shine into the hole aperture, it may accompany few reflection light scattering.

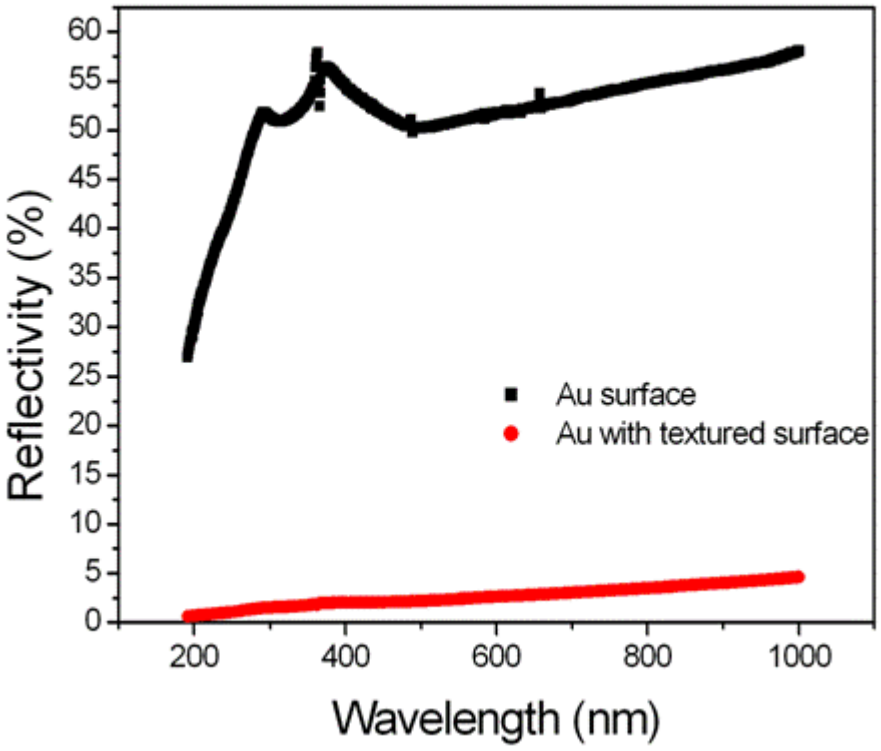

Figure 4-4 The reflectivity of silicon substrate with and without textursation process by N&K analyzer. The reflectivity of TMAH textured with a thin gold film is down to 2.00 % at 400 nm light wavelength.

4.1-2 Surface Energy of the Pyramidal Structure

The definitions of surface energy have involved consideration of the behavior of liquids in contact with solids materials and the formation of droplets. One convenient way of quantifying this behavior is to measure the contact angle formed by the liquid-solid interfaces shown in figure 4-5. The total surface energy is based on the Young–Dupre equation, which is described the interfacial tension between the liquid (L) and the polymer surface (S): [68]

$$(1+\cos\theta)\gamma_L = 2(\sqrt{\gamma_S^{LW}\gamma_L^{LW}} + \sqrt{\gamma_S^{+}\gamma_L^{-}} + \sqrt{\gamma_S^{-}\gamma_L^{+}}) \quad 6$$

$$\gamma_i = \gamma_i^{LW} + \gamma_i^{AB} = \gamma_i^{LW} + 2\sqrt{\gamma_i^{+}\gamma_i^{-}} \quad 7$$

The equation 6 is together with the Lifshitz–van der Waals (LW) and Lewis acid–base (AB) theories. The equation 7 is surface tension (γ_i) of a phase *i* can be expressed and γ_i^{+} and γ_i^{-} are the electron acceptor and electron donor parameters, respectively. The contact angle θ is determined using three different liquids with water, ethylene glycol and diiodomethane. The surface properties of optimal textured process are studied by the drop contact-angle technique shown in table 4-1. For the contact angles of water, ethylene glycol, and diiodomethane, the total surface energy can be calculated. From the Young–Dupre equation, the surface tension of van der Waals (γ_S^{LW}) has larger contribution than acid–base (γ_S^{+}, γ_S^{-}), and therefore the textured surfaces provide the apolar interface in table 4-2. With longer etching time leads to higher surface energy and relatively unstable surface duo to larger surface area and surface tension. [69] However, when coating a gold thin film, the total surface energy becomes lower and it represents more stable surface. When we drop the liquid, the water drop become spread out over the surface and the contact angle tends to 5.97 degrees, this means the interface of textured surface are super hydrophilic. The surface-hydrophilic suggests the immobilization of lipase on the textured surface with gold thin film can be more uniformly for SAM, since the lipase is water-soluble. Moreover, lipase has amphlpathic structure and can catalyze the esters at lipid/water interfaces, a phenomenon known as interfacial activation, which has been discussed in chapter 2.

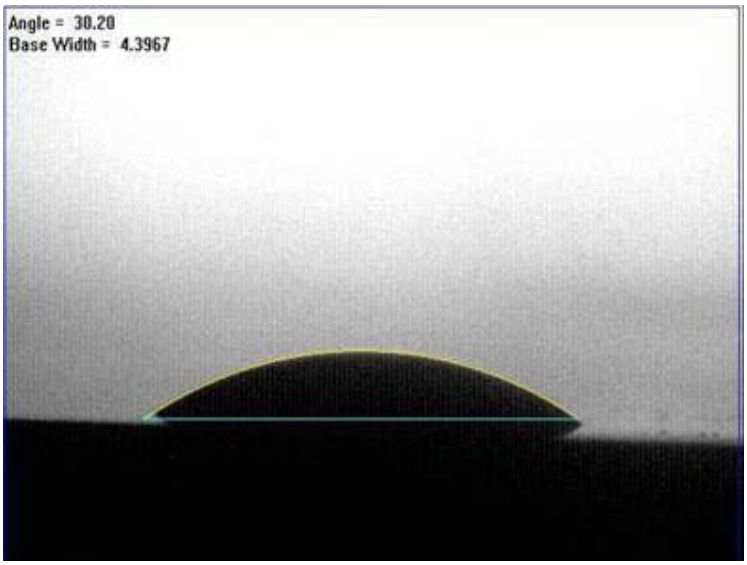

Figure 4-5 The drop of DI water on the textured surface coated a gold thin film. The contact angle dipped by DI water is 30.2 degree which means the hydrophilic interface of optimal texturing substrate the in the conditions of 1.19 % TMAH and 50 % of IPA solution at 80 ^{0}C for 120 min.

Table 4-1 The measurement of contact angle at different etching time by 1.19 % TMAH and 50 % of IPA solution at 80 ^{0}C.

	Water (degree)	Ethylene glycol (degree)	Diiodomethane (degree)
30 min	17.91	28.14	35.26
60 min	12.73	15.05	30.2
90 min	9.36	10.75	24.09
120 min	5.97	7.56	14.65
120min coated gold film	30.20	28.77	22.37

Table 4-2 The measurement of surface tension and total surface energy at different etching time.

	γ_S^{LW} (mJ/m^2)	γ_S^+ (mJ/m^2)	γ_S^-(mJ/m^2)	Total surface energy (mJ/m^2)
30 min	41.91	0.10	60.26	46.85
60 min	44.14	0.29	57.15	52.25
90 min	46.47	0.22	57.05	53.48
120 min	49.16	0.12	57.00	54.36
120min coated gold film	47.04	0.03	48.05	49.32

4.2 Activity and Stability of Immobilized Enzyme

Enzymes are biomolecules that catalyze the chemical reactions. Enzymes may be unstable and may not have the optimal activity. In this way, immobilization of enzymes with its relevance for the performance could be used as a tool to improve and optimize some of these activity and stability. [24] [70] Immobilizing enzymes to supporting materials can make enzymes reusable and affect their stability. Since enzymes may become activated when localized to a different environment, higher temperature or extreme pH value, during immobilization process. Furthermore, an optimized enzymatic process can have the effect of higher enzyme activity and stability for biodiesel manufacture to improve the conversion yield.

In this section, we discuss the optimal operation conditions of pH, temperature and concentrations of lipase. First, the lipase is immobilized on the gold substrate by SAM method. Then based on the Bradford assay and p-NPP reaction to calculate and measure the specific activity of lipase on the substrate. They are all carried out at the same area of samples, 1x1 cm^2 pieces.

4.2-1 Effect of pH on Lipase Activity and Stability

The pH stabilities of free lipase and immobilized lipase are compared in the range of pH 6~9 shown in 4-6. They are incubated for 1hr at 25 ^{0}C and then determining the activity at its optimum pH. The pH-stability profiles of the two enzyme preparations are stable at pH 7. The RSA is then calculated considering the lipase activity at highest specific activity as 100 %. At the condition of pH 6, acidic environment, the amino groups of lipase may be protonated, and decreasing the lipase activity. As pH increasing, it is found in figure 4-1 that lipase activity will decrease because of the lower stability in basic environment.

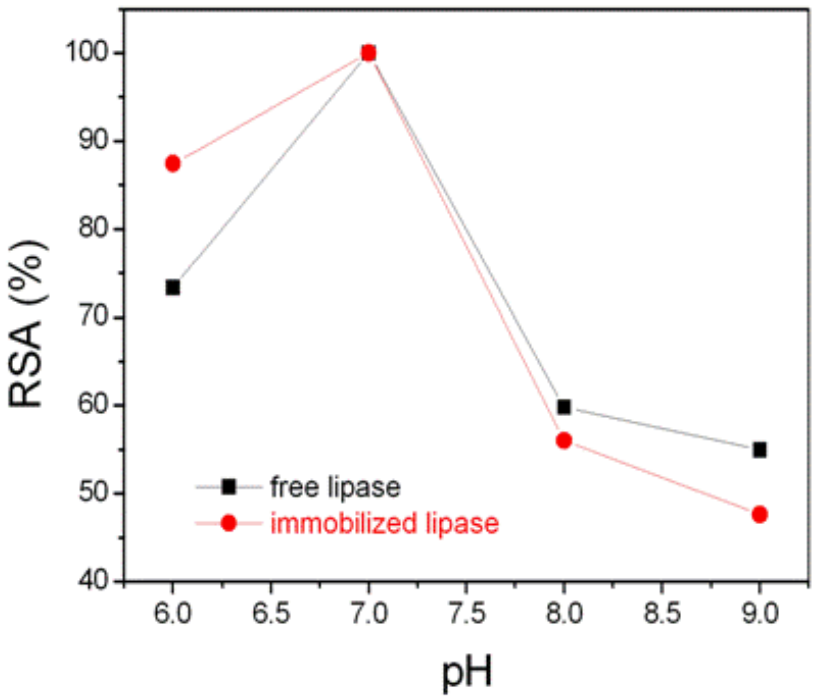

Figure 4-6 Effect of optimal pH on the activity of free and immobilized lipase.

4.2-2 Effect of Temperature on Lipase Activity and Stability

Measurements of enzyme activity are carried out in standard reaction mixture at different temperatures covering the range of 25–35 °C. Thermal stability was

investigated by incubating the free lipase and lipase immobilized at pH 7 for 1hr and then determining the activity at its optimum reaction temperature. As shows in figure 4-7, with the increasing the temperature, the lipase activity will increase until 30 °C due to enhance the collision of lipase molecule frequency in the reaction. After 30 °C, there is enough energy to destroy the protein conformation and denature since the protein itself is temperature sensitive. This result suggests that the temperature increase may cause the change in lipase binding mechanism. In figure 4-7, the immobilized lipase has better stability than free lipase under varying temperature. This may base on the assumption that there is microenvironment between the lipase and substrate. Microenvironment surrounds the active site of lipases is the one mainly involved in the solid surfaces. Thus, lipases recognize the functional surfaces to those of their chemical environment and they suffer interfacial activation during immobilization. [59]

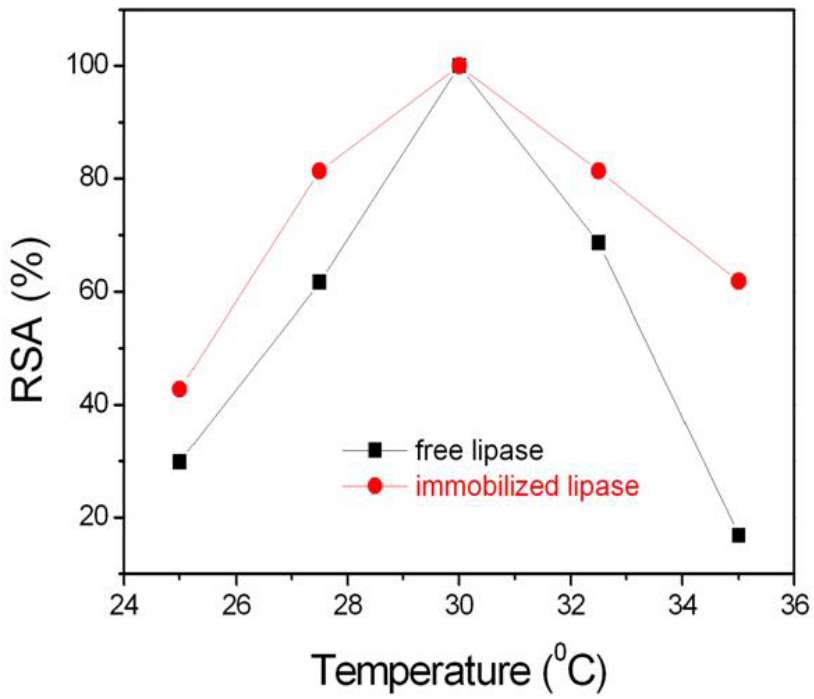

Figure 4-7 Effect of the optimal temperature on the activity of free and immobilized lipase.

4.2-3 Effect of Lipase Concentration on Lipase Activity and Stability

In the section, crude *Candida rugosa lipase* powder is used as the biocatalyst with water contenting rather than any additional organic solvent.[60] The lipase can catalyze both the hydrolysis and the synthesis of ester groups in insoluble substrates and activate in the presence of a water/lipid interface. Since the different concentration of lipase has the relationship with the rate of immobilization and it also will affect the cost we used in lipase. To study the effect of the water content in the reaction mixture, we investigate the efficiency of immobilization at a range of enzyme concentrations to determine the immobilization capacity of the lipase.

The immobilization lipase is discussed for enzyme concentrations from 0.25% (w/w) to 1.25% (w/w) under pH 7 and 30 °C for 1hr shown in figure 4-8. As the concentration increasing, the lipase activity will increase until 0.75% (w/w), and the activity of free lipase and immobilized lipase are 4.938 U/ml and 0.361 U/ml respectively. The lower concentration will diminish the collision of lipase molecule frequency in the reaction compared to higher concentration. After the concentration of 0.75% (w/w), the lipase activity will decrease with increasing concentration. This means the quantification lipase-immobilized on the substrate may be achieved the saturation situation, and not advance the lipase activity. According to figure 4-8, we determine that the lipase concentration of 0.75% (w/w) is suitable for this experiment.

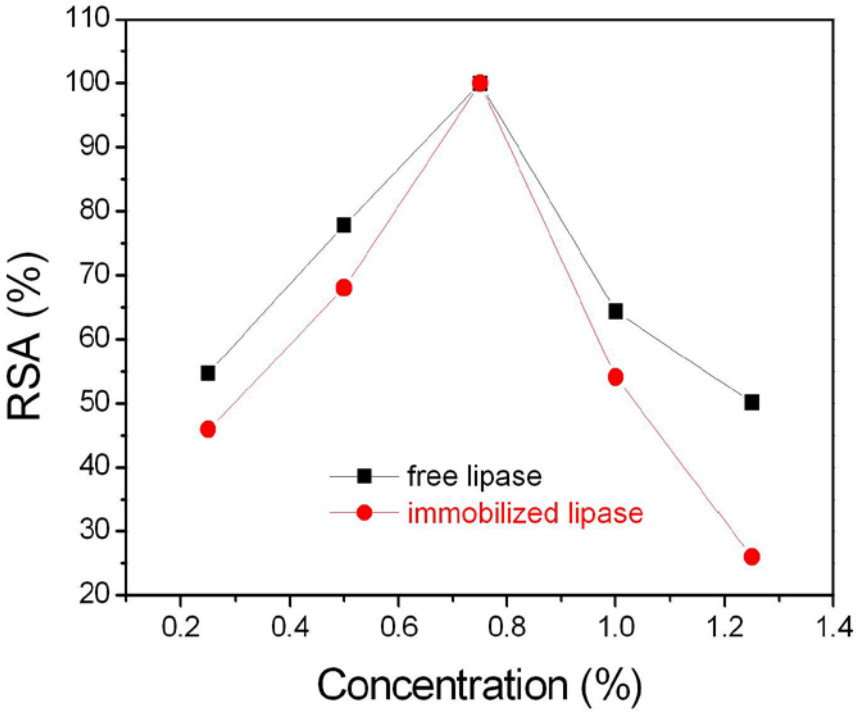

Figure 4-8 Effect of the optimal lipase concentration on the activity of free and immobilized lipase.

4.2-4 Quantitative Analysis of Lipase on the Textured Surface

The formations of pyramidal structures not only have lower reflectivity but also advance the surface areas for lipase-immobilized. There is a quantitative analysis of lipase-immobilized on the substrate with and without anisotropic texturisation shown in figure 4-9. This experiment is operational reused for 10 cycles and measured the effect of immobilized-lipase activity. It presents the reusability of lipase activity immobilized on the textured surface and the activity of immobilized-lipase up to 28.48 %. With the enhancing the amount of lipase-immobilized and lipase activity under the optimal immobilization process, thus improves the reaction of lipase-catalyzed as well.

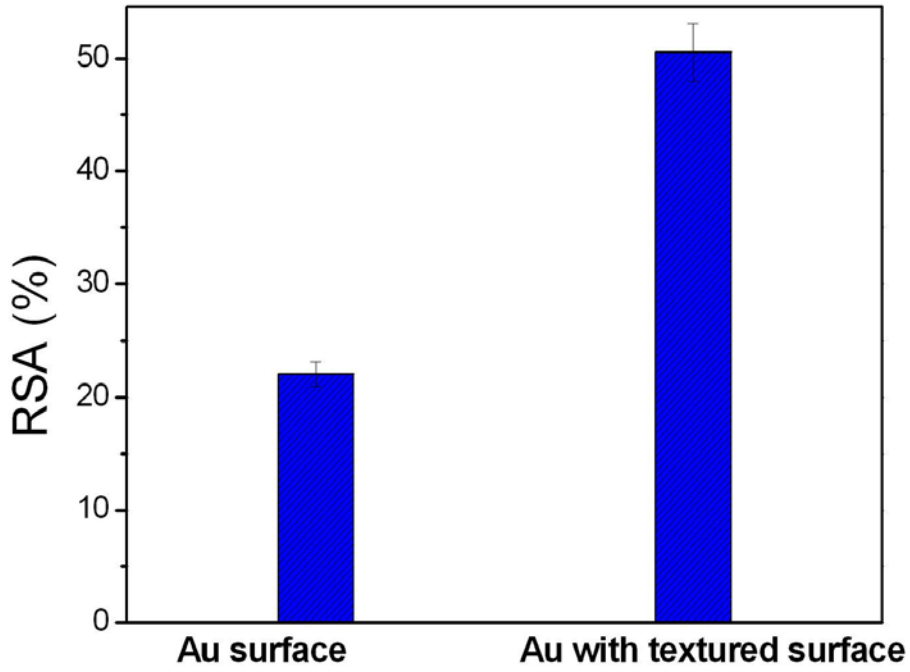

Figure 4-9 The quantitative analysis of lipase-immobilized on the substrate for 10 reused cycles. Right histogram stand for the anisotropic texturisation of 1.19 % of TMAH and 50 % of IPA solution at 80 °C for 120 min; the left histogram is without anisotropic texturisation. The substrate is already deposited 5 nm Cr and 10 nm Au for SAM and immobilized lipase.

4.3 Alcoholysis of Transesterification Reaction

The modification of the structure and the composition of oils and fats by enzymatic transeteresterification are currently of great industrial interest. For the applications of syntheses such as transesterification reactions are carried out either in organic media or in nonsolvent systems in which the water content can be controlled. Lipases can catalyze and synthesis of esters at lipid/water interfaces, a phenomenon known as interfacial activation, which covers the active site of lid.

[23] Interface-activated lipases occur in alternative conformation states with different activity, duo to the amphipathic nature of the lid. The alcoholysis reaction by lipase is activated by an oil–water interface. In the case of organic solvents, if the lids of the lipase molecules keep open in advance, lipase is expected to have a high activity because of the absence of oil-water interface shown in figure 4-10. [71]

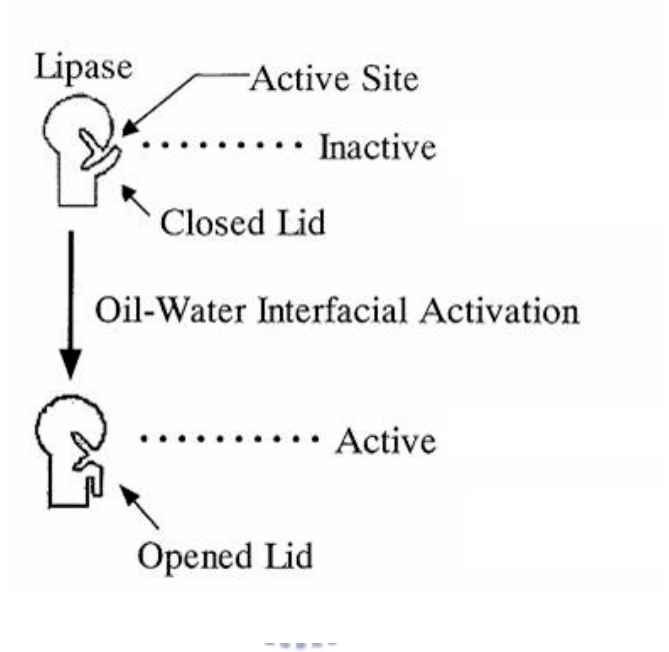

Figure 4-10 Schematic of lipase catalysis in the oil-water interface.

We have been detected the transesterification reaction with lipase-immobilized by vegetable oils and methanol. The mechanism of this catalysis reaction can be discussed in the oil-water interface shown in figure 4-11.

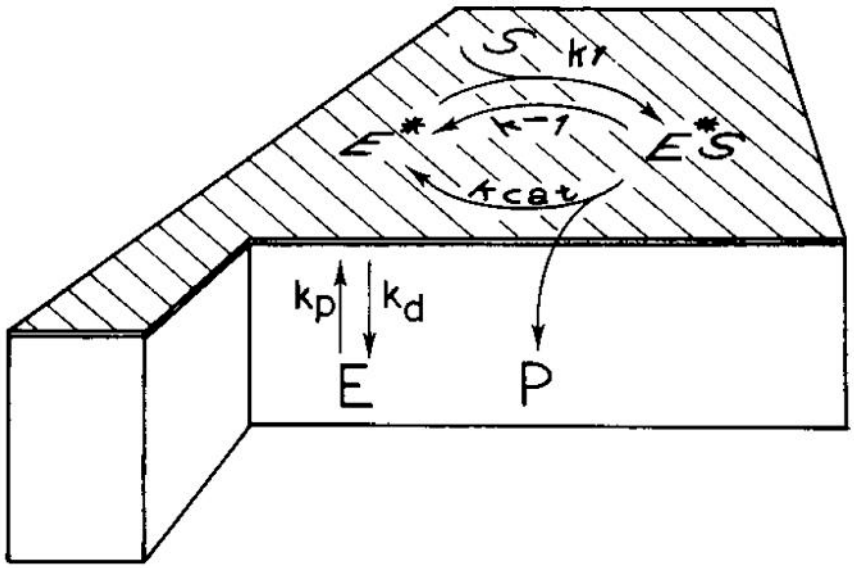

Figure 4-11 Proposed model for the action of a soluble enzyme at an interface.

The lid covers the enzyme active site, making it inaccessible to the substrate molecules. [33] When lipase catalysis in the oil-water interface with open conformation, the hydrophobic side faces the solvent and the lipase active site becomes exposed to the substrate-binding region. In figure 4-11, a simple model to describe kinetically action of soluble enzymes at interfaces. This model consists basically of two successive equilibriums. The first step describes the reversible penetration of a water-soluble enzyme into an interface. We call this first process penetration in contrast to a more general and rather unspecific adsorption. After this first step of penetration which leads to E* then follows a second equilibrium giving a kind of interfacial “Michaelis-Menten” complex. This complex denoted E*S is formed by the combination of a single substrate molecule with the penetrated lipase. [72] This can be justified by a simple calculation. The four following expressions describe in the simple model kinetically in figure 4-11:

$$E_0 = E + E^* \cdot \frac{I}{V} + E^*S \cdot \frac{I}{V}$$

$$\frac{dE^*S}{dt} = k_1 E^* \cdot S - (k_{cat} + k_{-1}) E^*S$$

$$\frac{dE^*}{dt} = k_p E + (k_{cat} + k_{-1}) E^*S - (k_d + k_1 \cdot S) E^*$$

$$\frac{dP}{dt} = k_{cat} \cdot E^*S$$

Figure 4-11 A simple model describes the kinetically action of soluble enzymes at interfaces.

We have used in the kinetic treatment the following symbols and abbreviations: E_O, total enzyme concentration (molecules/volume) ; E, free enzyme concentration (molecules/volume) ; E*, penetrated enzyme concentration (molecules/surface) ; E*S, penetrated enzyme-substrate complex concentration (molecules/surface) ; S, substrate concentration (molecules/surface) ; I, total interfacial area (surface); V, total volume (volume) ; kp, penetration rate constant (volume/surface) (time)$^{-1}$; kd, desorption rate constant (time)$^{-1}$; k_1, (molecules/surface)$^{-1}$ (time)$^{-1}$; k_{cat}, catalytic rate constant (time)$^{-1}$; P, product concentration (molecules/surface).

Kinetic analysis of soluble enzymes acting at interfaces cannot be treated by the classical Michaelis-Menten theory, because of the two-dimensional state of the substrate involved. Therefore, the first step is the reversible penetration of a water-soluble enzyme into an interface. The second is the equivalent of the Michaelis-Menten equilibrium.

Therefore, the interfacial processed lipase has a remarkable transesterification activity in the oil–water interface. We postulate that this activation is caused by the interface between oil and water makes the lipase lid open and enables the lipase to work effectively in the transesterification reaction.

4.4 Transesterification Reaction by Microfluidic Platform

As mentioned before, the study is focus on the microfluidic reactors for production the biodiesel and detection the transesterification reaction. The study uses microfluidic system by pumping 0.6 mm Teflon tubes through the channel and reactor chamber with lipase immobilized silicon surface or solar cell which is shown in figure 3-20. Teflon tubing is used to resistant the organic solvents, and has internal diameter appropriate for making connections to the feedstock, peanut oil and methanol, for the flow lines and detection.

We pumping the sample through relatively a tube and a channel and flowing in a large surface is to mix the sample well. Due to tendency to easily fabricate as well as low cost mixing approaches, the mixing is typically performed by diffusion, requiring a microchannel and reactor chamber. That means that the surface of the channel versus the volume of sample is large. In this situation, the substrate solution is constantly pumped through the microreactor tube. First, the feedstock solution is pumped through a Teflon tube with I.D. 0.6 mm, and then flow through a needle with I.D. is 0.25 mm, and the solution then flow through L-channel into a semicircle channel with I.D approximately 130μm. As the image, the intersection of the injection channel reveals straight edges with 90° angles in figure 4-12. The channel created in the PDMS replica has a nearly semicircle geometry with about 130 μm width and the height of semicircle is 55 μm. The side view of PDMS channel is shown in figure 3-16(b).

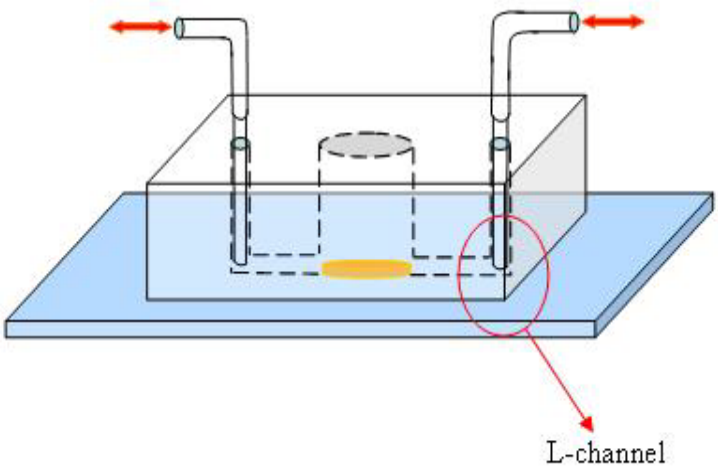

Figure 4-12 Schematic of microfluidic platform with the L-channel intersection.

The primary objective of the present work is to develop a simple fluidic system to enable for activity of immobilized lipase enzymes catalyzing transesterification in the microreactor. The substrate solution is pumped through the system with a syringe pump and the cut-off volume (pumping forward and reverse) for syringe pump is 0.06 ml at flow rate of 0.67 ml/min. A secondary objective is to explore the detection methods by UV–Vis spectrophotometer. Under this detection, the following are analyzing the characteristics by NMR and monitoring the biocatalytic process with photo-electronic detection. All experiments processed in microfluidic reactor and the conversion is much higher compared with other lipase biocatalysis. [73] The reactions are very slow, with requiring from 4 to 40 hours, or more. The experiment in the microfluidic system has higher conversion, duo to the optimal texturisation process for increasing the surface and activity of lipase-immobilized. The microfluidic platform for increasing the surface-to-volume ratio, and improve the conversion yield of transesterification reaction.

4.4-1 Ultraviolet-Visible Spectrophotometer Analysis

Biodiesel has been widely researched using many different types of vegetable oils. However, interest of this study is focused on peanut oil, due to lower coat and its different change of transmission during transesterification reaction. In order to faster and completely catalysis reaction, we first use the alkali-catalysis, KOH, just for comparison of the triglyceride (oil) and near 100 % of biodiesel. Figure 4-13 indicates the transmission in three different types of vegetables; (a) shows the transmission of soybean oil and (b) the transmission of soybean oil. In these two types of oil, there is not apparent change of transmission before and after transesterification; (c) shows the transmission of peanut oil which has obvious changes between the triglyceride (oil) and biodiesel in transmission, especially at the 400 nm wavelength with the difference of 29.26 %. In figure 4-13, the transmission change largest is using peanut oil for production the biodiesel which is using alkali-catalysis for easy observation.

(a)

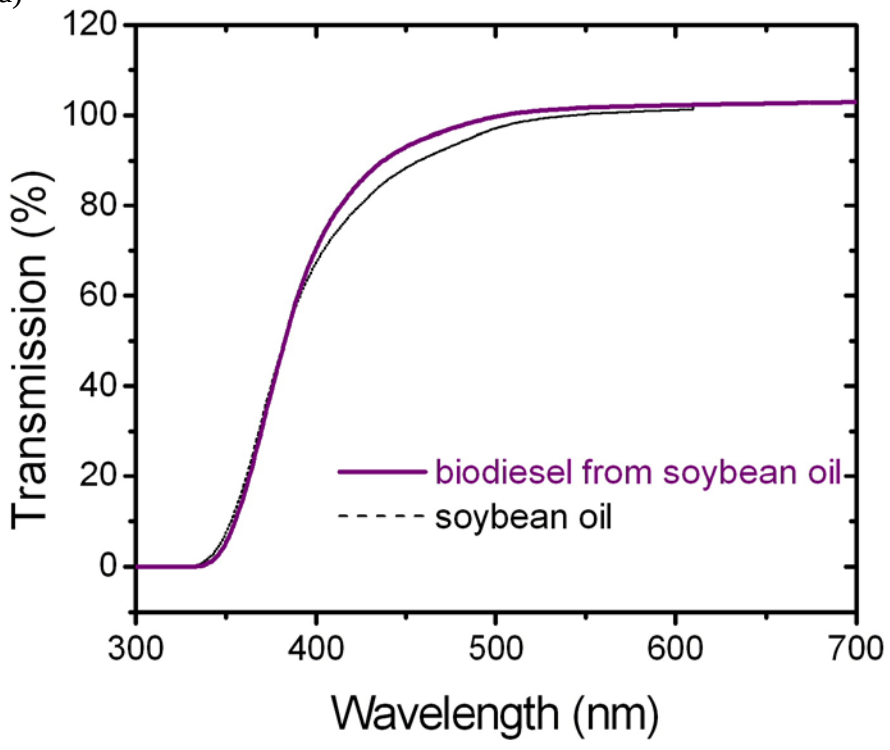

(b)

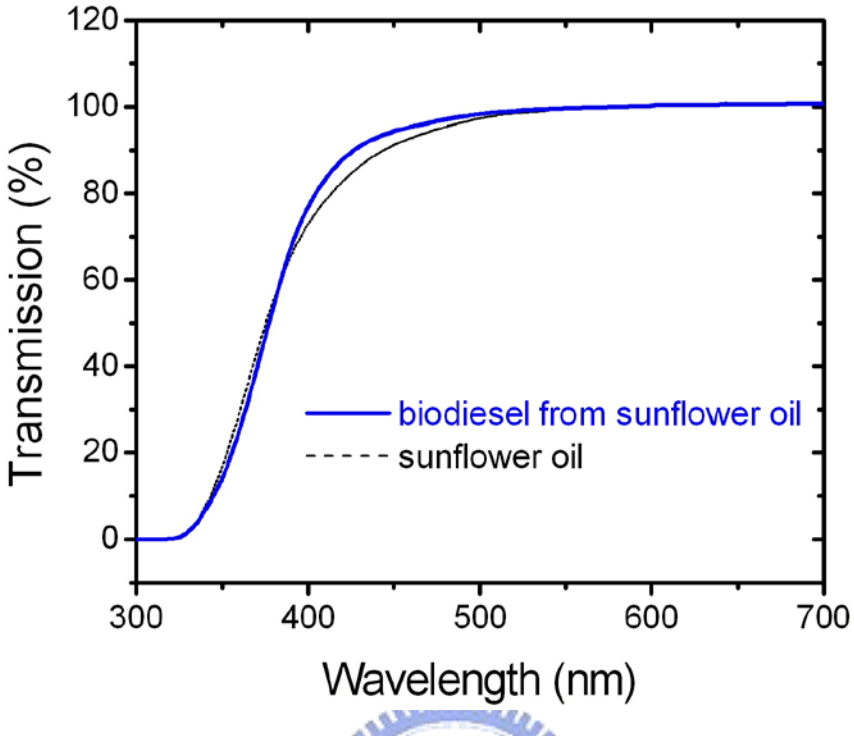

(c)

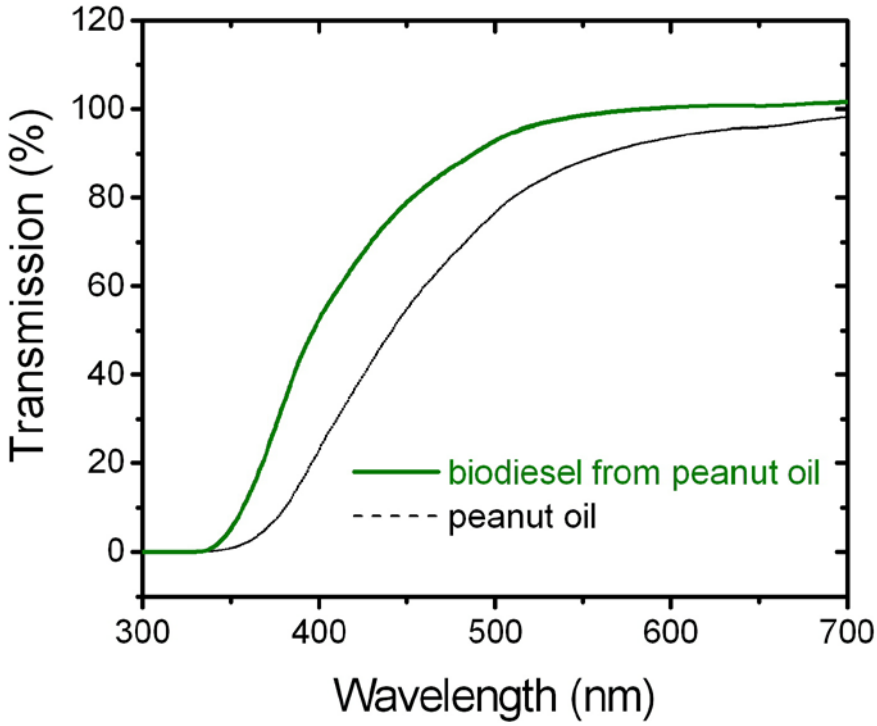

Figure 4-13 Comparison of the transmission with different vegetable oils by alkali-catalysis. (a), (b) and (c) are the transmission with oils and biodiesel by soybean oil, sunflower oil and peanut oil respectively.

According to this phenomenon, we can detect the transeaterification reaction with lipase-catalysis by using peanut oil and evaluating the transmission of UV-Vis spectrophotometer for the following analysis. As mentioned, the detection system is focus on microfluidic reactor with textured silicon surface. Once optimized with immobilization of *Candida rugosa lipase* on the textured silicon substrate, the microfluidic reactor is applied to detect transesterification reaction of pumping through a channel and measuring the transmission at the wavelength from 700 nm to 300 nm. Since the transmission increases with the transesterification reaction as shown in figure 4-13, we can detect optical responses with time. Figure 4-14 shows the detection of transmission with different incubation time and the reaction is using lipase-catalysis.

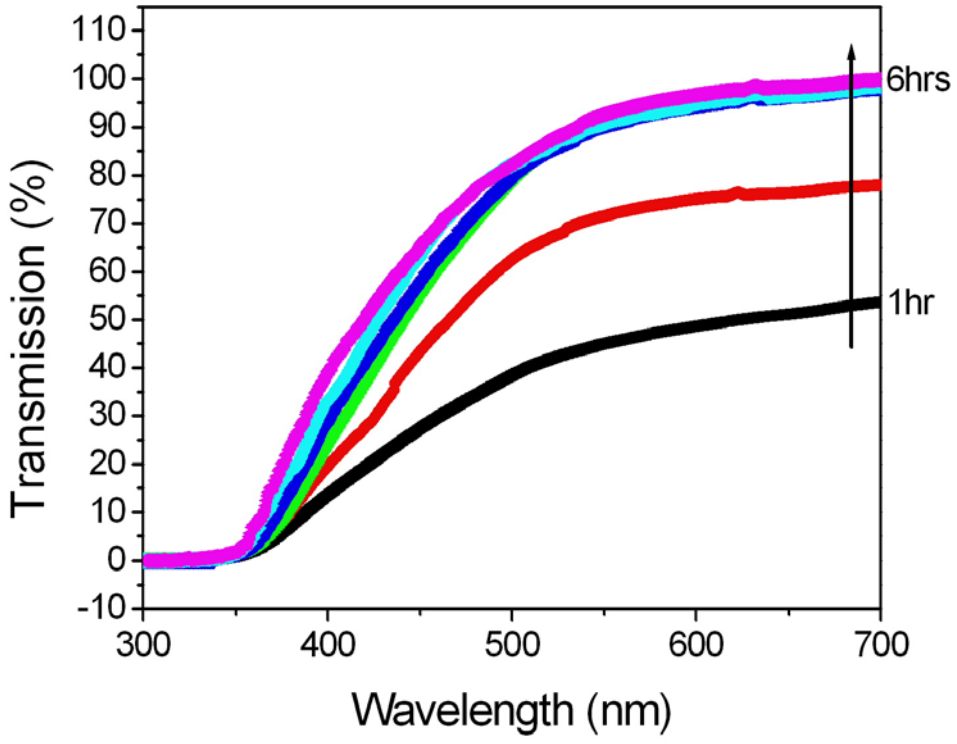

Figure 4-14 Measurement of the transmission spectrum by lipase catalyst with time.

The most different in the transmission curve from the all wavelengths is under 400 nm and the difference of 29.26 % which are 23.12 % and 52.87 % of peanut oil and biodiesel, respectively shown in figure 4-13 (c). Compared to the figure 4-13 (c) and 4-14, the transesterification reaction reacted with time, the trend of transmission curve from the oil moved toward the curve of biodiesel. That means the triglyceride has been catalyzed by lipase to form biodiesel and detected by the change of transmission. However, the transmission curves of the first two hours are below peanut oil transmission curve as shown in figure 4-15. The transmissions of first two hours are 13.5 % and 19.53 % and the triglyceride of peanut oil is 23.12 %. It is because the reactants are still under emulsifying and mixing. Then the transmission trends to increase with longer catalysis time.

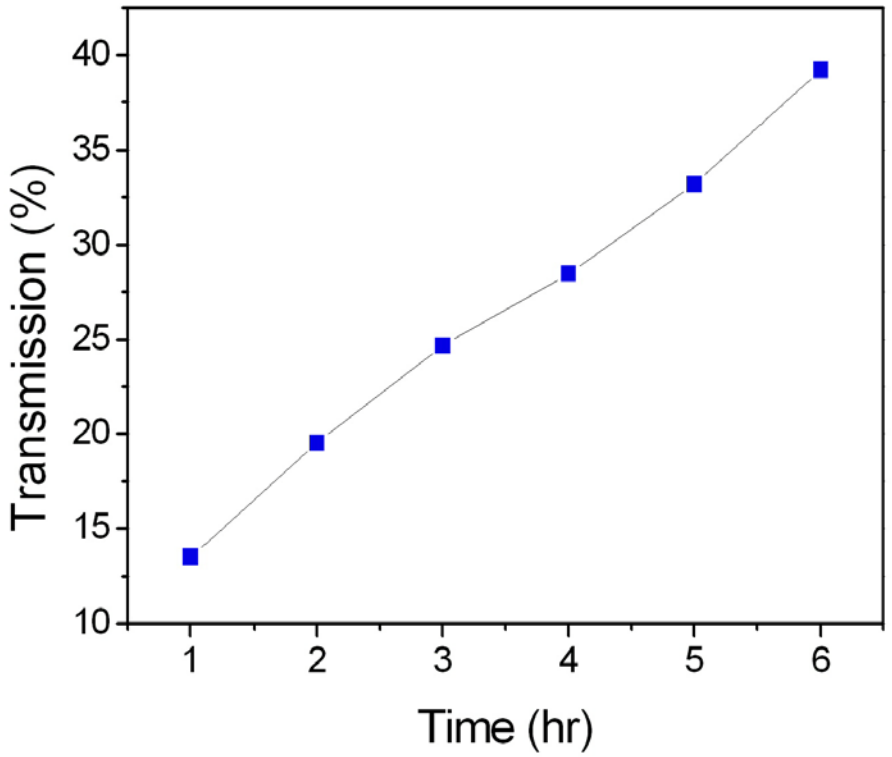

Figure 4-15 The relationship of transmission and catalysis time at 400nm. The transmissions of first two hours are 13.5 % and 19.53 %. For the next four hours, the transmissions are 24.67 %, 28.46 %, 33.2 % and 39.2 %, respectively.

This experiment proves the feasible and easy way for observation the transmission by UV-Vis spectrophotometer of driven biocatalytic system using immobilized lipase in a microreactor. We can determine the occurrence of transesterification reaction by the analysis of transmission changes. However, this method only can provide the phenomenon of transesterification reaction; it can not confirm the conversion yield. For more precise analyses the transesterification reaction, we use another methods which are discussed in next two sections.

4.4-2 Transesterification From NMR Analysis

Different from UV-Vis transmission, the Nuclear magnetic resonance (NMR) spectroscopy is given to exploit the magnetic properties of certain nuclei and identify the carbon-hydrogen framework of the compound during the transesterification reaction. In this section, we used the ^{1}H-NMR with respect to hydrogen, since the protons chemical shift of CH_3 groups between triglyceride and esters shown in figure 4-16. [27][28][74]

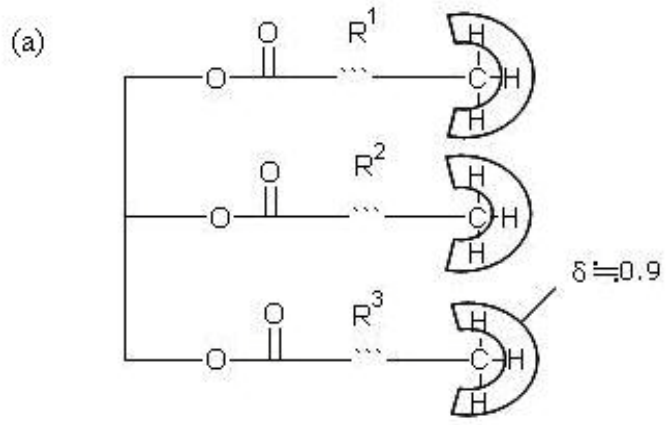

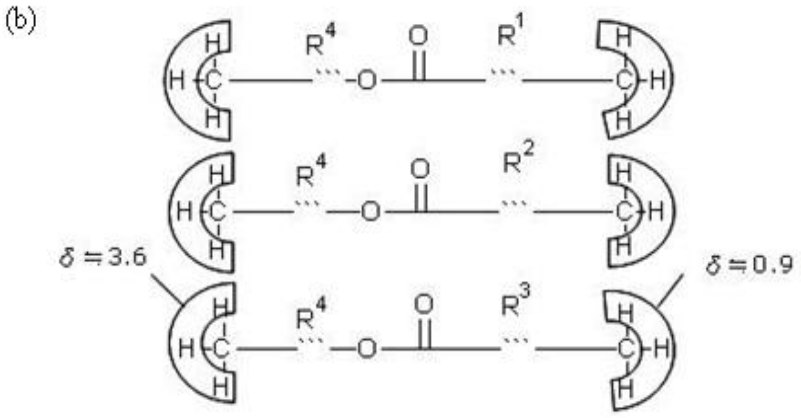

Figure 4-16 Schematic diagrams of the chemical shift of CH_3 groups. (a) Chemical shifts of proton in triglyceride, and (b) chemical shifts of proton in eaters (biodiesel).

The alkyl groups of methanol and alkoxy groups of triglyceride will react and exchange for production biodiesel during the transesterification shown in figure 2-1. The product of eaters (biodiesel) with two ends of CH_3 groups, shown in figure 4-16 (b), is made from the feedstock of one molar triglyceride with CH_3 groups and 3 molar methanols. The groups of R^1, R^2 and R^3 does not react the responses in the whole reaction, and the chemical shift of CH_3 groups with R^1, R^2 and R^3 is about 0.9 ppm and another site of esters with CH_3 groups is about 3.6 ppm. Since the two end sites of esters are with the same molar of CH_3 groups, the peak areas is equal to the H molar in H-NMR. Therefore, the conversion can be defined as the 3.6 ppm of peak areas divide by 0.9 ppm of peak areas shown in figure 4-17.

Depending on the local chemical environment, different protons in a molecule resonate at slightly different frequencies. Hence, both frequency shift and the frequency of the fundamental resonant are directly proportional to the strength of the magnetic field. The chemical shift is reported as a relative measure from reference resonance frequency for the nuclei ^1H.

The frequency shifts are extremely small in comparison to the NMR frequency. All of the ^{1}H-NMR experiments are performed on a Varian Unityinova 500 NMR spectrometer with description 5mm, 7" length tubes, and the solvent is d-Chloroform ($CDCl_3$). The typical frequency shift might be 500 Hz, and the chemical shift is generally expressed in parts per million (ppm). That means the percentage yield (weight conversion) was defined as (ppm of biodiesel ÷ ppm of initial peanut oil) × 100% and the percentage yield is estimated using peak area integrated by NMR spectrum. The ^{1}H-NMR spectrum is discussed with two-dimensional spectroscopy.

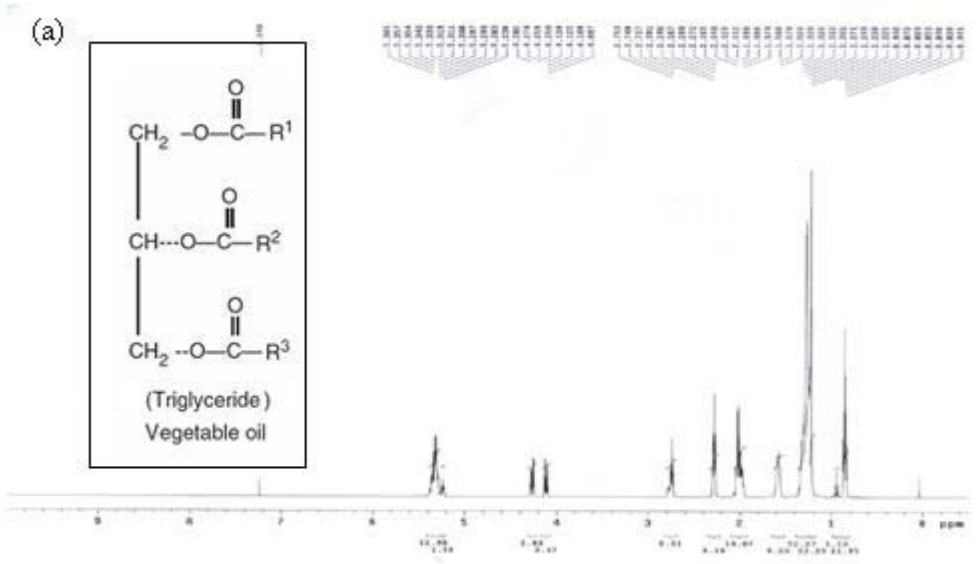

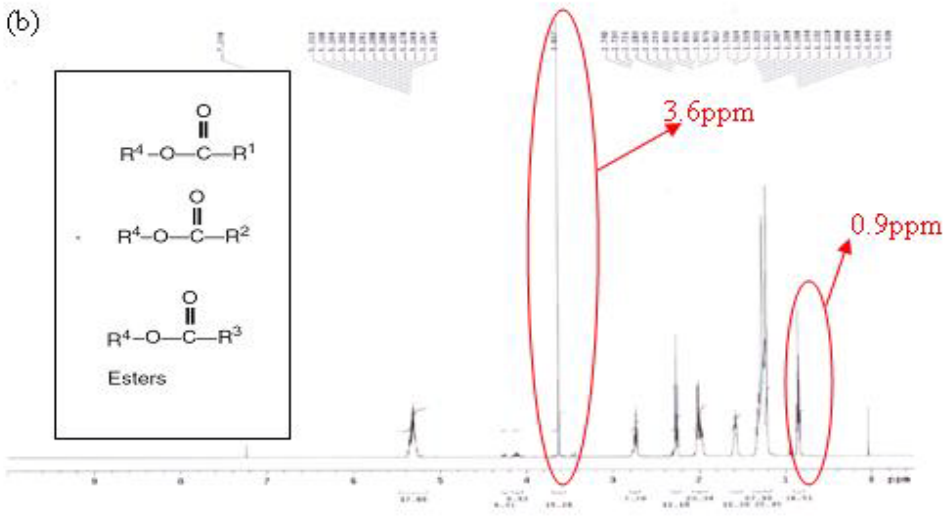

Figure 4-17 Comparison of ^{1}H-NMR spectrum before and after transesterification by Alkali-catalyzed for previously observation the chemical shift position of triglyceride and esters. (a) Before the reaction there is no peak in the chemical shift of 3.6 ppm which means there is not production of biodiesel, and (b) after the reaction the integrated of peak areas in chemical shift 3.6 ppm is 15.28 and 0.9 ppm is 16.51. The reaction conversion is calculated with 15.28/16.51 × 100 % = 92.55 %.

We have known that the ^{1}H-NMR spectrometers can be used to detect the transesterification reaction. In this study, the reaction is discussed on the microfluidic reactors and the microfluidic reactor with textured substrate is pumped continuous. After detection of transmission in the microfluidic reactor, the reaction solution is collected each hour for preparing ^{1}H-NMR sample (UV/Vis-NMR analysis system) shown in figure 4-18. The results of CH_3 groups with each hour in ^{1}H-NMR spectrum is shown in figure 4-19.

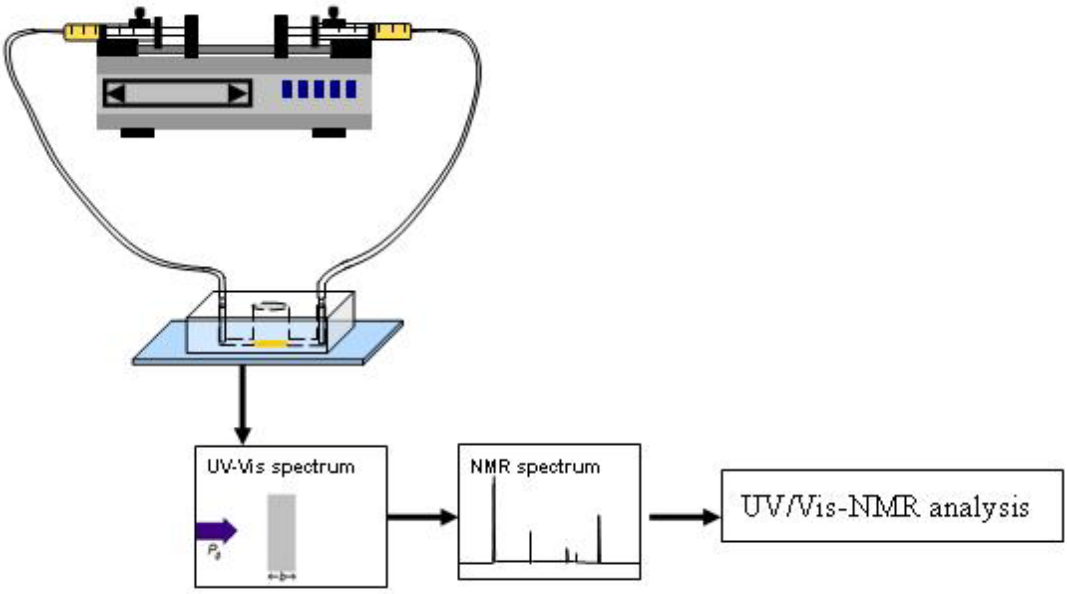

Figure 4-18 Schematic of UV/Vis-NMR analysis system.

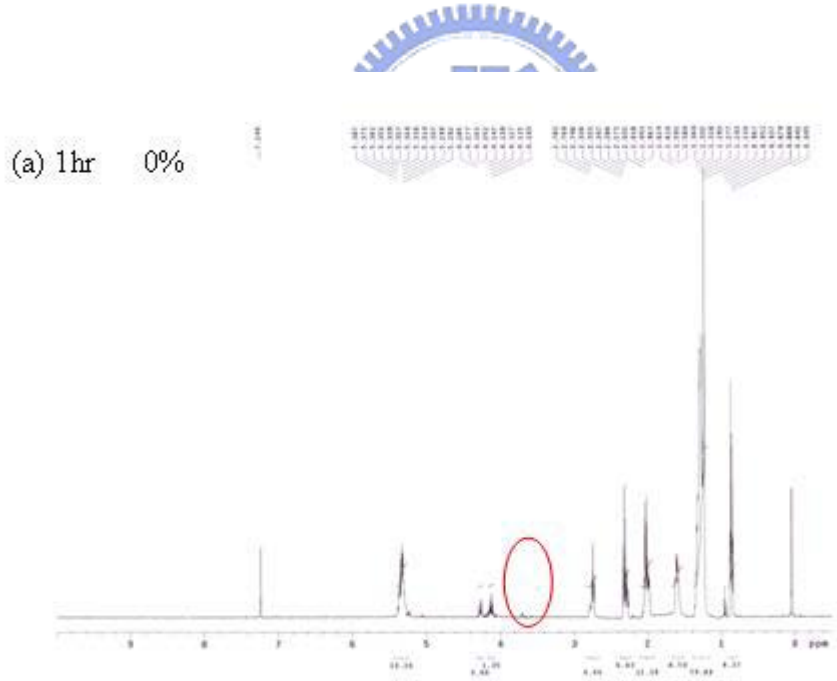

(b) 2hrs 0%

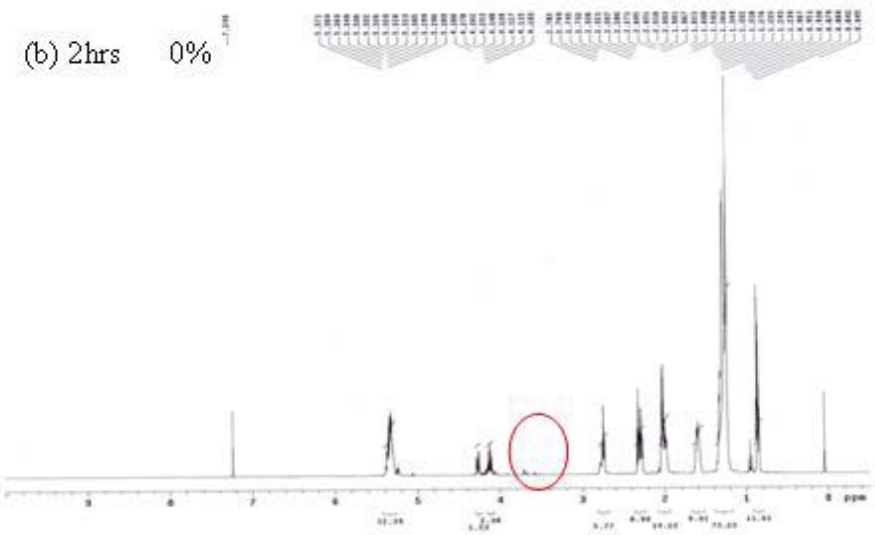

(c)

3hrs 1.91/15.65×100%=12.2%

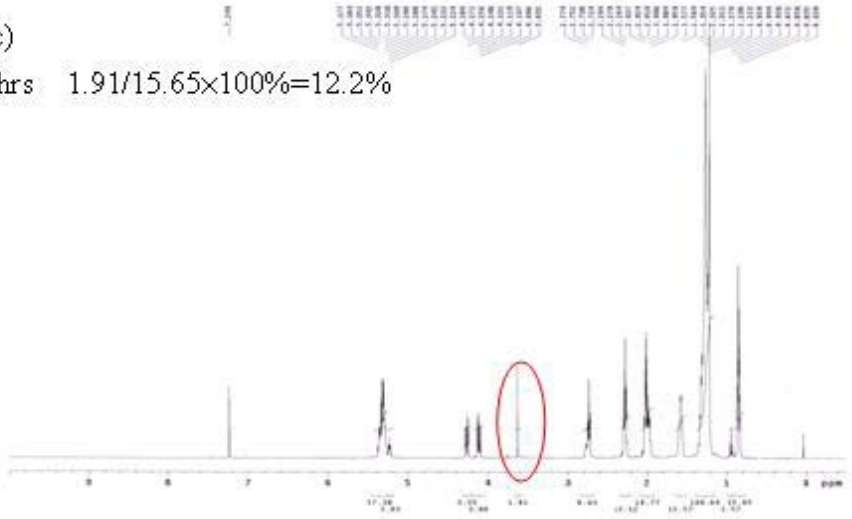

(d)

4hrs 6.18/29.22×100%=21.15%

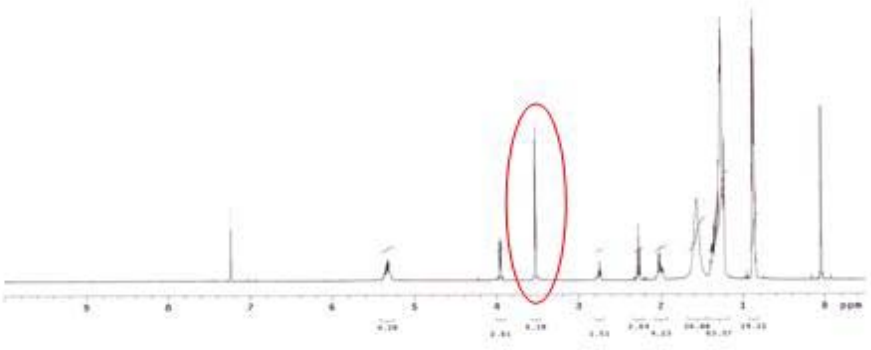

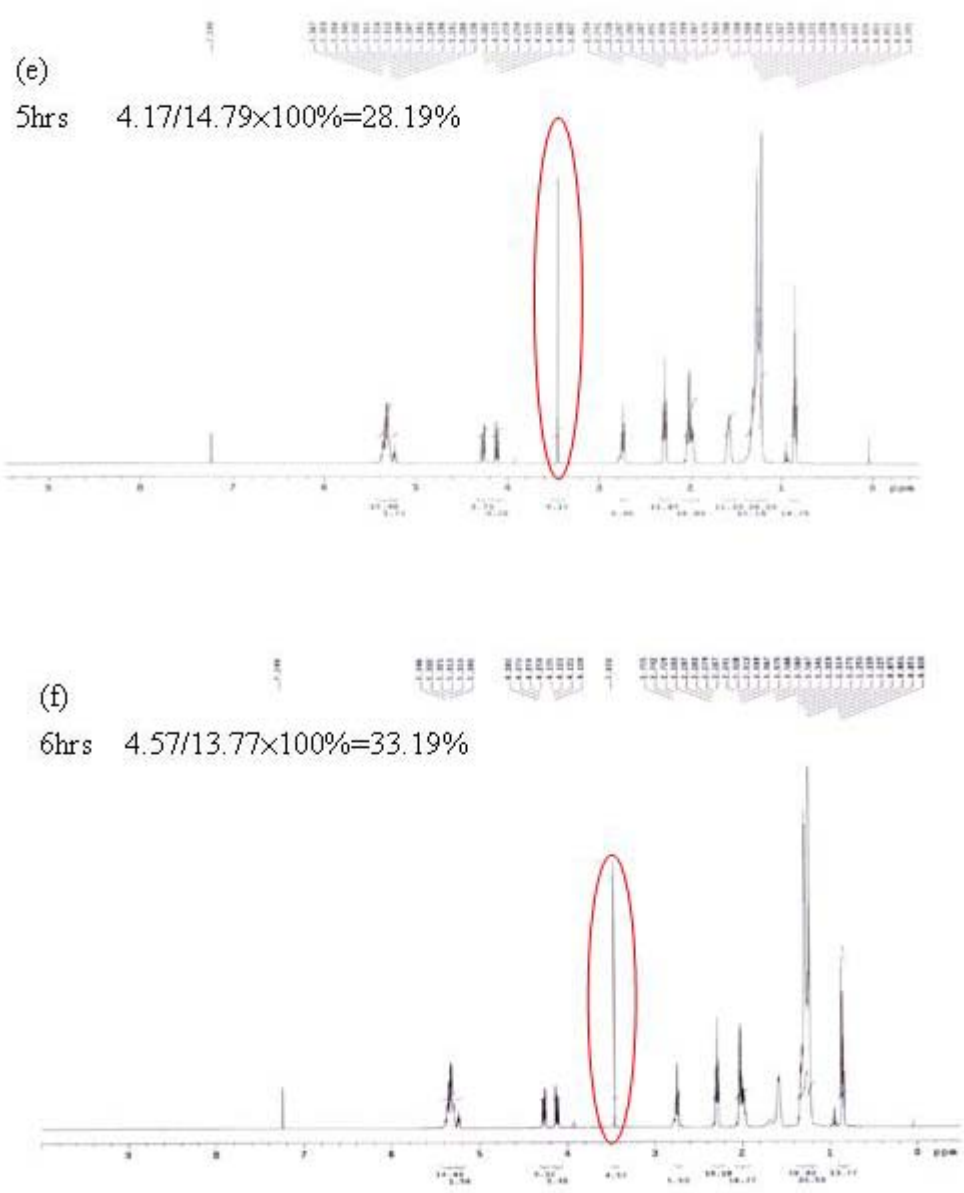

Figure 4-19 The ^{1}H-NMR spectrums exhibit the chemical shift of CH_3 groups with triglyceride and eaters for each hour. The peak of triglyceride and eaters are 0.9 ppm and 3.6 ppm respectively. The conversion is defined as the integrated of peak areas in 3.6 ppm divide by peak areas in 0.9 ppm.

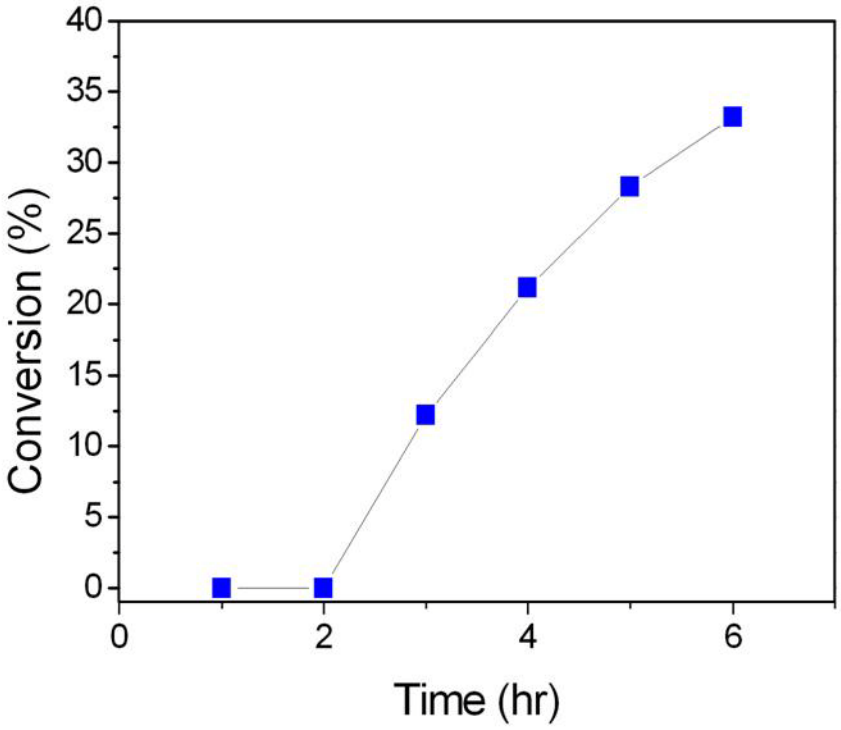

Figure 4-20 Effect of lipase catalyses the transesterification reaction for the conversion increasing with time.

The figure 4-18 shows the conversion increase with transesterifacation reaction progress, and that can be calculated. In this experiment, we propose a new approach for detection the transesterification reaction. With UV-Vis spectroscopy is a feasible and easy way for quickly detecting the reaction. Following are the analysis by ^{1}H-NMR can be quantity and calculated the conversion of transesterification reaction. The analysis is for detection of transmission in the microfluidic reactor, and the reaction solution is collected each hour for preparing ^{1}H-NMR sample (UV/Vis-NMR analysis system). Since the phenomenon of transmission can be expressed concretely quantity by calculated H-NMR. The relationship of them is shown in figure 4-21.

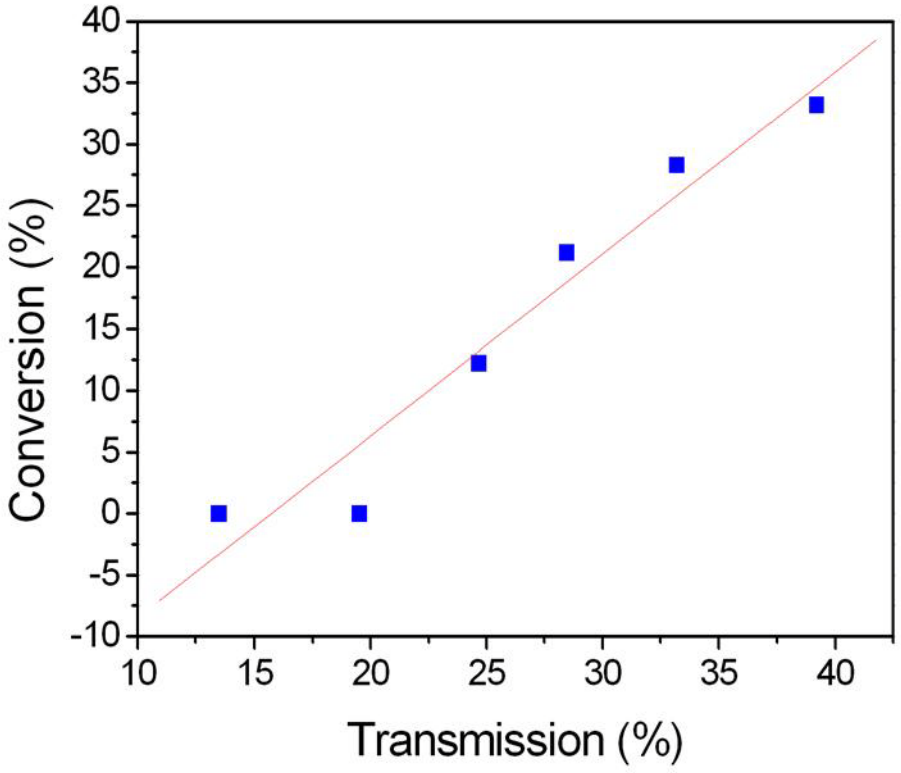

Figure 4-21 The relationship of transmission and conversion with the transeaterifacation reaction by lipase-catalyzed.

For the detection of transesterification reaction, the transmission in the first two hours is 13.5 % and 19.53 % which is under the transmission of triglyceride (oil), 23.12 %. We think reactants are still under emulsifying and mixing and the reaction is not really under biocatalysis. These results can be proved by the NMR which confirms the conversion is 0 % at the first two hours. After that, the conversion of reaction increase with longer time of biocatalysis, the appearance can also observe with increasing transmission. Therefore, this method allows either commercially available immobilized lipase or transesterification reaction to be tested in a short series of experiments.

4.4-3 Electrical Properties of Commercial Cell

The lipase-catalyzed reaction is evaluated by the UV –Vis spectrophotometer at 400 nm wavelength has been discussed in chapter 4.3-1. Application of enzymatic microfluidic reactors usually allows for continuous real-time monitoring of reaction progress. Here we would like to fabricate a photodetector to monitor the biocatalysis in the microfluidic system. We use a shadow mask for coating 5 nm Cr and 10 nm Au on the silicon substrate. The metal structure is composed of two contact pads and interdigitated lines, which form the active area of the device shown in figure 4-22.

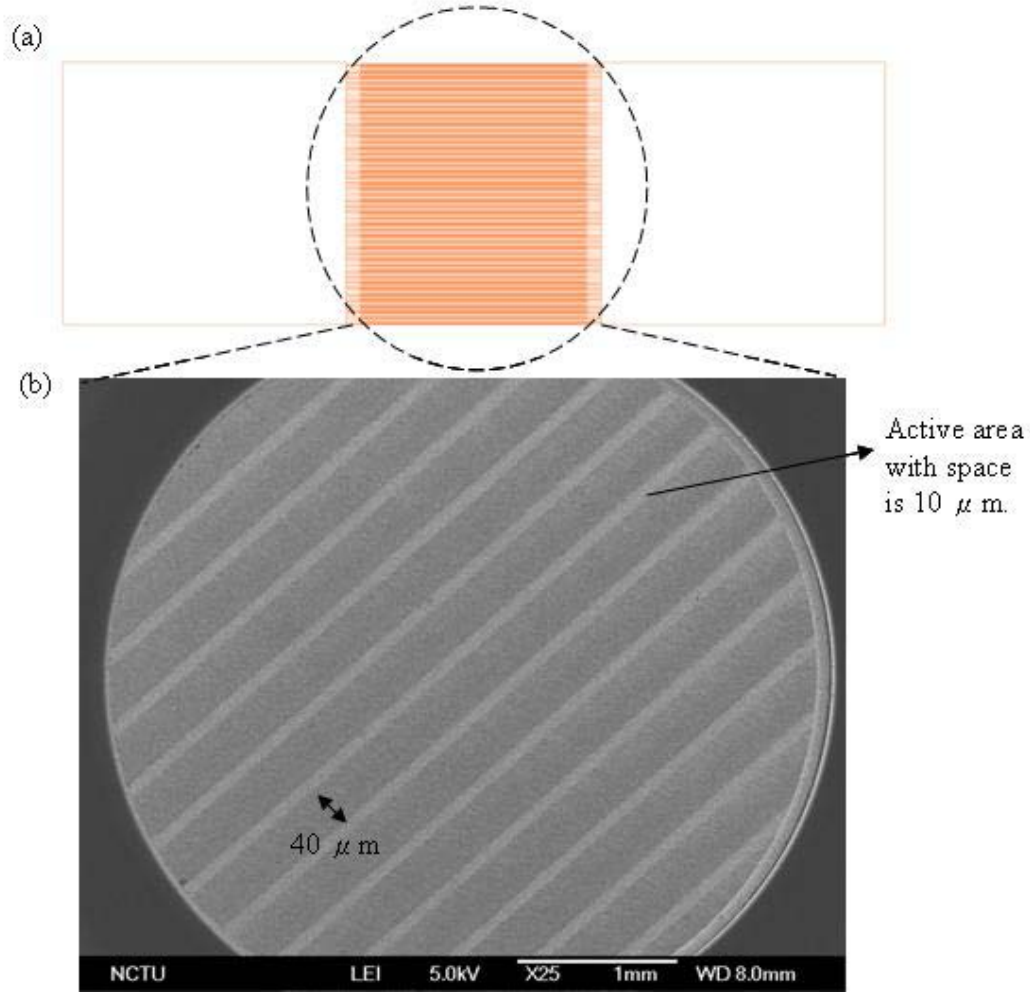

Figure 4-22 Schematic view of photodetector. (a) full layout of photodetector, the middle area is interdigitated lines, and the two squares in both side is contact pad, (b) the SEM image of interdigitated lines with metal part is active area.

The device works by absorbing optical energy and converting incident photons into a time-varying electrical signal. When the active area of the device is illuminated, carriers in the semiconductor absorption layer (also known as electron-hole pairs) are generated by incident photons having energy greater than the band gap energy (Eg). The carriers are transported to the metal contact pads, and current is detected in the external circuit under the application of an external bias voltage. However, the current of device is unstable and low on/off current is difficult to separate the photo-induced electrons shown in figure 4-23.

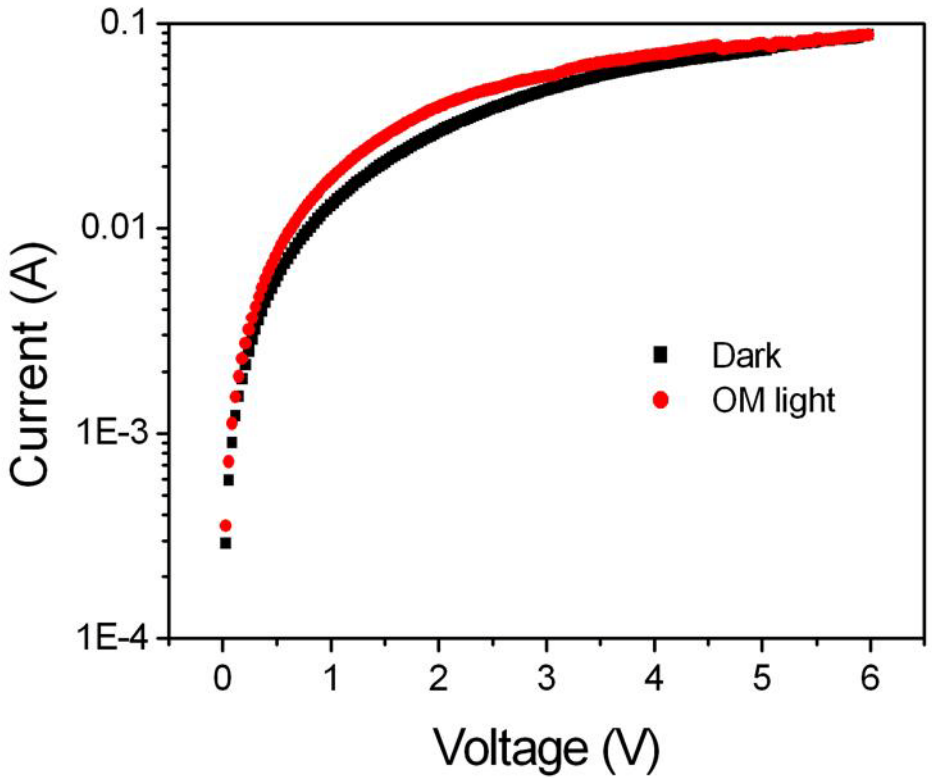

Figure 4-23 I-V characteristic of photodetector with interdigitated lines.

In figure 4-23, the device has low on/off current and not sensitive to the optical energy source. In this study, we focus on the phenomenon of difference transmission with the biocatalysis of transesterification reaction; therefore the sensitivity of light source is an important role for the detected device. The photodetector we used is

commercial solar cell for the same characteristic with random pyramids of textured surface by TMAH. [37]

The system utilizes a photo-electric transported work principles of real-time monitoring transesterifiaction reaction with lipase-catalyzed. Under the larger difference of transmission is at 400 nm, the lipase is immobilized on the solar cell and exposed to the 400 nm. This detection method is shown in figure 4-24.

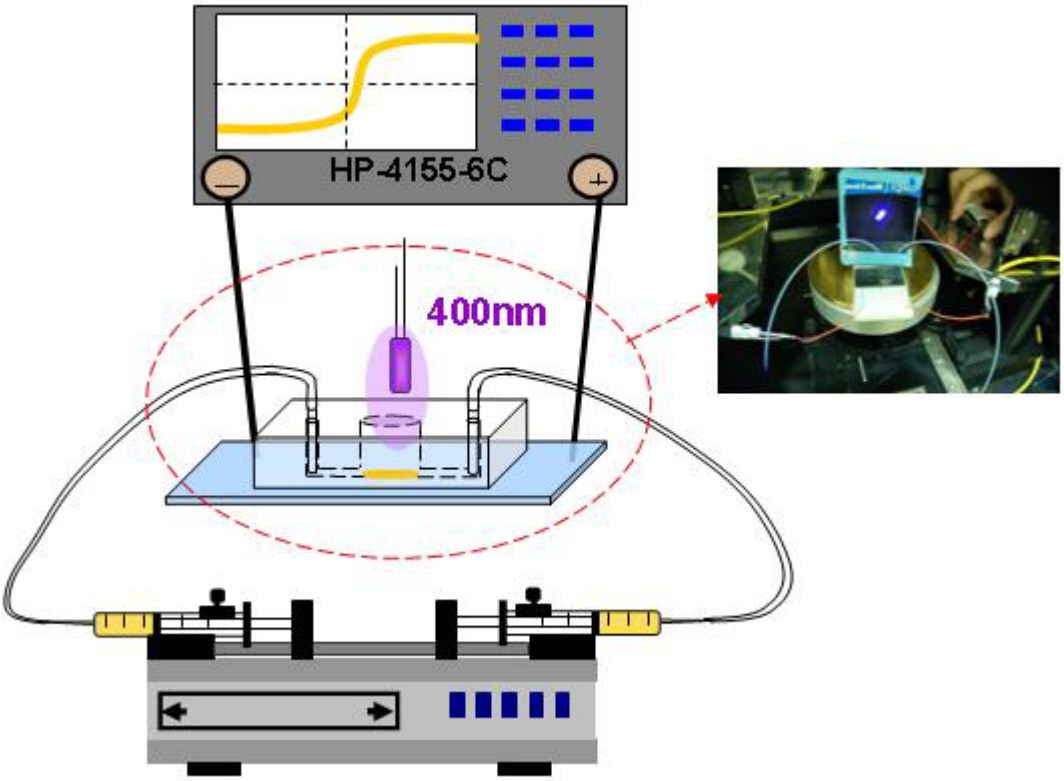

Figure 4-24 Schematic of UV/Vis-photodetector analysis system.

The solar cell is composed of the microfluidic reactor which is exposed to 400 nm light source and the output transducer is measured the photo-electrical signal. When the light is passing through the PDMS mold, the catalysis is evaluated in the exposed regions. The incident light of 400 nm is amethyst LED with InGaN material, 80 mcd of brightness, and operation at 20 mA of the current, and 3.5V of voltage. The

solar cell is amorphous silicon of SC 5030 with 50 mm in width, 29 mm in length, 2 mm in thickness, and operation at 26 mA in current and 1.8V in voltage.

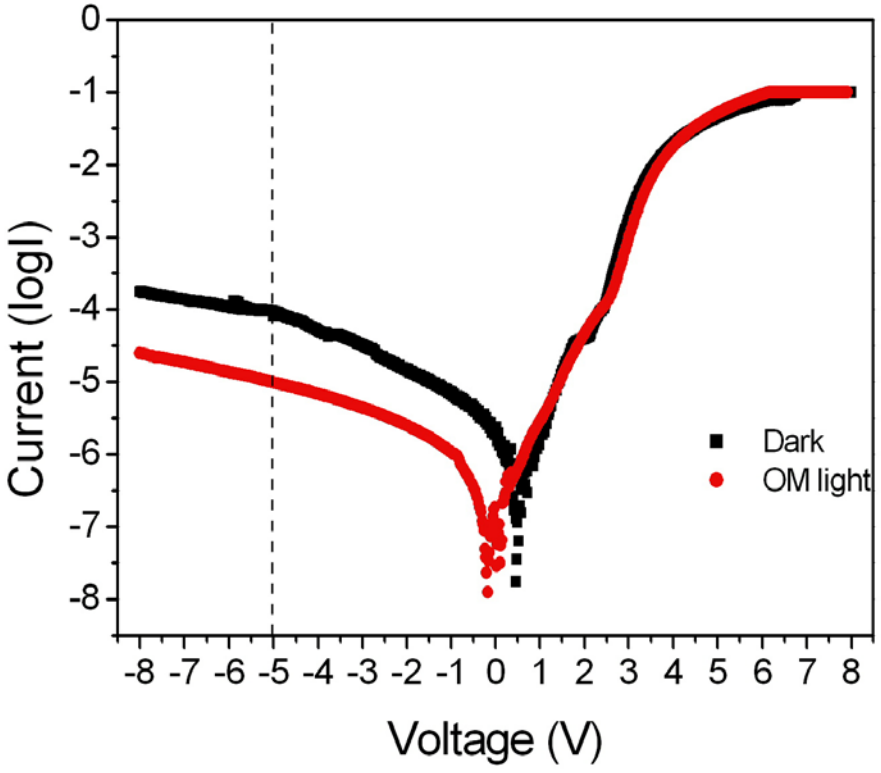

Figure 4-25 The relationship of log current and voltage with solar cells which are stressed the voltage from -8V to 8V. The solar cell has better sensitivity under external negative bias operation in -5V.

Under the under the application of an external bias voltage with -5V, the photo current of the solar cell was decrease from 50 μA to 5 μA, due to that lipase attachment of solar cell. With biocatalysis time increasing, the current increases from 20.50 μA to 33.11 μA shown in figure 4-26.

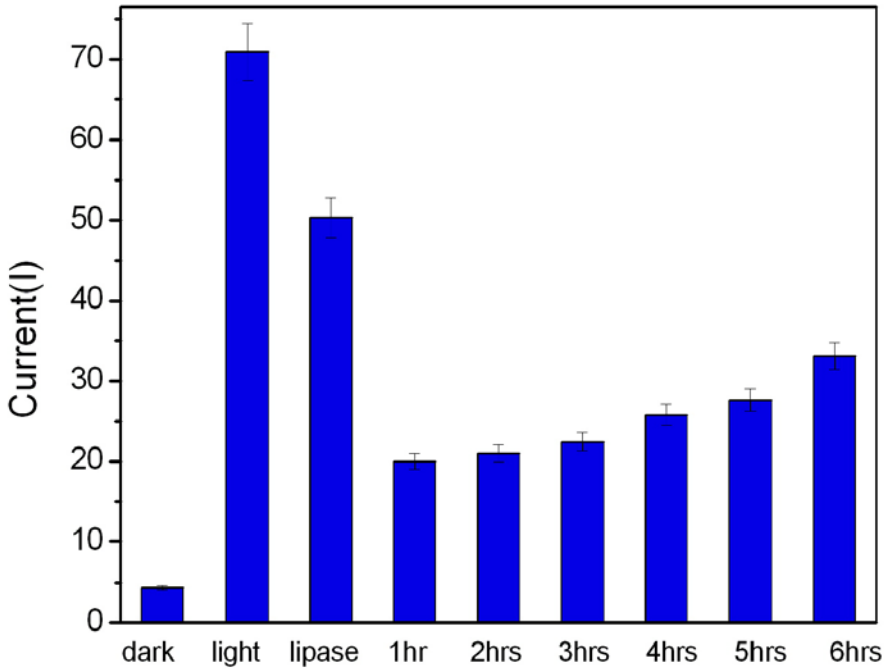

Figure 4-26 The I-t curve of lipase-immobilized on the solar cell and exposed to 400nm at bias of -5V.

After pumping the feedstock into the microfluidic system continuous, the photo signals decrease further attributed to the less transparent characteristic caused by samples mixing at the first two hours. This observation also is revealed in UV-Vis transmission spectrum at the first two hour. After mixing, the photo current signals increase gradually with time. The photo current here represents the amount of 400 nm light passed through product of transesterification reaction. Therefore, the gradually increasing photo current indicates the increasing catalysis reaction, the production of transesterification. This method allows photodetector to real-time monitoring amount of biodiesel by the electric signal. From the I-t curve, we can found the microfluidic platform has the sensitivity to detect the transesterification by lipase-catalysis. The results also present in the detecting and analysis by UV-Vis spectroscopy and ^{1}H-NMR spectrum which discussed before.

4.4-4 Analysis of Transesterification Reaction

One of our studies is directed towards using the photodetector for simultaneous real-time monitoring, which have the potential for using differential UV-Vis measurements and for commercial cell assays.

The understanding of the relationship between sensor parameters and performance would allow biosensors to more optimally meet the connection and consequence of those detection results. The analysis of solar cell with the lipase catalysis in the microfluidic reactor would be affected by transmission and photo-electrical current. However, we should consider the transmittance of PDMS, due to the incident light of 400 nm pass through the PDMS mold into the solar cell. Besides, the efficiency of solar cell and input power of 400 nm amethyst LED also are important factors in detecting solar cell.

The transmittance of PDMS mold is nearly 90.55 %, which is measured by a stable lamp. The power of light source is 70 mW and the efficiency of solar cell is 3.23 %. Here, we can calculate the electrical power accumulations of solar cell covered by microfluidic reactor, since the devices is illuminated and generated electrical signal by incident photons.

$$\text{Power (mW)} = 70\ \text{mW} \times 3.23\% \times 90.55\% \times \text{transmission} \qquad 8$$

In equation 8, the calculation power indicates that it has the relationship between the transmission and solar cell. In this experiment, the relationship of the transmission and photo-current signal of solar cell is shown in figure 4-27.

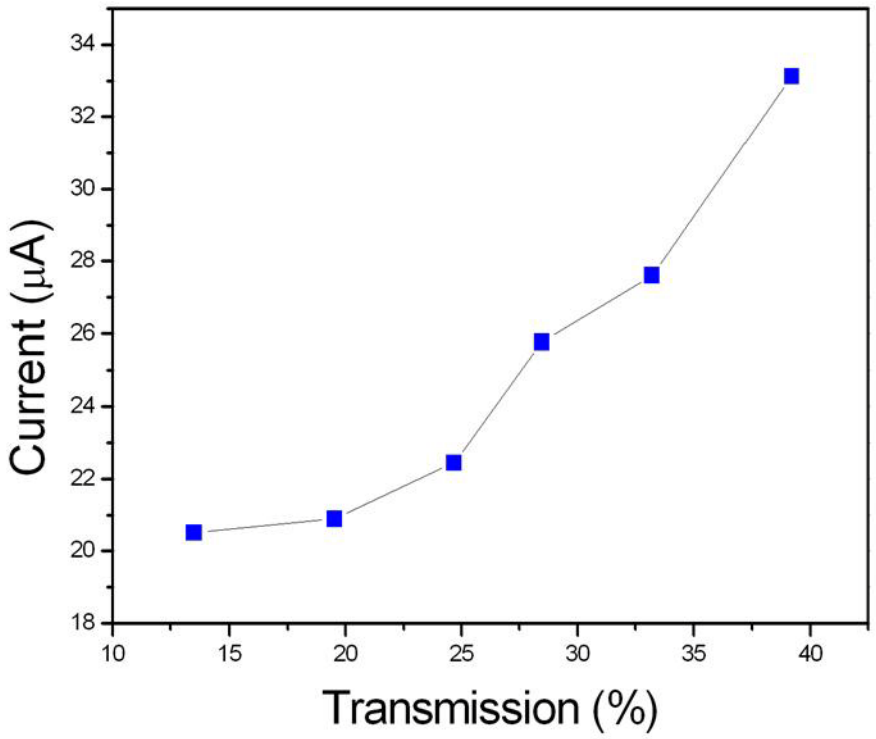

Figure 4-27 The relationship of transmission and current of solar cll with the transeaterifacation reaction by lipase-catalyzed.

As mentioned before, the activity of the lipases after surface immobilization can be evaluated by 400 nm wavelength. This method detected the different of transmission by the UV –Vis spectrophotometer, at the same time we detected by the ^{1}H-NMR and collected the electrical signal of solar cell for 6 hours. As the results of reaction catalysis, the detection of current increases with the transmission changes with time and enhance the conversion of reaction. Combine the figure 4-21 and 4-27, the connection between the three detecting method is studied and shown in the figure 4-28.

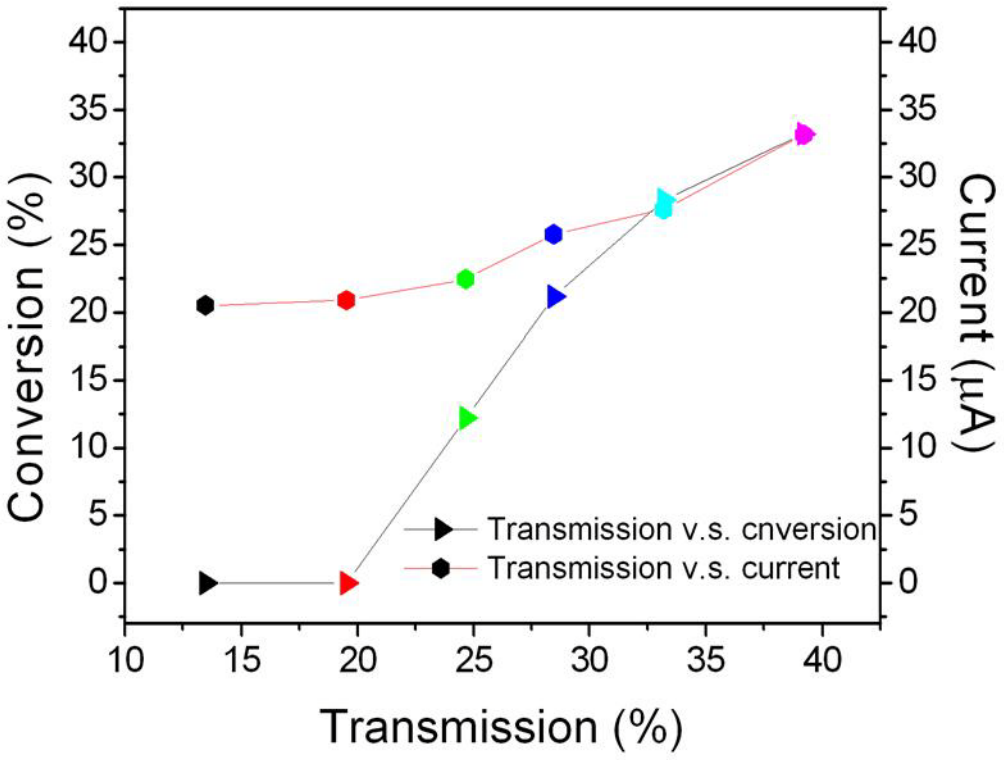

Figure 4-28 The relationship of the transesterification reaction compared with the UV/Vis-NMR (▲) and UV/Vis-photodetector (●) analysis system. The symbols with different colors represent different hours. The colours from black to purple represent sequential reaction time from 1 to 6 hours.

There is no obvious change of conversion at first two hours by NMR measurement, due to there is no reaction during solution emulsifying and mixing. Interestingly, the UV-Vis transmission is below the transmission of triglyceride and the photo current signal shows less change characteristic during the two hours of transesterification reaction. After that, the reaction catalysis with time and the result can be detected from the value of transmission. For the real-time monitoring, we used the solar cell for converting the light into the photo-electrical signal. In this experiment, we have the conclusion that the transesterification reaction has the characterization to the transmission and we have the conversion of the transmission

with time. Therefore, we can detect the reaction for real-time monitoring and, at the same time, know the convertion of the biocatalysis because of combining the UV/Vis-photodetector and UV/Vis-NMR analysis system.

Chapter 5 Conclusions

The microfluidic system has been successfully developed for biosensor detection and applications. The fabrication process of this platform is cheap, simple, fast, and very easy. In this study, we fabricate the microfluidic system with PDMS stamp and the TMAH textured silicon substrate, and solar cell microstructure as an on-chip biosensor for lipase-immobilized analysis. The microfluidic system transports the reagents through the Teflon tube and channel with in-line syringe pump.

For the section of immobilization, the optimal immobilization process is a challenge for lipase activity and stability. The self-assembly of the 3-MPA-NHS ester onto the substrate is through the amino groups of lipases by means of carbodiimide coupling agent such as EDC. The optimal condition for lipase-immobilized reaction is pH 7 under 30 ^{0}C environment in the 0.75 % (w/w) concentration of lipase. The textured substrate microstructure is developed for increasing the surface areas and decreasing the reflectivity. The anisotropic etching of silicon used for microfluidic system is under 1.19 % TMAH and 50 % of IPA solution for 120 min. The textured surface can improve the activity of immobilized-lipase up to 28.48 % and minimize the reflectivity down to 2.00 % at 400 nm light wavelength. We can detect the transesterification reaction by immobilized lipase onto the textured surface in the microfluidic chamber. We observe the change of transmission and know the occurrence of biocatalysis reaction by detection the absorbance of UV-Vis spectrophotometer, and the transmission change 29.26 % at 400 nm. The advantage of optical detection indicates the direct analysis of the biocatalysis reaction rather than using fluorescent tag or some photo-label attachment on the substance. The secondary feature is combining the UV-Vis and NMR analysis for precise identification of the chemical shift of CH_3 groups from triglyceride and esters. We can obtain precise

analysis for the conversion efficiency of transesterification reaction from the UV/Vis and NMR analysis system. The lipase is also immobilized onto the solar cell device and glass substrate for real-time monitoring at the wavelength of 400 nm light source for collecting the electric signal. This UV/Vis-photodetector analysis demonstrates the real-time detection of transmission in the microfluidic reactor with solar cell substrate and collected the electrical signal of currents for 6 hours.

For the combination of the UV/Vis-NMR and UV/Vis-photodetector analysis system, we successfully measure the transmission of the biocatalysis and then calculate and connecte the relationship of conversion and photo-current signal. We do not only propose an easy and feasible way to analyze and detect the characterization of transesterification reaction, but also provide a real-time monitoring platform for the characterization of transesterification reaction.

References

[1] T. Sakata, Y. Miyahara, *Biosens. Bioelectron.* **2005,** *21,* 827.

[2] S. P. Mohanty, E. Kougianos, *Potentials IEEE* **2006**, *25*, 35.

[3] A. Demirbas, *Energy Sources Part B* **2007**, *3*, 177.

[4] A. K. Agarwal, *Prog. Energy Combust. Sci.* **2007**, *33*, 233.

[5] A. J. deMello, *Nature* **2006**, *442*, 394.

[6] C. A. Marquette, L. J. Blum, *Biosens. Bioelectron.* **2006**, *21*, 1424.

[7] B. D. Malhotra, R. Singhal, A. Chaubey, S. K. Sharma, A. Kumar, *Curr. App. Phys.* **2005**, *5*, 92.

[8] C. Bartic, G. Borghs, *Anal. Bioanal. Chem.* **2006**, *384,* 354.

[9] R. B. Chaabane, M. Gamoudi, G. Guillaud, C. Jouve, R. Lamartine, A. Bouazizi, H. Maaref, *Sens. Actuator B-Chem.* **1996**, *31*, 41.

[10] R. K. Mendesa, R. F. Carvalhala, L. T. Kubota, *J. Electroanal. Chem.* **2008**, *612*, 164.

[11] B. Kuswandi, *Anal. Bioanal. Chem.* **2003**, *376*, 1104.

[12] W. Joseph, *Chem. Rev.* **2008**, *108*, 814.

[13] H. Noji, R. Yasuda, M. Yoshida, K. Kinosita, *Nature* **1997**, *386*, 299.

[14] S. Camou, A. Tixier-Mita, H. Fujita, T. Fujii, *Jpn. J. Appl. Phys.* **2004**, *43*, 5697.

[15] P. L. Urban, D. M. Goodall, N. C. Bruce, *Biotechnol. Adv.* **2006**, *24*, 42.

[16] M. A. Schwarz, P. C. Hauser, *Lab Chip* **2001**, *1*, 1.

[17] A. M. Jorgensen, K.B.Mogensen, J.P.Kutter, O. Geschke, *Sens. Actuator B-Chem.* **2003**, *90*, 15.

[18] L. Zhu, C. S. Lee, D. L. DeVoe, *Lab Chip* **2006**, *6*, 115.

[19] C. Eriksson, C. Agaton, R.Kange, M. Sundberg, P. Nilsson, B. Ek, M. Uhlen, M. Gustafsson, S. Hober, *J. Proteome Res.* **2006**, *5*, 1568.

[20] P. Andersson, G. Jesson, G. Kylberg, G. Ekstrand, G. Thorsen, *Anal. Chem.*

2007, *79*, 4022.

[21] H. Hisamoto, Y. Shimizu, K. Uchiyama, M. Tokeshi, Y. Kikutani, A. Hibara, T. Kitamori, *Anal. Chem.* **2003**, *75*, 350.

[22] N. J. Gleason, J. D. Carbeck, *Langmuir* **2004**, *20*, 6374

[23] K. Bunyakiat, S. Makmee, R. Sawangkeaw, S. Ngamprasertsith, *Energy Fuels* **2006**, *20*, 812.

[24] S. H. Chiou, W. T. Wu, *Biomaterials* **2004**, *25*, 197.

[25] S. Shah, S. Sharma, M. N. Gupta, *Energy Fuels* **2004**, *18*, 154.

[26] G.. Knothe, *J. Am. Oil Chem. Soc.* **2001**, *78*, 1025.

[27] G. Knothe, *Eur. J. Lipid Sci. Technol.* **2006**, *108*, 493.

[28] G. Knothe, *Trans. ASAE* **2001**, *44*, 193.

[29] Y. Zhang, M. A. Dube, D. D. McLean, M. Kates, *Bioresour. Technol.* **2003**, *89*, 1.

[30] A. Demirbas, *Prog. Energy Combust. Sci.* **2005**, *31*, 466.

[31] S. Brocca, F. Secundo, M. Ossola, L. Alberghina, G. Carrea, M. Lotti, *Protein Sci.* **2003**, *12*, 2312.

[32] A. R. Macrae, *J. Am. Oil Chem. Soc.* **1983**, *60*, 291.

[33] R. D. Schmid, R. Verger, *Angew. Chem.-Int. Edit.* **1998**, *37*, 1609.

[34] D. Iencinella, E. Centurioni, R. Rizzoli, F. Zignani, *Sol. Energy Mater. Sol. Cells* **2005**, *87*, 725.

[35] P. M. Sarro, D. Brida, W. V. d. Vlist, S. Brida, *Sens. Actuator A-Phys.* **2000**, *85*, 340.

[36] P. Papet, O. Nichiporuk, A. Fave, A. Kaminski, B. Bazer-Bachi M. Lemiti, *Mater. Sci.* **2006**, *24*, 1043.

[37] S. Koynov, M. S. Brandt, M. Stutzmann, *Appl. Phys. Lett.* **2006**, *88*, 203107-1.

[38] H. R. Luckarift, J. C. Spain, R. R. Naik, M. O. Stone, *Nat. Biotechnol.* **2004**, *22*, 211.

[39] R. B. Fair, *Microfluid. Nanofluid.* **2007**, *3*, 245.

[40] S. Haeberle, R. Zengerle, *Lab Chip* **2007**, *7*, 1094.

[41] B. J. Nehilla, K. C. Popat, T. Q. Vu, S. Chowdhury, R. F. Standaert, D. R. Pepperberg, T. A. Desai, *Biotechnol. Bioeng.* **2004**, *87*, 669.

[42] X. D. Zhou, D. P. Poenar, K. Y. L. ., W. Li, M. S. Tse, H. Chenc, C. K. Hengc, S. N. Tan, *Sens. Actuator A-Phys.* **2007**, *133*, 301.

[43] L. J. Lee, *J. Chin. Inst. Chem. Eng.* **2003**, *34*, 25.

[44] H. Becker, C. Gartner, *Electrophoresis* **2000**, *21*, 12.

[45] D. A. Skoog, F. J. Holler, T. A. Nieman, *Principles of Instrumental Analysis 5th ed.* **1998**.

[46] M. E. Smith, J. H. Strange, *Meas. Sci. Technol.* **1996**, *7*, 449.

[47] U. R. Prabhu, B. Baishya, N. Suryaprakash, *J. Magn. Reson.* **2008**, *191*, 259.

[48] K. F. Brennan, J. Haralson, J. W. Parks, J. A. Salem, *Microelectron. Reliab.* **1999**, *39*, 1873.

[49] C. Moldovan, R. Iosub, D. Dascalu, G. Nechifor, *Sens. Actuator B-Chem.* **1999**, *58*, 438.

[50] J. H. Li, G. J. Cheng, S. J. Dong, *J. Electroanal. Chem.* **1996**, *416*, 97.

[51] J. M. Slocik, E. R. Beckel, H. Jiang, J. O. Enlow, S. Jeffrey, J. Zabinski, T. J. Bunning, R. R. Naik, *Adv. Mater.* **2006**, *18*, 2095.

[52] Z. Grabarek, J. Gergely, *Anal. Biochem.* **1990**, *185*, 131.

[53] M. M. Bradford, *Anal. Biochem.* **1976**, *72*, 248.

[54] T. Spector, *Anal. Biochem.* **1978**, *86*, 142.

[55] L. Caseli, R. G. Oliveira, D. G. Masui, R. P. M. Furriel, F. A. Leone, B. Maggio, M. E. D. Zaniquelli, *Langmuir* **2005**, *21*, 4090.

[56] M. I. Toral, P. Richter, M. Cavieres, W. Gonzalez, *Environ. Monit. Assess.* **1999**, *54*, 191.

[57] P. Lotrakul, S. Dharmsthiti, *World J. Microbiol. Biotechnol.* **1997**, *13*, 163.

[58] C. M. Romero, M. D. Baigori, L. M. Pera, *Appl. Microbiol. Biotechnol.* **2007**, *76*, 861.

[59] R. Fernandez-Lafuente, P. Armisen, P. Sabuquillo, G. Fernandez-Lorente, J. M.

Guisan, *Chem. Phys. Lipids* **1998**, *93*, 185.

[60] M. Kaieda, T. Samukawa, A. Kondo, H. Fukuda, *J. Biosci. Bioeng.* **2001**, *91*, 12.

[61] M.W.Toepke, D. J. Beebe, *Lab Chip* **2006**, *6*, 1484.

[62] H. Makamba, J. H. Kim, K. Lim, N. Park, J. H. Hahn, *Electrophoresis* **2003**, *24*, 3607.

[63] R. Mason, J. T. Koberstein, *J. Adhes.* **2005**, *81*, 765.

[64] H. K. Wu, B. Huang, R. N. Zare, *Lab Chip* **2005**, *5*, 1393.

[65] K. B. Sundaram, A. Vijayakumar, G. Subramanian, *Microelectron. Eng.* **2005**, *77*, 230.

[66] I. Zubel, M. Kramkowska, *Sens. Actuator A-Phys.* **2001**, *93*, 138.

[67] P. Papet, O. Nichiporuk, A. Kaminski, Y. Rozier, J. Kraiem, J. F. Lelievre, A. Chaumartin, A. Fave, M. Lemiti, *Sol. Energy Mater. Sol. Cells* **2006**, *90*, 2319.

[68] F. H. Ko, C. T. Wu, M. F. Chen, J. K. Chen, T. C. Chu, *Appl. Phys. Lett.* **2007**, *90*, 191901.

[69] X. P. Zhang, B. Q. Sun, R. H. Friend, H. C. Guo, D. Nau, H. Giessen, *Nano Lett.* **2006**, *6*, 651.

[70] S. Sigurgisladottir, M. Konraosdottir, A. Jonsson, J. K. Kfistjfinsson, E. Matthiasson, *Biotechnol. Lett.* **1993**, *15*, 361.

[71] T. Maruyama, M. Nakajima, S. Ichikawa, H. Nabetani, S. Furusaki, M. Sekib, *J. Am. Oil Chem. Soc.* **2000**, *77*, 1121.

[72] R. VERGER, M. C. E. MIERAS, G. H. D. HAAS, *J. Biol. Chem.* **1973**, *248*, 4023.

[73] Y. Y. Linko, M. Lamsa, X. Y. Wu, E. Uosukainen, J. Seppala, P. Linko, *J. Biotechnol.* **1998**, *66*, 41..

[74] L. G. Wade , *Organic chemistry 5th ed*. **2003**.